Scuola Internazionale Superiore di Studi Avanzati

Doctoral Thesis

Non-equilibrium dynamics in one-dimensional constrained quantum statistical systems

Author:
Paolo P. Mazza

Supervisor:
Prof. Andrea Gambassi

A thesis submitted in fulfillment of the requirements for the degree of Doctor of Philosophy

in

Statistical Physics

“Possano i giorni trascorrere senza meta.
Non si prosegua l’azione secondo un piano”

ABSTRACT

In this thesis we discuss the non-equilibrium dynamics of one-dimensional many-body quantum systems in the presence of "constraints". Constrained systems are characterized by the fact that, in a truly non-equilibrium process the Hilbert space can not be fully "explored" within time scales proportional to any microscopical parameter of the Hamiltonian. The importance of investigating these kind of problems is twofold: on the one hand it is fundamental from a theoretical perspective, in order to understand the robustness of *ergodicity* in quantum systems and when (and if) there is a breakdown of thermalization. On the other hand, it is important from the practical point of view, because the precise control of low-dimensional quantum systems is expected to be extremely useful for the future development of quantum technologies.

In this work we will describe two possible kinds of constraints: systems in which the quasi-particle excitations, which are responsible for the spreading of the information during the time evolution, interact with a "confining" potential and systems in which the dynamics is resctricted to a given sub-space due to energetic suppressions which make some states unaccessible.

The structure of the thesis is as follows: in the first chapter 1 we will review some fundamental aspects concerning thermalization both in quantum and in classical systems. This problem has always attracted the attention of physicists but there had been an increasing interest in the last twenty years due to extraordinary development of experimental techniques with trapped cold atoms. These techniques made the experimental observation of real-time dynamics in closed quantum systems for very long times possible and opened the era of *quantum simulators*. We will illustrate the mechanism that is believed to lead to thermalization, i.e., the so-called *eigenstate thermalization hypothesis (ETH)* and the two only accepted exceptions to this paradigm: many-body localization and quantum integrability.

In chapter 2 we will discuss in detail the effect of "confinement of excitations" on the relaxation properties. We will show how the thermalization of one-dimensional quantum systems, expected to follow the ETH, is hindered by the presence of confinement. We investigate, using both numerical simulation and analytical techniques, the dynamics of the transport of physically relevant quantities, e.g., the energy, starting from "regular" initial states. Our results suggest an unexpectedly long transient phase during which the system does not thermalize. This phenomenon, at least for finite times, is qualitatively similar to what happens in systems in the many-body localized phase.
In chapter 3 we will show some recent developments in the study of constrained quantum systems in the so-called Rydberg-blockade phase. In particular, starting by discussing some recent experimental results, we will see how Rydberg atoms chains, can be used to mimic theories which are extremely rich from the theoretical point-view and which seem to violate the ETH.
In chapter 4 we will briefly review the notion of *gauge theory*, which is of utmost importance in all the fields of modern theoretical physics and in the study of fundamental interactions and we will explain the importance and the difficulties in both simulations and experimental probes of lattice gauge theories. Then, we will discuss one of the main topics of this thesis, namely the connections between the phenomena of slow-dynamics observed in Rydberg-blockade atoms chains and the dynamics in abelian lattice gauge theories. These two models are connected by means of an exact mapping, This fact opens the doors to several interpretation of the experimentally observed phenomena and, moreover, it shows that with the-state-of-the-art experimental setups in cold atoms experiments it is possible to perform large-scale simulations of lattice gauge theories. We will also present some theoretical considerations that can help in the understanding the very origin of the apparent ETH violation observed in Rydberg atoms setups. Furthermore, we propose a set of experiments that generically show long-lived oscillations, including the evolution of particle-antiparticle pairs, and discuss how a tuneable topological angle can be realized, further affecting the dynamics following a quench. We will also show the connection between spin systems analyzed in chapter 2 and abelian lattice gauge theories.
In the last chapter we will present our conclusions summarizing briefly the content of the previous chapters and we will illustrate some of the several possible developments along the same research line.
The original contribution of this thesis is in the second and in the fourth chapter. Some results reported in the second chapter are still unpublished.

This thesis is based on the following publications and pre-prints:

- Paolo P. Mazza, Gabriele Perfetto, Alessio Lerose, Mario Collura and Andrea Gambassi, *Suppression of transport in nondisordered quantum spin chains due to confined excitations*, Phys. Rev. B **99**, 180302(R).

- Federica Surace, Paolo P. Mazza, Giuliano Giudici, Marcello Dalmonte, Andrea Gambassi, *Lattice gauge theories and string dynamics in Rydberg atom quantum simulators*, arXiv:1902.09551.

- Alessio Lerose, Federica Surace, Paolo P. Mazza, Gabriele Perfetto, Mario Collura, Andrea Gambassi, *Slow dynamics by quantum confinement of excitations*, in preparation.

During my PhD I worked also on a project concerning statistical inference on binary data, that are data which can take only two values. This kind of data are usually inferred using spin models with "many-body" interactions. In particular, we focused on the study of the most parsimonious model that can be used to describe a certain data-set according to some complexity measure. The results of this work are summarized in:

- Clelia De Mulatier, Paolo P. Mazza, Matteo Marsili, *Statistical Inference on minimally complex models*, in preparation.

CONTENTS

CHAPTER 1

INTRODUCTION

The investigation of non-equilibrium dynamics and relaxation of physical systems is something of utmost importance in theoretical physics and lies at the core of statistical mechanics. Since the beginning of the modern era of theoretical physics, scientists have been fascinated by the challenge of understanding how the time evolution in systems with many microscopical constituents can display non-trivial *global phenomena*. These phenomena belongs to the realm of the *macroscopic* world and can be studied with effective theories, as for example thermodynamics. However, they depend on an underlying *microscopic* world, sometimes governed by different law of physics, as, happens, for example, for quantum systems. Building a bridge between these two different physical worlds is the main ambition of statistical mechanics, which aims of pursuing this objective by means of fundamental dynamical principles and probability theory. Among the several different global phenomena that could be studied using statistical mechanics, one of the most difficult and profound, is the notion of *thermalization*, which is the relaxation toward a state to which it is possible to associate a temperature. This is the main subject of this thesis. The problem can be stated as follows: let us imagine a system constituted by a large number of microscopic particles, each of which is governed by single-body equations that can be either classical or quantum, depending on the nature of the problem we want to study. The question is, given that in principle we could solve the single particles equations, either exactly or with approximate methods, why one should introduce a statistical description of the problem? Under which circumstances (type of interactions, initial configurations, etc...) does the system display *ergodicity*? In order to try to give an answer to these fundamental questions let us start by briefly reviewing the state of the art from a classical point

of view. Since, ultimately, our interest is in the investigation of the dynamics of quantum systems, a general overview on the problem can not avoid to deal with concepts that include *quantum ergodicity*, *quantum relaxation* arising from unitary dynamics; on these topics will be largely dedicated the next sections and chapters of this work. In our view, however, a brief introduction on classical systems is a good starting point for discussing, in a more familiar framework, some concepts that will be of great importance, rephrased in a proper way, also in the study of quantum systems [1].

1.1 Ergodicity in classical systems

Although the main subject of this thesis is the study of non-equilibrium dynamics, in this section we will briefly recall some notions concerning the equilibrium statistical mechanics in classical systems. A classical physical system formed by f degrees of freedom can be described by using f generalized coordinates $(q_1, q_2, \dots q_f)$ and f conjugate momenta $(p_1, p_2, \dots p_f)$. Using these coordinates it is possible to build $2f$-dimensional space which is called *phase space*. Every point of this space identifies a microscopic state of the system under examination. Given a Hamiltonian $\mathcal{H}(p, q)$, the motion of the systems is determined by the canonical equations of motion:

$$\dot{p}_j = -\frac{\partial \mathcal{H}}{\partial q_j}, \qquad \dot{q}_j = \frac{\partial \mathcal{H}}{\partial p_j}, \tag{1.1}$$

and the time-dependent state of the system is a one-dimensional manifold in the phase space. This trajectory is called the *phase orbit* of the system. For conservative systems this orbit is forced to lie on a surface of constant energy. A stationary configuration is a configuration in which one does not observe changes in the expectation values of any observable, i.e., considering a generic observable A

$$\partial_t A(q(t), p(t)) = 0. \tag{1.2}$$

In the stationary state we have that

$$A(q(t), p(t)) = \langle A \rangle = \lim_{T\to\infty} \frac{1}{T} \int_{\partial S} dt A(q(t), p(t)), \tag{1.3}$$

where the line integral is taken over ∂S the trajectory of the system. The limit $T \to \infty$ should be realistically understood as performing the average over a time window $T_{obs} \gg t_{micro}$ where t_{micro} is the *smallest* microscopic time scale associated with the dynamics of the system. However, although it is fascinating to think about an equilibrium expectation value as the result of the time-average

over the system's trajectory in the phase space, it is not useful for practical purposes. In fact, it is utopian to keep track of the orbit of the system in phase space, because the time scales associated to the dynamical evolution are extremely small. What we mean here is that, although on a global scale the system is kept in a stationary state, which results in the fact that the expectation value of any observable does not change in time, from a microscopic point of view it continues to evolve exploring different microstates in the phase space. For this reason it is fundamental, in order to give some quantitative prediction, to introduce the concept *probability* of microstates. In particular, let us call $\mathcal{M}$ the set of possible microstates of the phase space of a system that are *indistinguishable* under some macroscopic condition (e.g. all they have all the same energy); classically this set $\mathcal{M}$ identifies a subspace of the phase space. The probability of finding the system in one of these different partitions of the phase space $\mathcal{M}$ is given by its volume measured according to some measure $f(p,q)$

$$\Pr(\mathcal{M}) = \int_{\mathcal{M}} f(\boldsymbol{p},\boldsymbol{q}) dq_1 dq_2 \dots dp_1 \dots dp_f, \tag{1.4}$$

this measure is the probability distribution function over the microstates. What we described here is essentially what in physics is called a *statistical ensemble*, that consists of set of accessible microstates and a distribution function. In this context the expectation value of an observable is given by

$$\overline{A} = \frac{1}{\mathcal{N}} \int_{\mathcal{M}} A(\boldsymbol{p},\boldsymbol{q}) f(\boldsymbol{p},\boldsymbol{q}) dq_1 dq_2 \dots dp_1 \dots dp_f, \tag{1.5}$$

where $\mathcal{N}$ is a normalization constant.
One of the most fundamental statistical ensemble is the *microcanonical ensemble* which contains, with equal probability, all the microscopic states of the systems which lie in an energy shell $[E, E+\delta E]$, with $\delta E \ll E$, namely, it describes isolated systems which have the energy as the only conserved quantity. In this case, the measure over the microstates of the ensemble is constant, meaning that all the microstates belonging to $\mathcal{M}(E,\delta E)$ have the *same probability*,

$$f(\boldsymbol{p},\boldsymbol{q}) = \left[\int_{E<\mathcal{H}<E+\delta E} dq_1 dq_2 \dots dq_f dp_1 dp_2 \dots dp_f \right]^{-1}. \tag{1.6}$$

This is the *apriori equal probability* principle [1, 2]. Let us rewrite Eq. (1.5) in another form. Considering the limit $\delta E \to 0$ in shell energy we obtain

$$\Pr(\Delta\sigma) = \int_{\Delta\sigma} f(\boldsymbol{p},\boldsymbol{q}) d\sigma, \qquad (\boldsymbol{p},\boldsymbol{q}) \in \sigma(E), \tag{1.7}$$

with

$$f(\boldsymbol{p},\boldsymbol{q}) d\sigma = \left(\frac{d\sigma}{|\nabla\mathcal{H}|} \right) \Big/ \left(\int_{\mathcal{H}=E} \frac{d\sigma}{|\nabla\mathcal{H}|} \right), \tag{1.8}$$

where $\sigma(E)$ is the surface of states in the phase space with constant energy E and $|\nabla\mathcal{H}| = \sqrt{\sum_i \left[\left(\frac{\partial\mathcal{H}}{\partial p_i}\right)^2 + \left(\frac{\partial\mathcal{H}}{\partial q_i}\right)^2\right]}$.
In this limit we have:

$$\overline{A} = \int_{\mathcal{H}=E} \frac{A(\boldsymbol{q},\boldsymbol{p})d\sigma}{|\nabla\mathcal{H}|} \Big/ \int_{\mathcal{H}=E} \frac{d\sigma}{|\nabla\mathcal{H}|}. \tag{1.9}$$

Having achieved this, we are ready to introduce the main point of this paragraph: is there any difference between the expectation value reported in Eq. (1.3) and the one in Eq. (1.9)?
The answer to this question is provided by the *ergodic theorem* which states that the average $\langle A\rangle$ of an observable A over a long time and the average $\overline{A}$ over the region of all possible microstates in the phase space are equal, i.e.,

$$\lim_{T\to\infty} \frac{1}{T}\int_0^T A(q(t),p(t)) = \int_{\mathcal{H}=E} \frac{A(\boldsymbol{q},\boldsymbol{p})d\sigma}{|\nabla\mathcal{H}|} \Big/ \int_{\mathcal{H}=E} \frac{d\sigma}{|\nabla\mathcal{H}|}. \tag{1.10}$$

The ergodic theorem was formulated as an hypothesis for the first time by Lud-

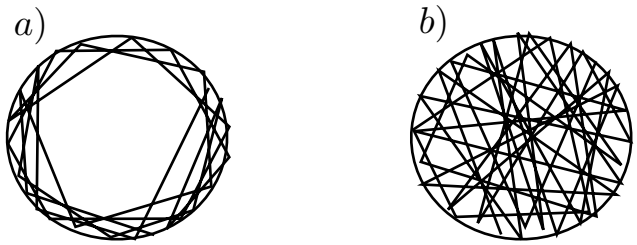

Figure 1.1: Sketch of a non-ergodic trajectory (a) and an ergodic one (b). In the latter case the trajectory covers *almost* the allowed surface of the phase space.

wig Boltzmann [3], who assumed that a phase space trajectory $\boldsymbol{P_t}$ of a system, in the course of time, completely covers a surface of allowed microstates, called ergodic surface, leading to the result of Eq. (1.10) and thus allowing for a statistical description of the equilibrium state of systems. His initial assumption, however, was not rigorously correct because a manifold ∞^1, as the phase trajectory, can not cover a manifold ∞^{2f-1} [1]. Therefore the Boltzmann's hypothesis was replaced by another, less stringent assumption, i.e., the quasi-ergodic hypothesis, stating that the phase trajectory passes through any neighborhood of any point of the ergodic surface, as sketched in Fig. 1.1.
The conjecture has been proved, becoming than a theorem, by the mathematicians Birkoff, von Neumann and Koopman only in the 1930's [4, 5, 6, 7].
The core of the proof is based on the fact that Hamilton equations reported in Eq. (1.1) preserve the volume of the phase space. This result is the well-known

Liouville theorem which states that the volume of an arbitrary subset of phase space is invariant under the transformation induced by the Hamilton equations. In other words, natural motion resembles a flow of an incompressible fluid occurring in a $2f-$dimensional space. The presence of conserved quantities constrains the motion to limited parts of the ergodic surface[1], however, *generic* systems do not have integrals of motion other than energy, angular momentum or linear momentum. Using the notions previously introduced with the Liouville's theorem it is possible to prove the ergodic theorem, however we will not discuss here the details of the proof, that can be found in classic literature of statistical mechanics (see, e.g., Chapter 5 of Ref. [8]).

The scenario discussed so far concerns generic systems; however, there is a special class of systems, which we want to focus on now, that do not follow the ergodic theorem: *integrable systems*. A classical systems with n degrees of freedom, and hence $2n-$dimensional phase space, is said to be integrable if there exist n independent, nontrivial integrals of motion, i.e. if we can find $\mathcal{Q}_1 \dots \mathcal{Q}_n$ quantities and a Hamiltonian $\mathcal{H}$ such that

$$\{\mathcal{H}, \mathcal{Q}_i\} = 0, \qquad \forall i = 1, \dots, n, \tag{1.11}$$

where the Poisson's bracket between two quantities $f(q_i, p_i)$ and $g(q_i, p_i)$ is defined as

$$\{f, p\} = \sum_{i=1}^{N} \frac{\partial f}{\partial q_i}\frac{\partial g}{\partial p_i} - \frac{\partial f}{\partial p_i}\frac{\partial g}{\partial q_i}. \tag{1.12}$$

Integrable systems rarely describe actual physical systems, but they are important because they are exactly solvable and, in addition, many real physical systems (e.g., planetary systems) can be described as suitable perturbations of integrable systems [9]. A remarkable aspect about integrable systems is reported in the Liouville-Arnold theorem [10], which states that a system with independent and commuting, meaning that they have mutually zero Poisson's bracket, integrals of motion (charges) satisfies the following properties:

- the phase space is partitioned into "level sets"

$$\mathcal{M}_q = \{\xi : \mathcal{Q}_i(\xi) = q_i, i = 1 \dots n\}, \tag{1.13}$$

  each of which is invariant under the flow generated by the time evolution.

- For a given value of the charges $q = (q_1, \dots, q_m)$, $\mathcal{M}_q$ is *diffeomorphic* to $T^m \times \mathbb{R}^{m-n}$, where T^m is a $m-$dimensional torus. This means that the phase space is divided in charge sectors.

[1] This argument will be treated in detail in the next sections, here we give just a small anticipation

- Assume that $m = n$, in this case $\mathcal{M}_q$ is diffeomorphic to a $n-$torus. Accordingly, it is possible to introduce a set of new variables in terms of which the motion on every torus is simpler. These new coordinates are called *action - angle variables* $J_1 \dots J_n$, $\theta_1 \dots \theta_n$ and evolve in time as

$$J_k(t) = J_k(0), \qquad \theta_k(t) = \omega_k(J)t + \theta_k(0), \qquad \omega_k(J) = \frac{\partial H}{\partial J_k}. \tag{1.14}$$

- Given an initial point $\xi(0)$ on $\mathcal{M}_q$, the time evolved trajectory point $\xi(t)$ is a multi-periodic function of the angles $\theta_1 \dots \theta_n$ which can be obtained by quadratures.

What this theorem is telling us is that for integrable systems the constraint induced by the conservation of charges affects the motion by dividing the phase-space in invariant $n-$tori depending on their initial value. It should now be clear why these systems are *nonergodic*: the phase-space can not be fully explored by the time-dependent trajectory. However, it interesting to analyze what happens if we restrict on one of these tori. Indeed, in this case, the dynamics reduces to a rotation on the torus and it can be decomposed into that of n independent one-dimensional harmonic oscillators. Note however, that the analogy is not completely correct, because the corresponding frequencies may depend in a highly nontrivial way on the action coordinates $J_1 \dots J_n$.
There can be two different scenarios, if the rotational frequencies are *incommensurable*, $\frac{\omega_m}{\omega_n} = k$ with k irrational, the trajectory on the torus will densely cover it, and with some abuse of language, we could say that the system is *ergodic on each torus*. In this case the equilibrium properties are effectively described in a probabilistic framework by means of the so-called *generalized Gibbs ensemble* (GGE):

$$\rho_{GGE} = \frac{\mathrm{e}^{-\sum_k \beta_k \mathcal{Q}_k}}{Z}, \tag{1.15}$$

where $\mathcal{Q}_k$ are the conserved charges. In fact, such a generalized Gibbs ensemble is constructed by taking into account, with proper Lagrange multipliers β_k, the constraint induced by the initial values of the conserved charges. The $k = 0$ charge is, usually, the energy itself. If there is only one conserved charge, the GGE reduces to the usual Gibbs ensemble and the system is ergodic. The functional form of the probability distribution is found by maximizing the entropy, this means, by finding the *less biased* distribution according to our knowledge of the system [11]. We will return on this topic in next section.
The other possible scenario occurs when the ratio between the oscillation frequencies is rational, $\frac{\omega_m}{\omega_n} = k$ with $k \in \mathbb{Q}$. In this case, after a finite number of oscillations, the trajectory comes back to its initial point and the motion is

periodic on the torus, resulting in the impossibility of using the ergodic theorem to describe the equilibrium properties of the system. These systems, as we discussed, are extremely "fine-tuned" , however the existence of these two scenarios is extremely important because when we perturb an integrable system the tori on which the motion is periodic (see Fig. 1.2) are destroyed by the perturbation, while the "ergodic tori", the ones fully covered by the trajectories, survive and affect the motion with quasi-periodic trajectories that induce long *prethermal phases*. This is the main result of the famous Kolmogorov-Arnold-Moser (KAM)

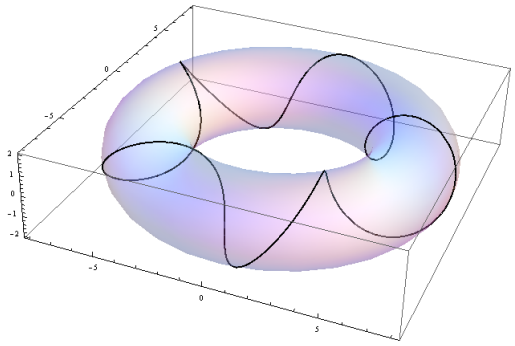

Figure 1.2: Sketch of a non-ergodic trajectory on a torus. The curve wraps several times but it returns periodically in its original position and the torus is not densely covered.

theorem [12, 13, 14]. In the next paragraph we introduce briefly the topic of quasi-integrable systems by discussing one of its most prominent examples, the Fermi-Pasta-Ulam -Tsingou problem[2]. [16, 17, 18].

Fermi, Pasta, Ulam and Tsingou decided, in 1953, to study the thermalization process in a solid. This work is considered pioneering for two reasons: on the one hand they found an apparent paradox concerning the relaxation properties of a classical many-body system opening the era of an intensive study of nonlinear physics. On the other, it is the first work in which there is a large use of computer simulations to inspect the dynamics of a statistical system. For this purpose it was used the computer *MANIAC*, which can be considered the first machine able to perform such calculations, it was settled in the Los Alamos Laboratories (USA). The main contribution of W. Tsingou was to write codes for this computer, a task that was not trivial in the 50's.

The idea of Fermi was to simulate the thermalization that occurs in solids using a model of N particles coupled by springs that follow Hooke's law but with a small nonlinear interaction term. This *anharmonicity*, in his mind, would have driven the system to equipartition of the energy among the oscillation modes (thus respecting ergodicity) starting from an initial state with only one mode populated.

[2] See Ref. [15] for an explaination of the long-unknown role of the female scientistW. Tsingou

To be more concrete, the Hamiltonian describing the system is:

$$\mathcal{H} = \sum_{i=0}^{N} \frac{p_i^2}{2m} + \sum_{i=1}^{N} \frac{1}{2}(r_{i+1} - r_i)^2 + \sum_{i=1}^{N} \frac{\alpha}{3}(r_{i+1} - r_i)^3 + \sum_{i=1}^{N} \frac{\beta}{4}(r_{i+1} - r_i)^4, \quad (1.16)$$

with N the number of particles, r_i their position, $\alpha, \beta > 0$. The terms proportional to α and β are the non-linearities that should be responsible for the thermalization of the system. It was, indeed widely known that a system $\alpha = \beta = 0$, would have not thermalized. It was observed that, after a transient phase in which all the modes of the oscillators ($k = 1, 2, \dots$) were equally populated obeying then equipartion of energy, the system returned to its initial configuration with almost all the energy in the initially populated mode. Therefore contrary to what it was expected, the system did not show thermalization. This problem puzzled physicists for decades and there were some attempt to link this peculiar behavior to the KAM theory, but this explanation was soon found to be unsatisfactory. The solution to this paradox requires to take into account the existence of localized excitations responsible for the drifting away from thermalization of the system; these localized excitations were named *solitons*.

Another interesting aspect of this problem is that the relaxation process can be connected to the classical Toda model, that is an integrable model. In particular, it is possible to see that, at short times, the state of the FPU chain is completely determined by ergodic Toda tori that are not "destroyed" by the perturbation. This fact thus enable a *transient* statistical description of the state in terms of a GGE (see Ref. [19] and references therein for details). We will not further treat this problem here because it is not the main topic of this thesis and especially because it would be impossible to give an exhaustive description of it in a few lines. We, however, considered interesting to touch on this argument in order to show how also the dynamics of very simple classical systems could be not yet fully understood and how it is still stimulating the interest of a large part of the statistical physics community.

To summarize this section, we have seen how from a classical point of view generic systems, with no extensive number of conserved charges, are ergodic. Integrable systems, instead, are non-ergodic, although, for the majority of them, a statistical description of the equilibrium state is still possible using the GGE. Quasi-integrable systems presents peculiar and highly nontrivial relaxation properties: the dynamics on short time-scales (compared to the inverse strength of non-integrable perturbation) display prethermal phases characterized by fictitious relaxation to a non-ergodic phase.

Some of these results have been obtained by studying the behavior of trajectories in the phase space. From a quantum point of view this approach does not

work, because it is not possible to introduce a phase space, due to the uncertainty principle, in the next section we will see how to deal with this problem.

1.2 Relaxation in quantum systems

In this section we introduce the main topic of this thesis: relaxation in quantum systems. By relaxation we mean the approach to equilibrium after a perturbation to the systems that took it in a non-equilibrium configuration. This equilibrium state can be either *thermal* (or chaotic, we will often use this term as synonyms here), meaning that it is possible to associate a temperature to the final state, or not, in the latter case we will talk about *ergodicity breaking*. As we have already stated in the previous section, for quantum systems the situation is a bit more involved compared to the classical case. This topic has stimulated the interest of physicists since the early days of quantum mechanics [20]. However, thanks to an incredible advance in this field occurred in the last fifteen years it is now possible to construct extremely controlled quantum systems which keep their coherence sufficiently long to observe, in actual experiments, time-evolution and relaxation. The impossibility to extend classical results concerning ergodicity to quantum systems does not mean that we can not use a statistical approach for describing the equilibrium properties in many-body quantum systems. It is possible to introduce the notion of Gibbs *ensemble* also in this case by means of the density matrix representation of quantum states, let us briefly review some basic notions about quantum statistical mechanics [1]. The representation of quantum states in terms of density matrix is particularly suitable when we deal with systems in which there is a lack of information that does not permit the construction of the entire system's wave function, namely, when we have *mixed* quantum states, that are an incoherent superposition of pure states [21]. Averaging over a mixed state in order to compute the expectation value of a generic observable A, has, in this case, a twofold nature. It considers both the average over the intrinsic probabilities of the quantum mechanical description and the average over the statistics of the mixture. Also pure systems can be described using density matrix representation, in this case only quantum fluctuations are taken into account. Before proceeding let us understand under which hypotheses the characterization of a thermal quantum state through the *ensembles* technique makes sense.

Let us consider a quantum system described by a Hamiltonian H and let us consider an initial state described by the wave-function $|\Psi(0)\rangle$ that is not an eigenstate of H. The $|\Psi(0\rangle)$ can be decomposed in terms of the eigenfunctions

$|\varphi_n\rangle$ of H:

$$|\Psi(0)\rangle = \sum_n c_n |\varphi_n\rangle. \tag{1.17}$$

The time evolved state is:

$$|\Psi(t)\rangle = \sum_n \mathrm{e}^{-iE_n/\hbar} c_n |\varphi_n\rangle \tag{1.18}$$

If we consider a certain observable A, its expectation value at time t is:

$$\langle\Psi(t)|A|\Psi(t)\rangle = \sum_{n,m} c_m^*(t) c_n(t) \langle\varphi_m|A|\varphi_n\rangle, \tag{1.19}$$

where $c_n(t) = \mathrm{e}^{-iE_n/\hbar t} c_n$.
In a system in thermal contact with a bath we can divide the Hilbert space as $S \otimes E$, where S is the system under investigation and E is the environment. The wave-function of this larger world can still be written as

$$|\Psi\rangle = \sum_j c_{j,E} |\phi\rangle_S, \tag{1.20}$$

however in this case the coefficients c_j's are elements of the environment E. If we consider an observable acting on the original system only: $\mathbb{1}_E \otimes O_S$, we have that its expectation value can be written as

$$\langle\Psi(t)\mathbb{1}_E \otimes O_S \Psi(t)\rangle = \sum_{m,n} \langle c_m(t) c_n(t)\rangle_E \langle\phi_m|O\phi_n\rangle_S. \tag{1.21}$$

In an actual measure what is detected is the average over a time that is large with respect to the molecular time scale, therefore we measure

$$\langle O\rangle = \sum_{m,n} \overline{\langle c_m(t) c_n(t)\rangle_E} \langle\phi_m|O\phi_n\rangle_S \tag{1.22}$$

usually, extremely difficult to describe exactly the interaction between the environment the the system we are studying. It is therefore postulated that, in this case:

$$\overline{c_m(t)^* c_n(t)} = |c_n|^2 \delta_{n,m}. \tag{1.23}$$

In statistical physics this postulate is known as *random phases postulate*, and states that a quantum subsystem in thermal equilibrium with a bath is an *incoherent superposition* of the eigenstates of the Hamiltonian H of the system. The physical meaning of this postulate is that the interaction between the system and the bath cancels all the quantum interferences among the states during the measure procedures. This is what is usually referred as a "statistical mixture". Under the assumption of the random phases postulate the value of a certain observable can be written as:

$$\langle A\rangle = \mathrm{Tr}(\rho A), \tag{1.24}$$

where $\rho = \sum_n |c_n|^2 |\phi\rangle\langle\phi_n|$ is the density matrix of the mixed state.
Let us consider a simple example that will clarify a bit why the random phases postulate is physically reasonable. Let us take a system S with two eigenstates ($|1\rangle_S$ and $|2\rangle_S$) in thermal equilibrium with an environment E that is in the state $|E\rangle_0$, and let us suppose that the environment E is much bigger than the system. The initial state $|\phi_0\rangle_{S+E}$ of the composed system $S+E$ is generically described by the wave function:

$$|\phi_0\rangle_{S+E} = (\alpha|1\rangle + \beta|2\rangle) \otimes |E\rangle_0 = \alpha|1, E_0\rangle_{S+E} + \beta|2, E_0\rangle_{S+E}. \tag{1.25}$$

If we suppose to have a weak interaction H_{in} between the environment and the system of the type:

$$H_{in} = C_1|1\rangle\langle 1| \otimes V + C_2|2\rangle\langle 2| \otimes V,$$

where V is the Hamiltonian of the environment, after a time interval t the state will evolve in

$$|\phi_t\rangle_{S+E} = \alpha|1, E_t^{(1)}\rangle_{S+E} + \beta|2, E_t^{(2)}\rangle_{S+E}, \tag{1.26}$$

in which $|E_t^{(1/2)}\rangle$ are the states of the environment which evolves due to the interaction with the system. The density matrix of the system S is

$$\rho_S = \rho_{11}|1\rangle\langle 1| + \rho_{12}|1\rangle\langle 2| + \rho_{12}^*|2\rangle\langle 1| + \rho_{22}|2\rangle\langle 2|, \tag{1.27}$$

the matrix elements can be calculated by using the definition of the reduced density matrix $\rho_S = \text{Tr}_E[|\phi_t\rangle_{S+E}\langle\phi_t|]$:

$$\begin{cases} \rho_{11} = |\alpha|^2, \\ \rho_{22} = |\beta|^2, \\ \rho_{12} = \alpha^*\beta\langle E_t^{(1)}|E_t^{(2)}\rangle. \end{cases} \tag{1.28}$$

At this point we can make some observations. The environment has a lot of degrees of freedom, by hypothesis it is much larger than the system S. It is reasonable to assume that the states of the system are randomly coupled with the states of the environment, this results in the fact that $\langle E_t^{(1)}|E_t^{(2)}\rangle \ll 1$, which means that ρ_{12} can be neglected compared to ρ_{11} and ρ_{22} and the reduced density matrix ρ_s is practically diagonal. This argument can be extended to systems with more than two degrees of freedom.
What we have stated so far holds rigorously for systems coupled to a bath in the thermodynamic limit, however we are interested in the study of *isolated* quantum systems for which the situation is a bit different. If a system is prepared in a pure state:

$$\rho_{in} = |\Psi(0)\rangle\langle\Psi(0)|, \tag{1.29}$$

the unitary time evolution

$$|\Psi(t)\rangle = \mathrm{e}^{-\frac{iHt}{\hbar}}|\Psi(0)\rangle, \tag{1.30}$$

due to the Schrödinger equation will maintain it in a pure state all times. Accordingly, in order to adapt the argument previously introduced for systems coupled to a bath with many degreees of freedom, we have have to introduce some additional notions, first of all the concept of *locality*. An observable O is said to be local if depends on a limited portion of the system, i.e., $O(x_i, x_{i+1}, x_{i+2})$, with x_j spatial coordinates. The actual mechanism behind thermalization in isolated quantum systems will be defined properly in the section concerning the eigenstate thermalization hypothesis (ETH), however, let us specify here precisely the meaning of relaxation in isolated systems. Let us consider a quantum system,

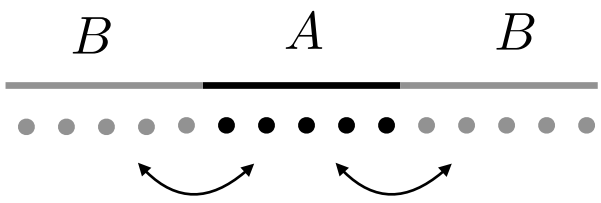

Figure 1.3: Interaction between subsystems in an isolated quantum system

and let us divide it in two parts, A and B, as in Fig. 1.3. Let us imagine to concentrate on the subsystem A. In this case we can describe our subsystem integrating out the degrees of freedom of the rest

$$\rho_A = \mathrm{Tr}_B|\Psi_{A+B}\rangle\langle\Psi_{A+B}|. \tag{1.31}$$

The obtained ρ_A is a statistical mixture, in this case we can say that the system acts as its own bath. In studying the dynamics, however, we have to pay attention to the proper definition of *infinite time* limit. In fact if we consider a finite subsystem of a finite system and we take naively the limit $t \to \infty$ for the time-dependent expectation value of a local observable, $O_x(t)$ with $x \in A$, i.e.

$$\lim_{t\to\infty}\langle O_x(t)\rangle, \tag{1.32}$$

we will observe quantum revivals, that are periodic restoring of the initial conditions, as long as the dynamics is unitary. In order to see a non-trivial approach to an equilibrium state we must pay attention in a proper re-scaling of the time with the *size* L of the system. To be more precise, we have to consider the thermodynamic limit for the system *before* considering the infinite time limit. The

correct order of the limits is, accordingly

$$\lim_{t\to\infty}\lim_{L\to\infty}\langle O_x(t)\rangle, \tag{1.33}$$

where L is a typical length scale of the system, the two limits do not commute. Therefore we can say that our system relaxes *locally* if

$$\lim_{t\to\infty}\lim_{L\to\infty}\rho_A(t)=\rho_A(\infty), \tag{1.34}$$

exists for any subsystem A. This is a definition of relaxation in an isolated quantum system, we stress, again that a system is said to be thermal if it is possible to associate a temperature T to the equilibrium state $\rho_A(\infty)$. In order to study the approach to equilibrium and to understand under which conditions (spatial dimensionality, interactions, conserved quantities...) a quantum systems thermalizes we have to keep track of the time evolution of local observables in purely non-equilibrium processes.

Taking a system out of equilibrium means that we evolve it with a Hamiltonian of which the initial state describing our system is not an eigenstate [22]. There are many ways for driving a quantum system out of equilibrium: considering a quantum system in an eigenstate of H_{sys}, it is possible to add a time-dependent potential $H_{sys}+V(t)$ that periodically drives the system out of equilibrium, i.e. $V(t+T)=V(t)$. Another possibility is to consider a potential $V(t)$ which acts as a ramp, meaning that it perturbs the system for a given finite time window. The protocol in which we are interested in is the so-called quantum quench. A quantum quench is an abrupt change of a parameter λ of the Hamiltonian $H(\lambda)$ that describes our system. By "abrupt" we mean that the change of the parameter λ from the initial value λ_0 to a final one λ_f should be done in a time δt that is smaller than the smallest time-scale τ of the system, that usually coincide with the largest difference among two contiguous energy levels $\tau^{-1}=E_{l+1}-E_l$, in proper units. In discussing approach to equilibrium we will focus mainly on one-dimensional quantum systems for the following reasons: one dimensional quantum systems are experimentally realized in many contexts, e.g., cold atoms quantum simulators, quantum wires, quantum carbon nano-tubes and also higher dimensional quantum magnets with particular symmetries [23]. Secondly, they are simpler to treat with respect higher-dimensional quantum systems from the numerical point of view because of the lower dimensionality of the Hilbert space and the smaller entanglement entropy growth. Furthermore one dimensional systems presents highly non-trivial aspects. As we will see in the next section, for example, it is possible to have strongly interacting models that can be exactly solved and presents an extensive number of non-trivial conserved quantities, this last aspect is crucial in the discussion about approach to equilibrium, as we have seen in the

classical case. Accordingly, the study of non-equilibrium one-dimensional quantum systems is extremely interesting, especially in view of the fact that exactly solvable higher-dimensional systems are essentially free models [24] with trivial conserved quantities that relax towards Gibbs thermal ensembles.

1.2.1 Integrable systems

One-dimensional quantum integrable models are *fine-tuned* models which present peculiar and extremely interesting properties of the equilibrium state reached after a quantum quench. By *fine-tuned* we mean that these systems are extremely sensitive to external perturbations; given an integrable Hamiltonian $H_{int} = \sum_j g^j O_j$, with j spatial indices (which we will consider discrete as we will mainly focus on lattice models) and O_j local operators, if we *perturb* our system with *non-integrable* operators $H = H_{int} + \sum_s g_s O_s$ the integrability (and all the characteristics of the equilibrium state that ensue) is destroyed. The theoretical interest in these models has raised again only recently, in fact it is now possible to construct highly controlled quantum setups that mimic extremely well these systems by reducing as much as possible the breaking of integrability due to noise and experimental imperfections, making it possible to probe the fascinating relaxation properties. In the last section of this chapter we will show some examples of experimental implementations. In this section, we will closely follow what is reported in a very nice collection of reviews [25] about this topic that summarizes the last ten years of intense theoretical effort. In particular, we will focus on the reviews concerning the role of local charges in equilibrium properties of one-dimensional spin chains and the construction of the generalized Gibbs ensemble (GGE) [26, 27].

There are different ways of defining a quantum integrable system, but none of the possible definitions is rigorous. A suitable working definition of quantum integrability can be done starting from the classical case discussed earlier. We can assert that a quantum system is integrable if one can find an *infinite* set of *local* (or *quasi-local*) integrals of motion. Let us note that this definition resembles the classical one upon the substitution of the Poisson bracket with the commutators

$$\{,\} \to \frac{i}{\hbar}[,]. \tag{1.35}$$

We therefore obtain the following definition: a one-dimensional quantum system in thermodynamic limit is integrable if there exists an infinite set $\{I_m\}$ of local operators such that

$$[H, I_m] = 0 \qquad \text{and} \qquad [I_m, I_n] = 0, \qquad \forall m, n. \tag{1.36}$$

By *local* we mean that $I_m = \sum_j \mathcal{I}_j$ where j is a spatial index running on the lattice sites and $\mathcal{I}_j$ are densities involving only a *finite* number of sites, e.g. $\mathcal{I}_j = O^{j-1,j,j+1}$. The role of quasi-local operators, i.e. operators whose density decades exponentially in space is discussed in Ref. [28]. The request of locality or quasi-locality of the integrals of motion is of fundamental importance. In fact, in a quantum system it is always possible to find an infinite set of mutually commuting conserved charges. For example, if we consider the projectors P_k on the eigenstates $|k\rangle$, i.e.,

$$P_k = |k\rangle\langle k| \tag{1.37}$$

they fulfill these conditions. Without requesting locality it would turn out that every quantum system is integrable, which is clearly not the case. It could seem artificial to impose the locality of the integral of motion but actually this request is very profound. In fact, as we stated in the previous section, an isolated quantum system relaxes *locally* and behaves as a mixed state only when the degrees of freedom external to the subsystem A of interest are integrated out (see Fig. 1.3). Accordingly, it is reasonable to concentrate on local conserved charges since we want to inspect the local properties of the system. As we have pointed out earlier, in a system which has only the energy E as conserved quantity,

$$E = \mathrm{Tr}(\rho(t)H) = \mathrm{Tr}(\rho(0)H), \tag{1.38}$$

the equilibrium state is described locally by an ordinary Gibbs ensemble

$$\rho_{loc} = \rho^{\mathrm{Gibbs}} = \frac{\mathrm{e}^{-\beta_{\mathrm{eff}}H}}{\mathrm{Tr}(\mathrm{e}^{-\beta_{\mathrm{eff}}H})}, \tag{1.39}$$

in which the effective temperature β_{eff} is fixed by the initial energy density

$$e = \lim_{L\to\infty} \frac{1}{L}\mathrm{Tr}(\rho(0)H) = \frac{1}{L}\mathrm{Tr}(\rho^{\mathrm{Gibbs}}H). \tag{1.40}$$

In case we have an extensive set of local conserved charges, as in Eq. (1.36) we have to consider the fact that the presence of integrals of motion influence the non-equilibrium dynamics of the system after a quantum quench. In fact, the constraint imposed by the conservation laws:

$$\langle\Psi(t)|I_m|\Psi(t)\rangle = \text{const.} \qquad \forall m, \tag{1.41}$$

restricts the dynamics on a fixed sector of the Hilbert space where the operators have a given expectation value. Accordingly the equilibrium state can not be longer described by a simple Gibbs ensemble, but we have to introduce a generalized Gibbs ensemble (GGE) wihch takes into account the charges' sector in which we are. The generalized Gibbs ensemble can be constructed, as we have already

outlined in the previous section, using the maximum entropy principle [11]. The GGE distribution can be therefore written as

$$\rho^{\mathrm{GGE}} = \frac{\mathrm{e}^{-\sum_n \lambda_n I_n}}{\mathrm{Tr}(\mathrm{e}^{-\sum_n \lambda_n I_n})}, \tag{1.42}$$

in which the I_n are the local integrals of motion whose initial values fix the Lagrange's multipliers λ_n, as it happens for the temperature in the case of the Gibbs distributions. Let us show a concrete example of generalized Gibbs ensemble: for this purpose we consider the prototypical transverse field Ising chain (TFIC) with Hamiltonian

$$H(h) = -J \sum_{j=1}^{L} \left(\sigma_j^x \sigma_{j+1}^x + h \sigma_j^z \right), \tag{1.43}$$

where σ_j^α are the usual Pauli's matrices on site j. This model, as the others that we will consider in this thesis, is short ranged. Hamiltonian (1.43) is an example of integrable model and it is exactly solvable in terms of free fermions [29], accordingly, in the thermodynamic limit $L \to \infty$, it has infinitely many conserved charges [30],

$$I^{(1,+)} = H(h) \tag{1.44}$$

$$I^{(n,+)} = -J \sum_j \left[(S^{xx}_{j,j+n} + S^{yy}_{j,j+n-2}) + h(S^{xx}_{j,j+n-1} + S^{yy}_{j,j+n-1}) \right] \equiv \sum_j \mathcal{I}_j^{(n,+)} \tag{1.45}$$

$$I^{(n,-)} = -J \sum_j (S^{xy}_{j,j+n} - S^{yx}_{j,j+n}) \equiv \sum_j \mathcal{I}_j^{(n,-)}, \tag{1.46}$$

where $S^{\alpha,\beta}_{j,j+l} = \sigma_j^\alpha \left[\prod_{k=1}^{l-1} \sigma_{j+k}^z \right] \sigma_{j+l}^\beta$ and $S^{yy}_{j,j} = -\sigma_j^z$. A remarkable aspect of free theories, as the TFIC once we have written (1.43) in terms of Jordan-Wigner [31] fermions, is that the GGE can be cast, equivalently, in terms of mode occupation number [32]. In fact, following [26], let us consider a tight-binding fermionic model

$$H = -J \sum_j c_j^\dagger c_{j+1} + \mathrm{h.c.} - \mu \sum_j c_j^\dagger c_j \qquad \{c_i^\dagger, c_j\} = \delta_{i,j}, \tag{1.47}$$

where the c_j are zero-spin fermionic operators. Moving to Fourier space the Hamiltonian can be written as

$$H = \sum_k [-2J \cos k - \mu_k] c^\dagger(k) c(k). \tag{1.48}$$

It is easy to find for such Hamiltonian a set of mutually commuting conserved charges, e.g., the occupation number $n(k) = c^\dagger(k)c(k)$ of the modes. However, these charges are not local and therefore, apparently, these conserved operators

are not proper for building the GGE. A suitable set of charges for this purpose, in this case, is:

$$I^{(n,+)} = 2J \sum_k \cos(nk) c^\dagger(k) c(k) = J \sum_j c_j^\dagger c_{j+n} + \text{h.c.}, \tag{1.49}$$

$$I^{(n,-)} = \mathrm{i}2J \sum_k \sin(nk) c^\dagger(k) c(k) = \mathrm{i}J \sum_j c_j^\dagger c_{j+n} - \text{h.c.}. \tag{1.50}$$

Nevertheless it is possible to show that these integrals of motion $I^{(\pm)}$ can be written as a linear combination of the mode occupation number $n(k)$. It is for these reason that the generalized Gibbs ensemble for free theories can be, in general, cast in the form

$$\rho^{\text{GGE}} = \frac{\mathrm{e}^{-\sum_k \mu_k n_k}}{\mathrm{Tr}(\mathrm{e}^{-\sum_k \mu_k n_k})}. \tag{1.51}$$

It is important to emphasize the fact that the generalized Gibbs ensemble is profoundly different from a thermal Gibbs ensemble: the existence of an infinite number of conserved charges makes it possible for the quantum state to retain an infinite amount of memory of its initial conditions. Accordingly, the equilibrium states described by the GGE are extremely different from the ones predicted by a thermal ensemble. In order to show this aspect let us show an example [32] considering a Hamiltonian of *hard-core* bosons:

$$H = -J \sum_j b_j^\dagger b_{j+1} + \text{h.c.} + \sum_j V_j b_j^\dagger b_j. \tag{1.52}$$

"Hard core" means that they behave as fermions, i.e., they cannot occupy the same quantum state, but they do not have exchange antisymmetry. This Hamiltonian can be straightforwardly diagonalized using a Jordan-Wigner transformation and therefore it is equivalent to a free fermionic one. An important aspect of this model is that is easily realized experimentally using cold atoms. Let us consider, for the model in Eq. (1.52), a non-homogeneous initial state and let it evolve for a given period of time, until we observe a relaxation towards an equilibrium state. A particularly interesting observable is $m_k(t) = \langle \Psi(t)|m_k|\Psi(t)\rangle$, the time-dependent momentum occupation number, where $m(k) = b_k^\dagger b_k$. This observable is particularly suitable also for experimental purposes. In Fig. 1.4, it is reported the time-evolution of $m(k)$ after a quantum quench and its equilibrium value; this is compared with the expectation value given by Gibbs ensemble and by the generalized Gibbs ensemble. As it is possible to observe, after non-equilibrium dynamics the modes occupation number relax on a steady state that is perfectly described by a GGE and it is different from the values predicted by the Gibbs ensemble. In particular, in the middle panel it is possible to compare the steady

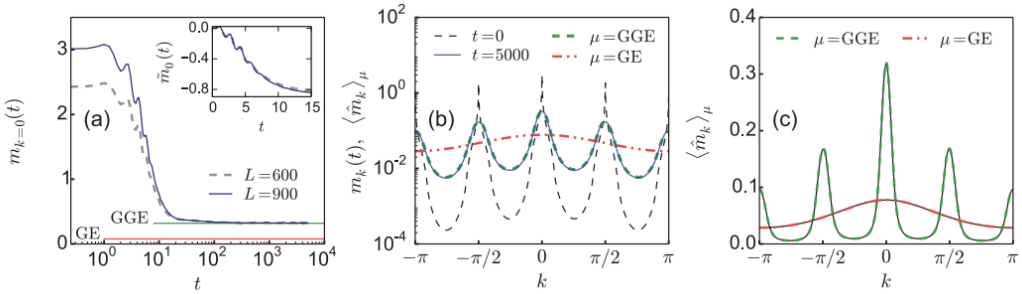

Figure 1.4: Fig. from Reference [32]. Comparison between the dynamical expectation value of m_k and the equilibrium states predicted by a generalized Gibbs ensemble (GGE) and a thermal Gibbs ensemble (GE).

state with the initial state, the peaks in the momenta persist also in the infinite-time limit as a consequence of the conservation of the integrals of motion.

The presence of conserved charges in integrable systems divides the Hilbert space in different sectors which are dynamically disconnected among each other. Such mechanism resembles, *mutatis mutandis*, the division of the phase-space in invariant tori that occurs in classical systems. This partition of the Hilbert space in sectors does not only influence the dynamics of local observables, as we have seen, but it has effects also on the *spectral properties* of the system, affecting the distribution of the energy levels. For a generic thermal systems in the thermodynamic limit we expect the Hamiltonian to be close to *random matrix*[3] that takes into account the symmetries of the system [33]. Eugene Wigner [34, 35, 36, 37], studying the spectrum of nuclei with finite Hilbert space, was the first who proposed the connection between the local statistical behavior of the energetic levels of nuclei in a "simple sequence"[4] and the eigenvalues of a random matrix. A statistical theory of the energy levels is not supposed to predict in detail their structure in any physical system, but instead it is expected to describe their general distribution. It can be shown that for generic chaotic systems the statistics of the energy levels follow the so-called *Wigner-law* typical of random matrices belonging to the Gaussian Orthogonal Ensemble (GOE) [38]. To be more precise, given $s_l = (E_{l+1} - E_l)/\Delta E_{avg}$, the separation between two contiguous energy levels normalized, with ΔE_{avg} the average distance of energy levels, in the system we have, for chaotic[5] systems, that

$$P(s) = \frac{1}{2}\pi s \mathrm{e}^{-\frac{1}{4}\pi s^2}. \tag{1.53}$$

[3]The connection between ergodic Hamiltonians and random matrices will be discussed more precisely in the section of this chapter concerning eigenstate thermalization hypothesis.

[4]A simple sequence is one whose levels all have the same spin, parity, and other strictly conserved quantities

[5]In this section we will refer often to ergodic systems as *chaotic*.

Let us note that in this case we observe *level repulsion*, i.e., $P(s) \to 0$ as $s \to 0$. For an integrable system, instead, the level statistics is generically described by a Poisson law, as conjectured by Berry and Tabor [39]:

$$P(s) = \mathrm{e}^{-s}. \tag{1.54}$$

This fact can be understood with the following intuitive argument [40]: in an integrable system the eigenstates are labelled by an infinite set of quantum numbers, it is therefore highly probable that states with different quantum numbers have the same energy, giving a Poisson distribution. In chaotic systems, instead, we have level repulsion because the Hilbert space is not partioned in different sectors according to the initial value of the conserved charges. In Fig. 1.5 we report the two distribution in order to highlight the different behavior. An important

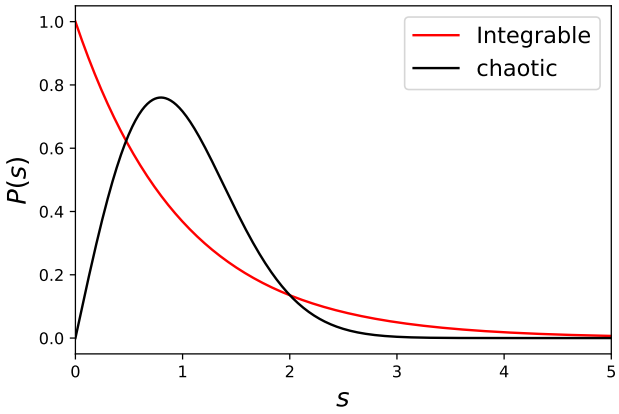

Figure 1.5: Level statistics for an integrable and a chaotic system, the behavior in the proximity of $s = 0$ is what maximally distinguish the two cases i.e. level attraction vs. level repulsion.

parameter that can be introduced in order to distinguish between the two cases, i.e. Poisson distribution or Wigner-Dyson, is the *r-factor* [41] that is defined as

$$\tilde{r}_n = \frac{\min(s_n, s_{n-1})}{\max(s_n, s_{n-1})} \tag{1.55}$$

where s_n has been previously defined as the normalized difference among the ordered energy levels. This quantity has the advantage that it allows a more transparent comparison with experiments compared to the traditional level spacing distribution. It can be shown by studying the distribution of the r for different types of spectra [42] that for Poissonian level statistics the average value is $\langle r \rangle = 2 \ln 2 - 1 \approx 0.38629$, while for Wigner-Dyson statistics one has $\langle r \rangle = 4 - 2\sqrt{3} \approx 0.53590$.

1.2.2 Transport in quantum systems

One of the main topics concerning the study of quantum systems out-of-equilibrium is the *transport* of physical quantities [43]. In order to understand how the system behaves in non-equilibrium configurations, the study of the transport of physical quantities plays, in fact, a privileged role. In order to understand the reason of that, let us take a step back; one could think of relaxation in non-equilibrium dynamics following a quantum quench in terms of *spreading* of quasi-particles excitations generated by the energy pumped in the system. These quasi-particles travel in the system and correlate different parts of it eventually leading to smoothing the initial inhomogeneities [44]. Transport of physical quantities and relaxation toward an equilibrium state are two connected phenomena. The quasi-particle generated in a quantum quench can spread also measurable quantities across different parts of the system (e.g. energy, magnetization), however, they are not the same thing. In fact, in order to observe transport we must consider always *inhomogeneous* initial states. The quasi-particles responsible for the relaxation in non-equilibrium process are generated also when we consider a *homogeneous* initial states. In order to show how transport can occur in quantum systems let us outline two prototypical examples [43]. Let us consider a free system (as for example the TFIC) which is initialized in a state with two disconnected reservoirs at different temperature and chemical potential that are connected at $t = 0$. This

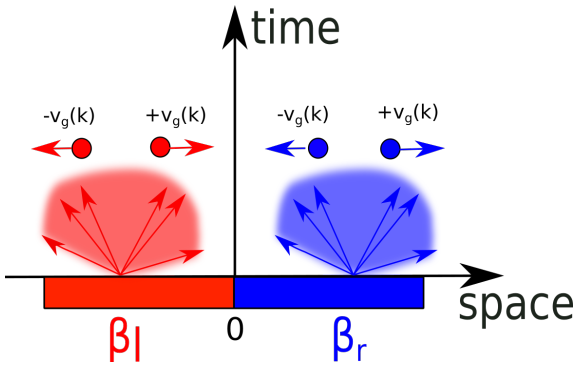

Figure 1.6: Initial setup in a prototypical inhomogeneous quench. We have two disconnected reservoirs at different temperature that are connected at $t = 0$, for $t > 0$ the quasi-particles spread across the system.

.

process is called inhomogeneous local quench, each part of the system is a source of quasi-particles which will travel across it, as reported in Fig. 1.6. For $t > 0$ there will be quasi-particles from the right part of the system that will move to the left (left-movers) and particles arising from the left part of the system that

will move to the right (right-movers). Accordingly as time increases, there is a larger and larger central region, opening as a *light-cone* (see Fig. 1.7) over which the local state of system can be described as having a distribution of left-movers equivalent to the distribution of right-movers. In order to characterize quantita-

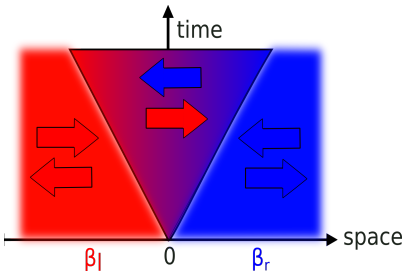

Figure 1.7: Cartoon of the time evolution in a typical free theory, the quasi-particles do not interact this causes a light-cone opening of the non-equilibrium steady stated zone in the middle

.

tively the transport let us consider the example of a one-dimensional free system at criticality which can be described by a *conformal field theory*. In this case, it can be demonstrated that the late-time energy current in the central region is

$$J_{t\to\infty}(E) = \frac{\pi c k_B^2}{12\hbar}(T_L^2 - T_R^2), \tag{1.56}$$

in which c is the central charge of the conformal field theory $T_{L/R}$ are the temperatures of the right and left part and k_B is the Boltzmann's constant. An easy way to understand relation (1.56) is that the energy current is proportional to the difference in the power radiated by the two halves. This is nothing but the Stefan-Boltzmann law which in $(1+1)$-dimensions predict a dependence on the square of the temperature. A similar functional shape is found also for other models which are not described by conformal field theories. A different behavior is instead observed in systems in which the quasi particles interact among each other, this can happen also in exact solvable statistical systems. In fact, it has been recently shown that, in inhomogeneous quenches, the spreading of the physical quantities follows a diffusion equation [45]. To conclude we the spreading of information and the transport in inhomogeneous quenches can be either *ballistic*, meaning that the spatial densities and currents can be written as a function of $\xi = x/t$, i.e. $f(\xi = x/t)$, and *sub-ballistic*. In the latter case the transport of physical quantities is described by a diffusion equation.

Transport phenomena and spreading of quasi-particles occur in integrable and non-integrable systems, as we have seen, in different way: in one case ballistically in the other diffusive, eventually lead to relaxation either to Gibbs ensemble or to GGE. However, there are cases in which the diffusion of the quasi-particles is

completely *suppressed* and the relaxation is therefore hindered. This happens, for example, in one-dimensional quantum systems which are in the so-called *many-body localized* phase due to the presence of disorder in the Hamiltonian.

1.2.3 Many-body localized systems

Many-body localization (MBL) is a *robust* dynamical phase of matter that makes interacting *disordered* systems perfect insulators also at finite temperature, thus breaking ergodicity and hindering the relaxation in non-equilibrium processes (see Ref. [46] for a comprehensive pedagogical introduction). Furthermore it is the only known *robust* mechanism that prevents thermalization in an isolated quantum system, thus keeping an infinite amount of information about its initial conditions. In fact, if on the one hand MBL shares this peculiar property with quantum integrability, as seen in Sec. 1.2.1, on the other, an important difference with quantum integrable systems is that MBL persists also if a small perturbation is added.
The fact that the presence of certain type of disorder in the couplings of a Hamiltonian can lead a system to behave as a perfect insulator, has been studied for the first time in a seminal paper by Anderson [47]. In his work he considered free particles on a lattice with random on-site potential and shown that the single particle wave-function localizes, this phenomenon is in fact known as *Anderson localization* (see panel ***b*** in Fig. 1.8). Anderson localization is an extremely interesting

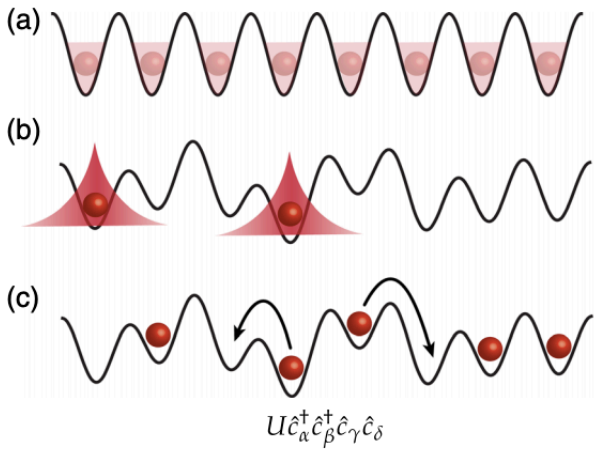

Figure 1.8: Figure from Ref. [46]: (a) In a crystal with no random potential the occupation number is equal on all the sites because the single-particle eigenstates are completely delocalized. (b) Adding a disorder can localize the wave-function and suppress the smoothing of inhomogeneities (Anderson localization). (c) This phenomenon of localization persists, in certain conditions, also when an interaction among the particles is switched on.

phenomenon, in fact in the absence of disorder the single-particle eigenstates are

Bloch-propagating waves de-localized across the system. When a disordered potential is switched on, the nature of the single-particle eigenstates, $\Psi(x)$, changes completely and they *localize* spatially in the system with $\Psi(x) \approx \mathrm{e}^{-\frac{x}{\xi}}$, where ξ is the so-called localization length. Disordered potentials are characterized by a quantity called *strength*, which is nothing but the variance of the distribution from which the values of the *in-situ* potential are sampled. The origin of localization for disordered systems can be easily understood in the limit of *strong* disorder, in which the variance W of the random potential is much larger than the tunneling between neighboring sites of the lattice. Let us consider, for example, the following Hamiltonian

$$H = t \sum_j (c_j^\dagger c_j + \text{h.c.}) + \sum_j \epsilon_j c_j^\dagger c_j \tag{1.57}$$

with ϵ randomly sampled with equal probability from $[-W, W]$. In the limit $t \ll W$, resonant transitions between neighbouring sites are impossible. The same holds also for transition between lattice sites at distance n, in that case the process that allows a resonant transition would be at the n^{th} order in perturbation theory and the amplitude of tunneling would decay as $t_n \approx (t/W)^n$. In spatial dimensions $d = 1$ and 2 it can be proved that *any* amount of disorder leads to Anderson localization. For $d \geq 3$, instead, there is a transition depending on the strength of the disorder, between a metal phase, in which the system is a conductor, and an insulating phase. It is, however, unrealistic to consider in an actual system, non-interacting particles. Accordingly, a natural question that arises is how much the picture depicted by Anderson changes when an interaction among the particles is added in the system. This problem is highly non-trivial because interactions can in principle open decay channels for highly excited localized single-particle states into lower-energy states, thus restoring transport. The first attempt in order to understand this problem was made in 2006 by Basko, Aleiner and Altshuler [48]. They considered the broadening of a single particle highly excited localized state with localization length ξ using a self-consistent Born approximation. Within this approach they were able to capture the maximal possible number of excitations in an avalanche decay process that would have led eventually to delocalization of the eigenfunction. They found that this problem of single-particles level broadening was similar to the problem of studying Anderson localization on a *tree* with a temperature-dependent connectivity $K \approx T$; *a posteriori* this is expected, because, the available phase space in the decay process grows as the temperature is increased. In particular, they estimated a critical temperature $K_c \approx T_c \approx 1/[\lambda \ln |\lambda|]$, in which λ is the strength of the interaction, below which the model presents localization. In fact, it can be shown that below that threshold the probability of having non-vanishing decay

rate for a localized single-particle state is zero, while for $T > T_c$ the many-body eigenstates of the model delocalize.

An important contribution to the problem, which opened the door to the systematic study of many-body localization, was the seminal work by Oganesyan and Huse [41]in which they studied a one-dimensional lattice with *finite-dimensional* local Hilbert space and with *disorder*. They stated that in these conditions there could be localization even at high temperature. For this purpose they considered a free fermionic model (like the one considered in Eq. (1.57)) with on-site disorder and next-nearest-neighbour interactions. A more detailed analysis was made slightly later in 2008 by Prosen et al. [49]. They considered a disordered XXZ chain and studied the transition between many-body localized and thermal phases as a function of the disorder and of the interaction strength. They considered the Hamiltonian

$$H_{XXZ} = \frac{J_\perp}{2}\sum_{i=1}^{L}(\sigma_i^x\sigma_{i+1}^x + \sigma_i^y\sigma_{i+1}^y) + \sum_{i=1}^{L}\left(\frac{J_z}{2}\sigma_i^z\sigma_{i+1}^z + h_i^z\sigma_i^z\right) \tag{1.58}$$

where σ^α are Pauli's operators and h_i^z are randomly distributed on-site magnetic fields h_i^z sampled uniformly from $[-W, W]$. This model is not different from the one considered in Ref. [41]: in fact, by means of a Jordan-Wigner transformation, it is possible to cast Eq. (1.58) into the Hamiltonian of a free fermionic model with on-site disorder, in which $J_\perp$ and J_z are transformed into the fermion hopping and the nearest-neighbours interaction respectively. The phase diagram of this model is schematically reported in Fig. 1.9. It can be observed that in order

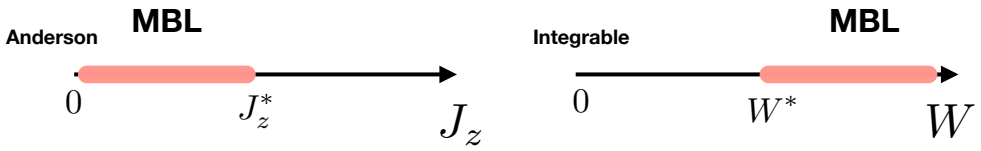

Figure 1.9: Schematic phase diagram of the disordered XXZ model. In the absence of disorder $W = 0$ the model is integrable via Bethe-Ansatz. In the absence of interaction the model is equivalent to free fermions therefore there is Anderson localization.

to have many-body localization there should be a trade off between the interaction strength and the disorder strength. In the extreme case of zero interaction $J_z = 0$, the model is essentially equivalent to the one studied by Anderson and therefore any amount of disorder can lead to localization. If we fix the disorder W to a value comparable with $J_\perp$ (i.e. $W/J_\perp \approx 1$) it is possible to identify a critical value of the interaction $J^*(W)$ above which the system is delocalized. Similarly, by fixing $J_z \approx J_\perp$ there is a critical value of the disorder $W^*(J)$ above which the system is in a many-body localized phase.

In order to detect the existence of an MBL phase, both in Ref. [41] and in Ref. [50], the *r-parameter*, that we introduced in Eq. (1.55), it is studied. As we have previously discussed, for ergodic systems the statistics of the level spacing is follows a Wigner-Dyson distribution on the contrary for non-thermalizing systems we expect a Poisson distribution. In Ref. [50] Pal and Huse studied how the r-parameter for the spectrum of the Hamiltonian (1.58) changes as a function of the disorder strength W with $J_\perp = J_z$; a summary of their analysis is reported in Fig. 1.10. In a region around $W^* \approx 3.5h$ one can observe a drop between

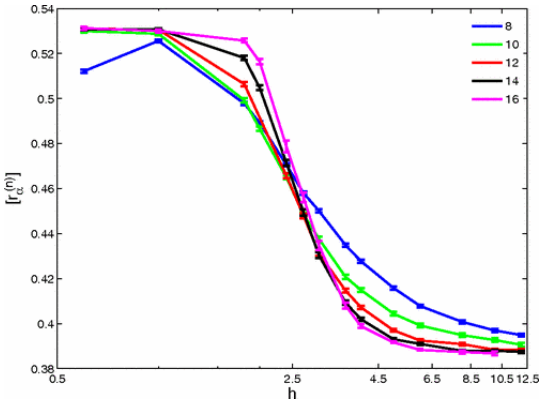

Figure 1.10: Figure from Ref. [50]. r-parameter as a function of the disorder strength for the model (1.58). At the critical value of $W^* \approx 3.5h$ there is apparently a transition between an ergodic and a MBL phase.

$r \approx 0.54$, the value typical of a Wigner-Dyson distribution, and the value $r \approx 0.38$, typical of a Poissonian distribution. For this reasons it is believed [6] that at $W = W^*$ a phase transition occurs between a many-body localized phase and an ergodic phase. These results moreover suggest that there can be an effective quasi-integrability picture behind the lack of thermalization in a many-body localized system.

A quantity that can provide insights about the time evolution of the system is the time-dependent bipartite entanglement von Neumann entropy, that is defined as (referring to Fig. 1.3)

$$S_A(t) = -\mathrm{Tr}_A(\rho_A(t) \ln \rho_A(t)), \tag{1.59}$$

and is a *very sensitive* quantity in order to detect the amount of information that is shared by the two subsystems A and B. For symmetry reasons it holds that $S_A = S_B$, where S_B is the same quantity defined in Eq. (1.59) with the role of A and B exchanged. If we perform a global quantum quench in a generic

[6] Recently some criticism about the effective validity of type of analysis has been raised. See Ref. [51] for details.

system, a linear growth of the entanglement entropy in time is observed [52, 44]. This fact can be understood in terms of quasi-particles spreading in the system; for integrable models, since the quasi-particles move balistically, it is possible to give exact analytical predictions [44, 25]. For finite systems it is observed that the entanglement entropy, after the initial growth mentioned above, saturates to a value that is proportional to the volume V of the systems $S_{t\to\infty} \propto V$. In particular, in integrable systems that in the scaling limit are described by a conformal field-theory, the final entanglement entropy can be proven to be equal to

$$S_A = \frac{c}{3} \ln l + c \tag{1.60}$$

in which c is the central charge of the conformal field theory and l is the length of the sub-system A [53]. In many-body localized systems, on the contrary, the entanglement entropy growth in time is logarithmic, i.e. $S(t) \propto \ln t$ [54, 55].
It is interesting to note that, although the system is in a localized phase, a perturbatively small interaction can activate a *glassy dynamics*, i.e. extremely slow evolution, signaled by a slow spreading of correlations, contrary to what is observed in Anderson localization where the entanglement does not grow in time after an initial bump. The fact that the entanglement entropy evolves slowly reveals a completely different behavior of the system with respect to both the ergodic and the integrable cases, in which a linear growth of S_A is observed, signaling a breakdown of relaxation toward an equilibrium state. In Ref. [54] this fact was observed by using matrix product states (MPS) numerical simulations on the XXZ random system that we already introduced in Eq. (1.58). In particular, they studied how the temporal growth of the entanglement entropy changes as a function of the interaction strength $J_z/J_\perp$, as can be seen in Fig. (1.11). The logarithmic growth of the entanglement entropy in the MBL scenario can not be explained as a consequence of the diffusion of the quasi-particle, because in this case they are truly localized. In order to understand this peculiar behavior of S we should take into account the fact that the wave functions $\Psi(x)$ of the particles in the system, as we have already stated, are exponentially localized with a decay length given by the confinement length, i.e., $\Psi(x) \approx \mathrm{e}^{-x/\xi}$. The dephasing induced by the two particles will grow exponentially with the distance d between them, because the interaction strength is proportional to the overlap between their wave functions [55]. Since this fact is important also for the rest of our discussion let us see in detail how it works in a simplified framework. Let us consider two particles that are created in an initial state that is an equal weight superposition of two neighbouring sites, $|\Psi_0\rangle = 1/2(c_1^\dagger + c_2^\dagger)(c_3^\dagger + c_4^\dagger)|0\rangle$, where $c_i^\dagger$ creates a particle localized around the site i and $|0\rangle$ is a state without particles. We can, for fixing the ideas, consider c_i's as fermions operators, however

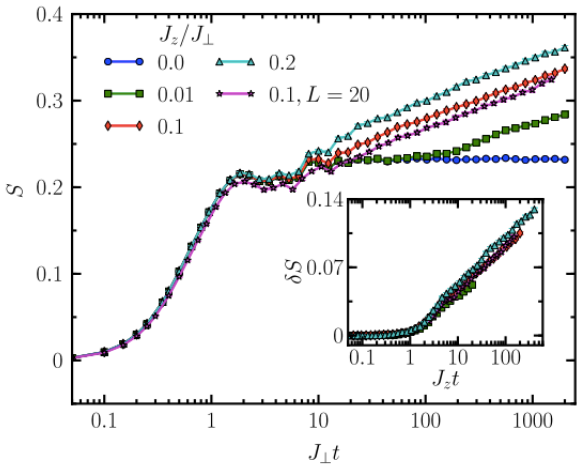

Figure 1.11: Figure taken from Ref. [54]. Growth in time of the bipartite entanglement entropy as a function of the interaction strength $J_z/J_\perp$ in the disordered XXZ model (1.58) in the many-body localized phase.

the argument is completely generic. in the absence of interactions, these two particles do not communicate and a generic two-particles state can be written as a product state $|\Psi_0\rangle = |\alpha\beta\rangle$, with α and β the single particle states. In this case the total energy is just the sum of the single particle energies, $E_{\alpha\beta} = \epsilon_\alpha + \epsilon_\beta$. The introduction of an interaction between the two particles adds a correction term to the energy proportional to the overlap between the two single-particles wave functions and to the interaction strength V, $\Delta E_{\alpha\beta} = CV\mathrm{e}^{-x/\xi}$, because the interaction term we consider is short-ranged, i.e. $H_{\text{int}} = \sum_{\langle i,j\rangle} V n_i n_j$ where $n_j = c_j^\dagger c_j$. If we consider the time-dependent reduced density matrix of one of the two particles, i.e.,

$$\mathrm{Tr}_\beta(\rho_{\alpha,\beta})(t) = \frac{1}{2}\begin{pmatrix} 1 & F(t) \\ F^*(t) & 1 \end{pmatrix} \tag{1.61}$$

in which $F(t) = \mathrm{e}^{-i\Omega t}(1-e^{-i\delta\Omega t})$, $\delta\Omega = \delta E_{14} - \delta E_{24}$ and $\Omega = \epsilon_1 - \epsilon_2 + \delta E_{13} - \delta E_{23}$, it is possible to show that the two particles are maximally entangled, with $S = \ln 2$, when $F(t) = 0$ and this happens at time $t_{\max} \approx \hbar/V\mathrm{e}^{x/\xi}$. The dephasing, therefore, leads to the decreasing of the off diagonal elements of the density matrix which is a clear sign of decoherence. Generalizing this argument, let us divide our one-dimensional system in two halves L and R and let us focus on the reduced density matrix ρ_L. As the time passes an increasing part of L will correlate with an increasing part of the system R. In concrete, at time $t(x) = t_{min}\mathrm{e}^{x/\xi}$, with x a spatial coordinate and t_{min} a microscopic time-scale, the degrees of freedom at a distance $x(t) \approx \ln(t/t_{min})$ will be correlated. This creates an entropy among the two halves that is proportional to the diagonal entropy $S_{ent} \propto S_{diag}$ that is

the maximum entropy within the subsystem $x(t)$. Since the maximum entropy achievable by a subsystem in an initial product state is proportional to its size, the final entropy at time $t \gg t_{min}$ is

$$S_{diag}(t) \propto \xi \ln(Vt/\hbar). \tag{1.62}$$

The correctness of this formula has been verified by comparing it with numerical results [55]. It is important to emphasize that in the previous argument we never introduced the concept of disorder; this mechanism, in fact, works every time that there are localized excitations described by wave functions exponentially localized in space.

So far, we have addressed the behavior in time of entanglement entropy after a quantum quench and we have seen that in systems in a many-body localized phase the growth has peculiar properties compared to the other cases. This peculiarity can be found also in the bipartite entanglement entropy of the eigenstates of MBL systems. In fact, considering the eigenstates $|e_i\rangle$ and computing their entanglement entropy,

$$S_e = -\mathrm{Tr}_A(\rho^A_{e_i} \ln(\rho^A_{e_i})), \qquad \rho^A_{e_i} = \mathrm{Tr}_B |e_i\rangle\langle e_i| \tag{1.63}$$

it has been noted that they have a lower amount of entanglement compared to thermal systems [56]. In particular, for generic systems following the eigenstate thermalization hypothesis, that we will review in the next section, the entanglement entropy of the eigenstates is volume-law, meaning that is is proportional to the volume of the sub-system, i.e. $S \propto V$. Instead for the eigenstates of MBL systems it is *area-law*, meaning that $S_e \propto \partial V$, in particular, for one-dimensional systems it is constant. This fact can be intuitively understood with the following argument, as we have already discussed, in a MBL system only the degrees of freedom at distance of the scale of the localization length ξ correlate. This property persists, surprisingly enough, also at the spectral level for *high-energy* eigenstates, contrary to what happens for other non disordered gapped systems in which area-law scaling of the entanglement is observed only in the ground state [57].

Area-law scaling of the entanglement entropy of the eigenstates together with a poissonian distribution of the energy levels show that the MBL properties can be detected also at spectral level. This behavior is similar to what it is usually observed in integrable models, in order to formalize this idea let us consider the following argumentation [55]. Since the eigenstates have a small amount of entanglement, they are *close* to product states: by "close" we mean that they can be cast in a product state form by applying a series of quasi-local unitary transformations. These unitary transformations diagonalize the Hamiltonian of the

system and, since they are quasi-local, they can be used to map physical degrees of freedom into quasi-local charges. To be concrete, let us consider a Hamiltonian

$$\hat{H} = \hat{H}_0 + \hat{H}_{int}, \tag{1.64}$$

in which $\hat{H}_0$ is the disordered Hamiltonian and $\hat{H}_{int}$ is a nearest-neighbours interaction. Let us suppose that there are N local operators $\hat{\sigma}_i$ such that

$$[\hat{H}_0, \hat{\sigma}_i] = 0, \qquad \forall i = 1, \dots, N, \tag{1.65}$$

with N the number of sites, which consider finite. The eigenstates of $\hat{H}_0$ can be written in terms of product states of eigenvectors of $\hat{\sigma}_i$, i.e. $|\{\bar{\sigma}\}\rangle = |\sigma_1 \sigma_2 \dots\rangle$. If we turn on a weak interaction term, the $|\{\bar{\sigma}\}\rangle$ will be no longer eigenstates of the Hamiltonian $\hat{H}$, but it is possible to act with unitary transformations on them in order to find the actual eigenstates. For this purpose, let us consider quasi-local unitary transformations $\hat{U}$ that can be factorized in terms of multi-sites local operators, i.e. $\hat{U} = \prod_i \hat{U}^{(2)}_{i,i+1} \hat{U}^{(3)}_{i,i+1,i+2} \dots$. The crucial point is that since our system is in a many-body localized phase the global unitary operators (given by the product of local ones) will be *exponentially* close to the identity,

$$||\mathbb{1} - \hat{U}^{(n)}_{i,i+1,\dots,i+n}||^2_F < \mathrm{e}^{-n/\xi}, \tag{1.66}$$

where $||\cdot||_F$ is the Frobenius norm. Accordingly, it is possible to define a new set of operators $\hat{\tau}_i$, such that $\hat{U} : \hat{\sigma}_i \to \hat{\tau}_i$. These operators can be written as

$$\hat{\tau}_i = C\hat{\sigma}_i + \sum_{i=1}^{N} V^{(n)}_i \hat{O}^{(n)}_i, \tag{1.67}$$

with $O^{(n)}_i$ local operators and $V^{(n)}_i \approx \mathrm{e}^{-(n-i)/\xi}$. This implies that the Hamiltonian $\hat{H}$ can be written in terms of some local integrals of motion (LIOMs) as

$$\hat{H}_{MBL} = \sum_i \alpha_i \hat{\tau}_i + \sum_{i>j} \beta_{i,j} \hat{\tau}_i \hat{\tau}_j + \sum_{i>j>k} \gamma_{i,j,k} \hat{\tau}_i \hat{\tau}_j \hat{\tau}_k + \dots, \tag{1.68}$$

in which the long-range couplings decay exponentially, i.e. $\beta_{i,j} \propto \mathrm{e}^{-|i-j|/\xi}$. In this perspective it is clear why the level statistics follow a Poisson distribution and it is also explained the breakdown of the thermalization: as in integrable systems, the presence of local quasi-conserved quantities implies a preservation of the initial conditions during time evolution.

1.2.4 Eigenstate thermalization hypothesis

Hitherto we have analyzed in detail the two known cases in which relaxation toward a thermal state is hindered, i.e. integrable systems and MBL systems.

However, we have not yet discussed what is the mechanism behind the thermalization in closed quantum systems, which is known as *eigenstate thermalization hypothesis* (ETH) [58]. Before introducing ETH let us take a step back and let us focus to Eq.(1.19). As we have seen, the time-dependent expectation value of an observable A in a closed quantum system can be written as:

$$A(t) = \sum_n |c_n|^2 A_{n,n} + \sum_{m \neq n} c_m^* c_n \mathrm{e}^{i(E_m - E_n)t/\hbar} A_{n,m}. \tag{1.69}$$

In the limit $t \to \infty$ the off-diagonal terms average to zero in Eq.(1.69), if there are no degeneracies in the spectrum, and therefore we obtain

$$\lim_{t\to\infty} A(t) = \sum_n |c_n|^2 A_{n,n}. \tag{1.70}$$

The crucial question at this point is [59]: is it possible to interpret the r.h.s. of (1.70) as emerging from the expectation value on the microcanonical ensemble, appropriate for isolated systems? This aspect is absolutely non-trivial for two reasons: first of all, thermal expectation values should be *independent* of the single states, i.e., on the values of the c_ns, and they should depend only on the initial *energy*. Furthermore, the time required for the off-diagonal elements in Eq. (1.69) to vanish could be extremely large, also larger than the age of the universe, especially for actual systems in which the energy levels may be exponentially close.

In section 1.2.1, we stated that an ergodic quantum system, i.e., a systems which thermalizes, whose equilibrium state is described by a thermal ensemble, has a Wigner-Dyson statistics of the energy levels which is typically found in random matrices. The connection between random matrices and thermal systems is formalized in the ETH picture. In fact, if the Hamiltonian describing our system was a true random matrix we could rewrite relation (1.69) (in the thermodynamic limit) as

$$A(t) = \bar{A} \sum_n |c_n|^2 = \bar{A}, \tag{1.71}$$

because $A_{m,m}$ would be independent of m and the off-diagonal elements would be exponentially suppressed upon increasing the system size. However, in Eq. (1.71) there is no initial energy dependence: the states are all weighted equally, accordingly, it can be considered the thermal expectation value of a state at infinite initial temperature. In order to describe expectation value of ergodic systems for *every* temperatures, it is necessary to include an energy dependence. Eigenstate thermalization hypothesis is a way of achieving this goal, going *beyond* the random matrix theory. It was Srednicki in Ref. [58] who first provided an adaptation of random matrix theory to real physical systems. In this sense, the eigenstate

thermalization hypothesis can be formulated as an ansatz for the expectation value of local a observable A in ergodic quantum systems:

$$A_{m,n} = A(\bar{E})\delta_{mn} + \mathrm{e}^{-S(\bar{E})/2} f_A(\bar{E}, \omega) R_{m,n}, \tag{1.72}$$

where $\bar{E} = (E_m + E_n)/2$, $\omega = (E_m - E_n)/2$, $S(E)$ is the thermodynamic entropy at energy E and R_{mn} is a random real or complex variable with zero mean and unit variance. It is crucial that both $A(\bar{E})$ and $f_A(\bar{E}, \omega)$ are smooth function of the energy and that $A(\bar{E})$ coincides with the value predicted by microcanonical ensemble. The physical interpretation of ETH is of outstanding importance: what Eq. (1.72) is telling us is that in ergodic systems the information about the thermal expectation values of observables is *encoded in every single eigenstate*, and for this reason it is called eigenstate thermalization hypothesis. Relation (1.72) should in principle hold for *all* observables and *all* the eigenstates, this is known as *strong*-ETH.

We can see how, in ETH picture, thermalization in closed quantum mechanical systems is *onthologically* different from what happens in classical ones. As we have seen at the beginning of the chapter, in classical systems the ergodicity is given by a *chaotic* time-evolution of the trajectory in the phase space and final thermal state has nothing to do with the initial state. In ETH, instead, information about thermalization is contained in *every* eigenstate, therefore time evolution has not the crucial role that had in classical systems, the only thing that it does is to uncover thermalization by inducing decoherence in the initial state, as sketched in Fig. 1.12. Eigenstate thermalization hypothesis describes the approach to thermal ensemble for generic quantum systems irrespective of their spatial dimension. The validity of ETH has been numerically proven in many works in the last fifteen years (see Ref. [59] for a review). However the statement according to which every eigenstate of an ergodic system must show the signals of thermalization seems to not hold: some systems can have "rare" states in the spectrum which violate ETH. Nonetheless, as long as the number of these states is exponentially small, thermalization will still occur, because in the dynamics following a quantum quench these states will have a negligible weight. Such scenario is usually referred to as "weak" thermalization (or weak ETH) [61].

A completely different problem is the one concerning violation of ETH in non-integrable systems with no generic symmetries. In particular, it is interesting to understand how and in which sense this occurs in order to test the robustness of the ETH. These arguments will be treated in detail in the next chapters and actually represent the core of this thesis.

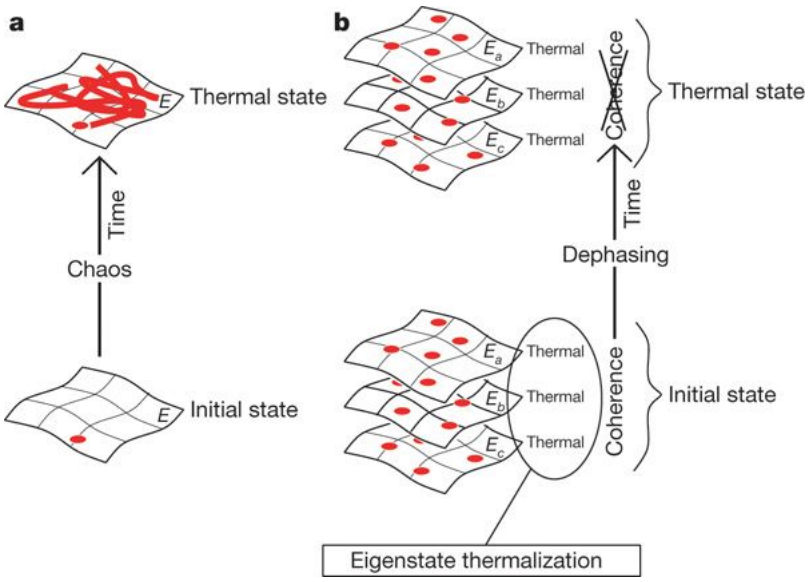

Figure 1.12: Figure taken from Ref. [60]. Schematic representation of the thermalization process in classical and quantum systems. In panel a we can se how the thermalization process in classical systems is given by chaotic time evolution. In panel b we see, instead, how the information about the thermal phase in quantum systems is encoded at the level of single eigenstates.

1.3 Experimental realizations of one-dimensional quantum systems

The last section of this introduction is dedicated to a brief review of some of the most important experiments concerning relaxation in isolated quantum systems. In the last years there had been an incredible advance in the experimental techniques involving both cold atoms and condensed matter systems, that made the observation of coherent dynamics possible for incredibly long times. These technological advances are of utmost importance since they have marked the beginning of the golden era of quantum simulations, fulfilling Feynman's prediction about the use of engineered quantum systems for the study of non-equilibrium quantum phenomena [62]. One of the main problem of numerical simulations in quantum systems is their feasibility. In order to simulate a truly extended statistical quantum system on a classical computer numerical techniques (MPS, DMRG, quantum MonteCarlo, etc...) must be used, but this results in strong limitations in the dimension of the systems one can simulate or in the maximum time achievable. The use of properly engineered quantum systems get automatically rid of these difficulties because the quantum nature of the simulation is naturally encoded in the system; the "only" price to pay is to keep the simulator coherent as long as possible. A particularly optimal setup for simulating quan-

tum spin systems is represented by Rydberg atoms. They are expressly suitable for being controlled by means of opto-acoustic traps and can mimic very well a two level system with nearest neighbours interactions, as depicted in Fig. 1.13.

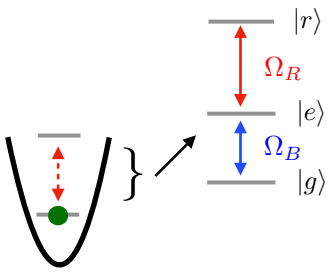

Figure 1.13: Schematic representation of Rydberg atom trapped in a harmonic trap.

The first experiment we are going to discuss is the famous quantum newton cradle [63]. This experiment is very important because it represents the first realization of a system that remains integrable for a time sufficiently long to observe non-thermalization[7]. In order to inspect the dynamics of the system, they prepared many arrays of trapped (with optical lattices) one-dimensional (1D) Bose gases, each containing from 40 to 250 ^{87}Rb atoms, and observed no equilibration even after thousands of collisions. Atoms in each array are described by a Lieb-Liniger Hamiltonian, in particular it is possible to tune interaction in the Tonks-Girardeau limit, in which the bosons behave as free fermions. The quench protocol consists in a trap-release, meaning that the frequency of the optical potential is abruptly changed. After that the bosons are free to move and to collide, but despite this fact coherent dynamics is observed for an unexpected long time, as reported in second panel of Fig. (1.14). Another recent remarkable work in which it is simulated an integrable model is reported in Ref. [64], in which there is the first experimental observation of a generalized Gibbs ensemble (GGE).
More challenging, from the experimental point of view, is the realization of disordered systems which show MBL transition. The main difficulty in this case is represented by the fact that in order to build a random or quasi-random potential, it is necessary to make different laser beams interfere properly. Also in this case it is important to keep isolation from external environment for a sufficiently long time. One the first experimental realization of a MBL system was carried out in 2015 [65] in the group of Immanuel Bloch. They considered a fermionic

[7] To be more precise, the perturbations to the systems, given by the coupling with external degrees of freedom or by the anharmonicity of the trap are perturbatively small and influence the dynamics only at longer time-scales

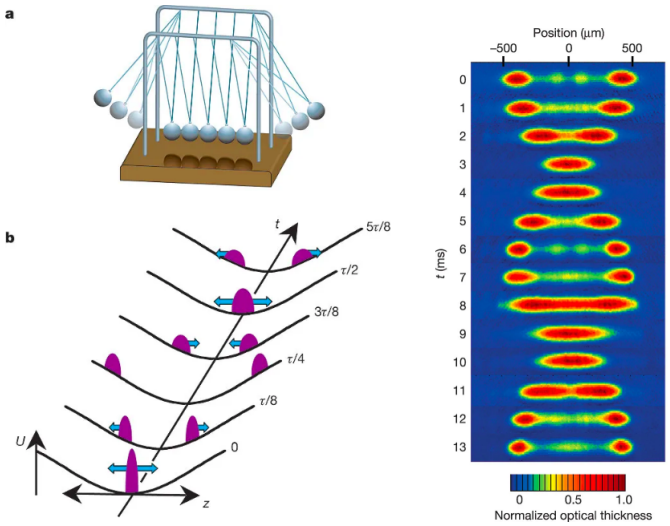

Figure 1.14: Figure from Ref. [63]. Left panel: schematic illustration of the experiment. Right Panel: density of bosonic cloud as a function of time.

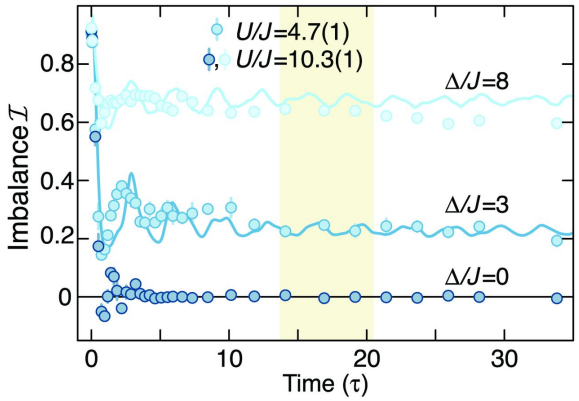

Figure 1.15: Figure from Ref. [65], experimental data for the population imbalance as a function of time for different values of the interaction.

system with quasi-periodic potential described by the Hamiltonian

$$H = -J\sum_{j,\sigma}(c^{\dagger}_{j,\sigma}c_{j+1,\sigma} + \text{h.c.}) + \Delta\sum_{j,\sigma}\cos(2\pi\beta j + \phi)n_{j,\sigma} + U\sum_{j} n_{j,\uparrow}n_{j,\downarrow}. \quad (1.73)$$

The system was initially prepared in a charge density wave initial state with only the even sites occupied and then let evolve. During the non-equilibrium time evolution the imbalance between even and odd sites, $I = \langle (N_e - N_o)/(N_e + N_o)\rangle$ was monitored. As it is reported in Fig. 1.15, when there is no disorder, $\Delta = 0$, the system thermalizes, as signaled by the fact that the initial inhomogeneity is smoothed out. But for $\Delta \neq 0$ the stationary value of the imbalance is different from zero, this is an hallmark of localization.

The last experiment we discuss is slightly different from the previous ones, as

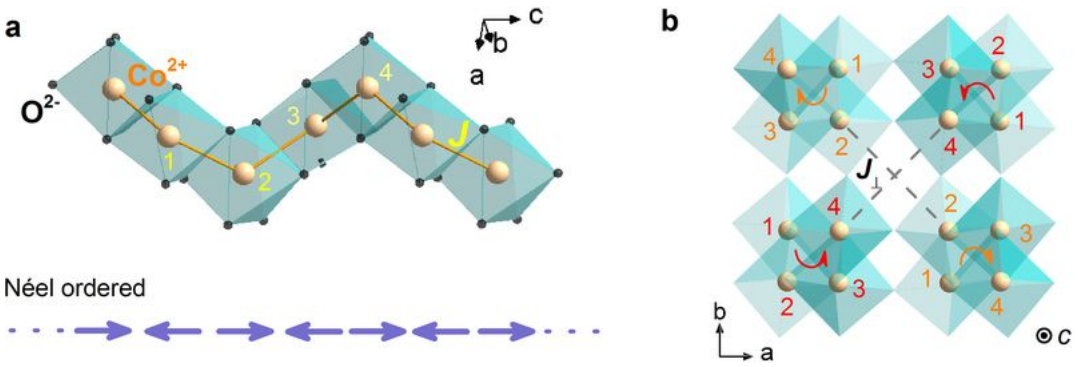

Figure 1.16: Figure from Ref. [23]. Structure of the $SrCo_2V_2O_8$ from two different perspectives. The role of the spin-1/2 degrees of freedom is played by the magnetic moment Co^{2+} ions, the interaction strength J, much larger than other inter-chains interactions, is responsible for the effective one-dimension of the material.

it represents an example of an actual condensed matter systems (quantum magnet) which is well described by a one-dimensional spin system. This experiment involves systems showing, *confinement* which we will extensively describe in the next chapter. Z. Wang et al. in Ref. [23] were able to observe *bound states* of magnons in a chain of $SrCo_2V_2O_8$ crystal that is described by a spin-1/2 XXZ anti-ferromagnetic Hamiltonian in a longitudinal magnetic field, i.e.,

$$H = \frac{J}{2}\sum_{n=1}^{N}(\sigma_n^x\sigma_{n+1}^x + \sigma_n^y\sigma_{n+1}^y + \Delta\sigma_n^z\sigma_{n+1}^z) - g\mu_B B\sum_{n=1}^{N}\frac{\sigma_n^z}{2} \tag{1.74}$$

where σ_i^α are Pauli's spin operators and B is the strength of an external magnetic field. The reason why a three-dimensional crystal can be effectively described by a one-dimensional chain is because the interaction strength between the Co^{2+} ions along the direction of the symmetry axis (J intra-chain coupling) is much larger than the interaction strength between the other chains in the ochtahedra ($J_\perp$, inter-chain coupling), in particular in their experiment $J_\perp/J < 10^{-2}$, as reported in Fig. 1.16. The main purpose of the experiment was to detect the first excited states above the ground state. This goal can be achieved using optical or neutron scattering on the sample material. In fact, by means of terahertz optical spectroscopy in a longitudinal field B up to $B \approx 30$ T, it is possible to see clear evidences of the existence of bound states of magnons, by observing the transmission spectra and resonances as a function of the frequency and of the magnetic field applied, Fig. 1.17. It is particularly interesting to observe how in the ordered phase the excitations have a linear dependence on the longitudinal field strength, as it should be expected in confining bound states.
The importance of this experiment relies on the fact that shows the possibility of building high controllable quantum systems using real crystals. Moreover, this

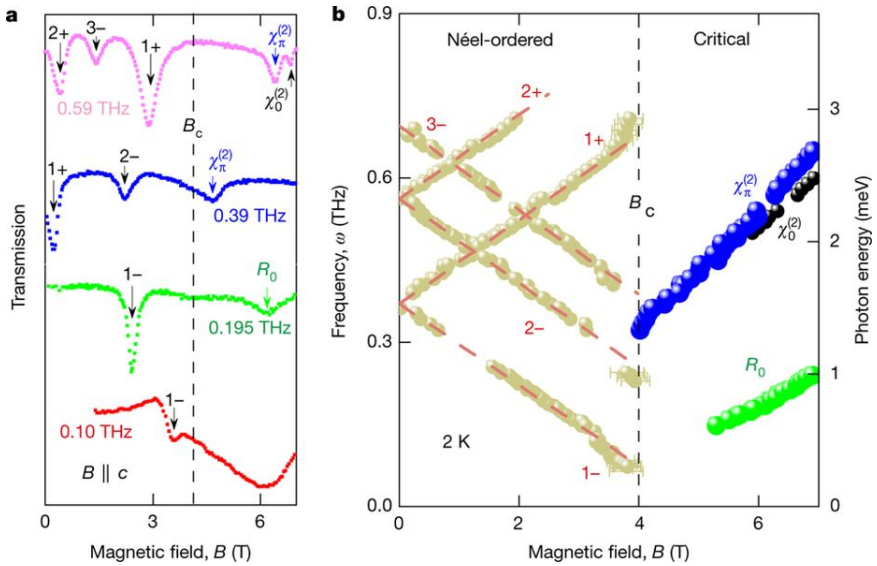

Figure 1.17: Figure from Ref. [23]. Experimental data for the transmission spectra and dispersion relation as a function of the magnetic field, either in ordered phase and in critical phase.

specific setup mimics systems whose excitations can be *confined* in bound states, this aspect leads to some crucial and unexpected feature in non-equilibrium dynamics that will be discussed in the next chapter.

CHAPTER 2

CONFINEMENT AND SLOW-DYNAMICS

In this chapter we discuss one of the main topics of this thesis: how the presence of a confining interaction can influence the approach to thermal equilibrium in systems that should follow the eigenstate thermalization hypothesis. All the results that we are going to present actually hold for general class of one dimensional quantum systems. In fact, the only thing that we require is that the excitations on top of the ground state can be described by quasi-particles that interact with a *linear* potential, i.e. $V(x_1, x_2) \propto |x_1 - x_2|$, with x_1 and x_2 the positions of the particles. Similar phenomena have been shown to emerge in several one-dimensional condensed-matter models [66, 67, 68, 69]. This kind of interaction can mimic the effect of the confinement typical of gauge theories, and, at least in one-dimension, the physical implications are qualitatively (and in some cases also *quantitatively*) similar. Therefore, the interest in studying this kind of systems is twofold: from the statistical physics point of view they represent an example of systems with a unexpected slow dynamics in the absence of disorder, from high-energy physics perspective the possibility of building condensed matter models with confinement can be an extremely powerful tool for the simulation of dynamical properties in gauge theories.

Here we will study in detail the prototypical case of the ferromagnetic quantum Ising chain with a transverse and a longitudinal magnetic field, h_z and h_x and we will discuss also the similarities between this and other models, as for example the XXZ chain. The Hamiltonian of Ising chain with longitudinal field is:

$$H(h_z, h_x) = -J \sum_{i=1}^{L-1} \sigma_i^x \sigma_{i+1}^x - h_z \sum_{i=1}^{L} \sigma_i^z - h_x \sum_{i=1}^{L} \sigma_i^x. \tag{2.1}$$

Here, as usual, $\sigma_i^{x,y,z}$ are the Pauli matrices acting on the site i, $J > 0$ is the Ising exchange parameter, L the system size. For $h_x = 0$, the model is exactly solvable

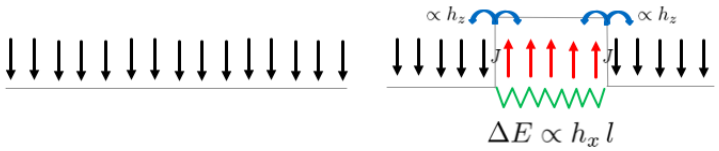

Figure 2.1: Graphical description of confinement of excitation in Hamiltonian (2.1).

in terms of free fermions [70] which, in the ferromagnetic phase with $|h_z| < J$, physically correspond to freely moving domain-walls (or kinks) connecting the two oppositely magnetized ground states with $\langle \sigma_j^x \rangle \neq 0$. Switching on a finite $h_x \neq 0$ causes a non-perturbative modification of the spectrum of the elementary excitations: it selects as a ground state the one with $\langle \sigma_j^x \rangle$ along h_x and raises the energy of configurations with domains of reversed spins by an amount proportional to their extension, as schematically reported in Fig. 2.1. This corresponds to a linear, V-shaped interaction potential between two consecutive kinks delimiting a domain, which therefore become *confined* into composite objects called *mesons*. This effect is qualitatively similar to the quark confinement in quantum chromodynamics, in particular in the *Lund parton-model* that, although it is a simple effective hadronic theory, is able to describe quite complex phenomena [71]. This modification of the spectrum has been studied in the vicinity of the critical point $h_z \to 1$ exploiting field-theoretical methods [72, 73, 74]. In these works the spectroscopy of the Ising field theory in an external magnetic field is studied and the masses of the particles, bound states of kink and anti-kink, are exactly calculated. in the absence of external magnetic field there are eight stable particles $A_i (i = 1, \ldots, 8)$[1], but five of them lie above the energetic stability threshold. When integrability is broken, $h_x \neq 0$, they become unstable and their decay width can be perturbatively computed [73].

Another interesting regime of this problem is the one in which the excitations are dilute in the ferromagnetic phase, i.e. $h_x \ll h_z < J$. This case has been recently faced both from high-energy physics perspective, studying the spectroscopy of the bound-states with a semiclassical approach [76], and from a statistical physics point of view, analyzing the non-equilibrium dynamics in a homogeneous quantum quench [77]. Since the strange properties of relaxation found in Ref. [77] have initially drawn our attention on problems with confinement, we will briefly summarize their result. We have to keep in mind, however, that we will be interested in the regime in which the transverse field h_z is the *lowest* scale of the problem, i.e. $h_z \ll J, h_x$.

[1] This fact is connected with the $E8$ symmetry group spectrum, see [75]

2.1 Homogeneous Initial State

The study of the non-equilibrium dynamics starting with homogeneous initial states in systems described by Hamiltonian (2.1) shows clearly the effect of the interaction between the quasi-particles on the thermalization. The quench protocol studied by Kormos et al. in Ref. [77] consists in preparing the system the ground state of Eq. (2.1) and then changing abruptly the fields $H(h_z^i, h_x^i) \to H(h_z^f, h_x^f)$. What one naively would expect is that the expectation value of local observables, as for example the magnetization $\langle \sigma^x \rangle$, should attain a thermal value predicted by the microcanonical ensemble, and that this should happen on a time scale that is related to some microscopical parameter of the Hamiltonian, e.g. $\tau \approx 1/Jh_x$. What is observed, instead, is that there are persistent oscillations that do not decay until surprisingly long times, see Fig. 2.2. In this case, as usual, the initial

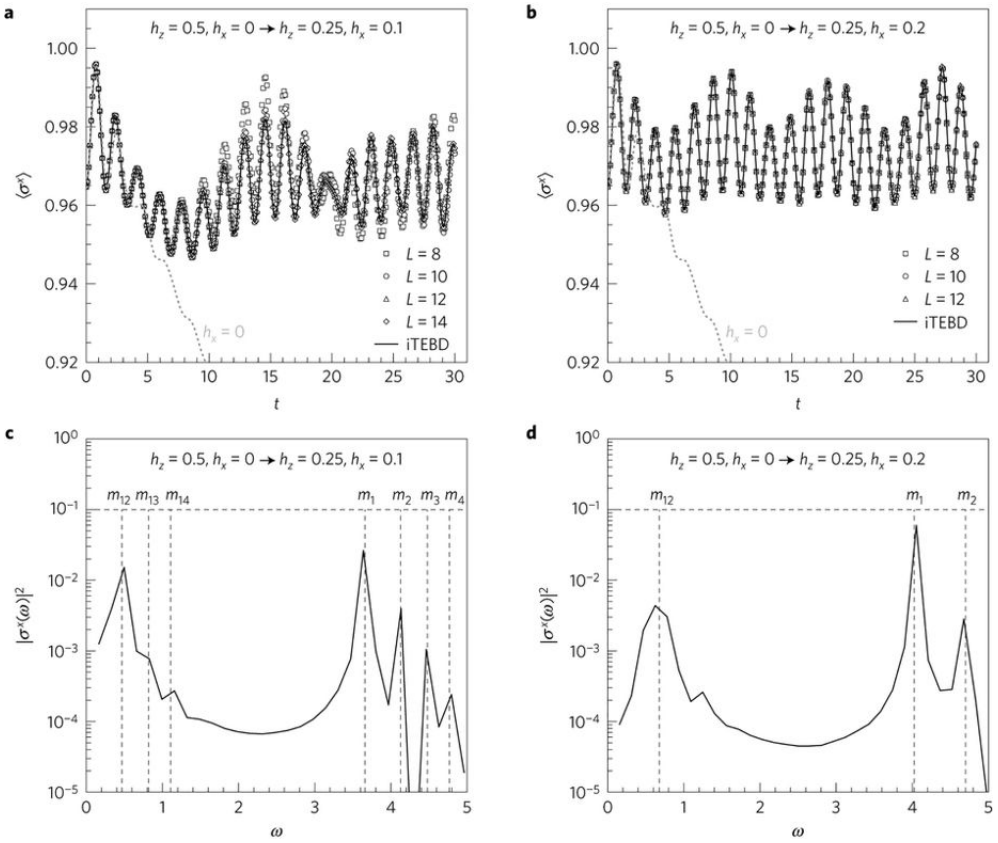

Figure 2.2: Figure from Ref. [77]. Time-dependent expectation value of the magnetization in a global quench in a system with confinement. Note the persistent oscillations given by the presence of a confining potential between the quasi-particles. The spectral analysis of this time series is peaked on the values of the masses of the mesons (or their difference) predicted in semiclassically in Ref. [76].

state behaves as a source of quasi-particles , however since they interact with a

linear potential they form bound states and *oscillate*, this phenomenon is similar to the Bloch oscillations which describe the motion of a particle (typically an electron) in a crystal under the action of a constant force. The fact that in Fig. 2.2 the data of the time series for different sizes obtained with exact diagonalization and the ones obtained with infinite Time Evolution Block Decimation (iTEBD) coincide, indicate that this a bulk effect. In other words, the bound states of kink anti-kink (mesons) are not propagating in the system. This effect can be explained considering that for $h_x = 0$ the initial state can be written in terms of the quasi-particles excitations as

$$|\Psi_0\rangle = \mathcal{N} \prod_{k>0} (1 + i\mathcal{K}(k) a_k^\dagger a_{-k}^\dagger)|0\rangle, \tag{2.2}$$

where $|0\rangle$ is the vacuum, $a_k^\dagger$ Bogolioubov fermions, k the momenta of the quasi-particles and $\mathcal{K}(k) = \tan(\Delta_k/2)$ with Δ_k the difference between the Bogolioubov angles in the pre-quench and post-quench Hamiltonians, in other words, Δ_k is a parameter that measures the "intensity" of the quench. If $h_x \neq 0$, with $h_x \ll h_z$, this picture still holds, the only effect of an external magnetic field, is a linear potential among the excitations. Therefore if $h_z^f \approx h_z^i$, i.e. if $\Delta_k \ll 1$, high-order terms like $\mathcal{K}(k)\mathcal{K}(k')a_k^\dagger a_{-k}^\dagger a_{k'}^\dagger a_{-k'}^\dagger$ with a non-zero total momentum, are suppressed resulting in non-propagating mesons. For comparison let us see what happens if we perform a big quench. For this purpose we prepare our system in the ground state of (2.1) with $H(h_z = 0, h_x = 0.2)$ and we let it evolve with $H(h_z = 0.7, h_x = 0.2)$, we perform a numerical simulation using Time Evolution Block Decimation (TEBD) [78]. As we can see in Fig. 2.3, in this case the time-

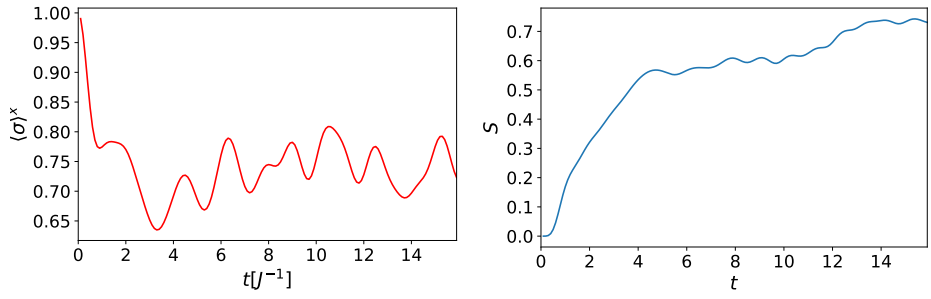

Figure 2.3: Time-dependent expectation value of the magnetization and of entanglement entropy in a "big" quench.

dependent expectation value of the magnetization is different, in particular it decays faster at the beginning with respect to what is observed in Fig. 2.2. This happens because there is a non-vanishing number of mobile mesons that enhance evolution of the initial state.

The slow dynamics of the system in presence of a confining field can be de-

tected also observing the time evolution of the bipartite entanglement entropy. In Fig. 2.4 are reported the numerical results performed in Ref. [77] for different quenches. In this case only a qualitative analysis is reported, it is not discussed if the presence of the longitudinal field h_x changes the temporal growth of the entanglement entropy from linear (as it is for $h_x = 0$) to logarithmic. We will study this aspect in the last section of this chapter. For small quenches, i.e. quenches in

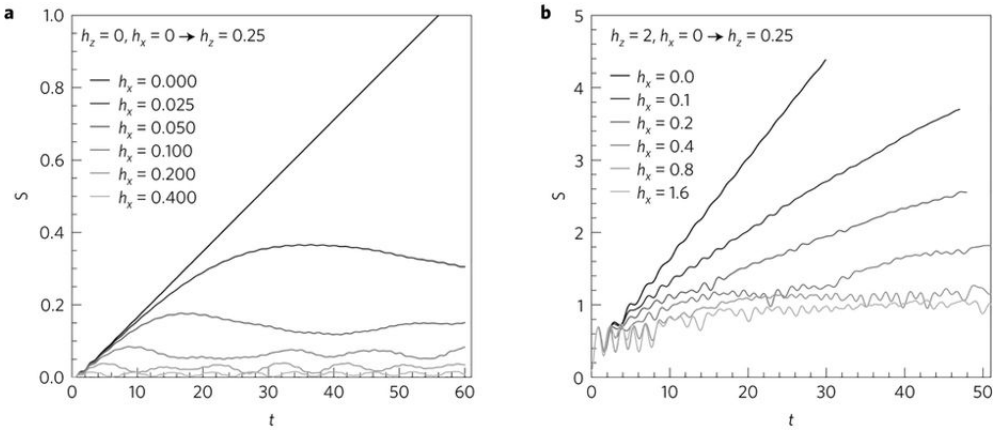

Figure 2.4: Figure from Ref. [77]. Entanglement entropy growth for different values of the longitudinal field h_x.

which $\Delta_k \ll 1$, only the first modes above the ground state are excited, and thus only small mesons are created. The oscillations observed in the time-evolution of magnetization in Fig. 2.2 are related to the masses of the created mesons that can be estimated using Bohr-Sommerfeld quantization of the phase space of an effective theory on lattice [76]. The dispersion relation of fermionic excitations, in the absence of longitudinal field, is:

$$\epsilon(k) = 2J\sqrt{1 - 2h_z \cos k + h_z^2} \tag{2.3}$$

for small longitudinal field, $h_x \ll h_z$ the only effect we have is a potential among the kinks that is proportional to the distance d between the two quasi-particles, i.e., $V(d) = \xi d$ with $\chi = 2Jh_x\bar{\sigma}$. Accordingly, it is possible to build an effective Hamiltonian that mimics the interaction between the quasi-particles

$$H(k_1, k_2) = \epsilon(k_1) + \epsilon(k_2) + \chi|x_1 - x_2| \tag{2.4}$$

If we perform a canonical transformation and express Hamiltonian (2.4) in terms of center of mass and relatives coordinates

$$X = \frac{x_1 + x_2}{2}, \qquad x = x_2 - x_1 \tag{2.5}$$

$$K = \frac{k_1 + k_2}{2}, \qquad k = k_2 - k_1, \tag{2.6}$$

the Hamiltonian (2.4) takes the form

$$H = \omega(k, K) - \chi(x), \tag{2.7}$$

with $\omega(k, K) = \epsilon(k + K/2) + \epsilon(k - K/2)$. We can interpret $q = k$ as a spatial coordinate and $x = -p$ as its conjugate momentum, at this point Eq. (2.7) describes the periodic motion of a particle with kinetic energy $\xi|p|$ in a potential $\omega(k, K)$. Using the Bohr-Sommerfeld quantization condition, paying attention to the fact that for $K < 2 \arccos h_z$ the function $\omega(K, k)$ has one minimum, but for $K > 2 \arccos h_z$ it has two minima, it is possible to find the masses of the first mesons that coincide with the peaks observed in the bottom panels of Fig. (2.2).

2.2 Inhomogeneous initial state

The physical picture described in the previous section seems to suggest a certain qualitative similarity with the slow dynamics typical of disordered systems in MBL phase. In order to understand if this similarity can be pushed forward we study the transport properties in systems with confinement [79]. The typical way through which transport properties are investigated, is by means of a so-called *inhomogeneous quench*. An inhomogeneous quench consists in joining, at time $t = 0$, two complementary subsystems that are initially prepared in two different equilibrium states, such that they evolve according to a common, homogeneous Hamiltonian. We preliminarly consider the simplest inhomogeneous initial state, namely a domain-wall with a single kink in the middle of the chain which reads, in terms of the eigenstates $|\uparrow\rangle_j$ and $|\downarrow\rangle_j$ of σ_j^x,

$$|\Psi_0\rangle = \bigotimes_{j=1}^{L/2} |\uparrow\rangle_j \bigotimes_{j=L/2+1}^{L} |\downarrow\rangle_j \equiv |\uparrow\uparrow \dots \uparrow\uparrow\downarrow\downarrow \dots \downarrow\downarrow\rangle\,, \tag{2.8}$$

and which is also an eigenstate of $H(0, h_x)$. The quench protocol consists in turning on, at time $t > 0$, a transverse field $h_z \neq 0$. We study the non-equilibrium evolution of the energy density profile $\langle \mathcal{H}_j(t) \rangle$ as a function of j, where

$$\mathcal{H}_j = -J\sigma_j^x \sigma_{j+1}^x - \frac{h_z}{2}\left(\sigma_j^z + \sigma_{j+1}^z\right) - \frac{h_x}{2}\left(\sigma_j^x + \sigma_{j+1}^x\right). \tag{2.9}$$

For $h_x = 0$, the initial energy density $\langle \mathcal{H}_j(t = 0) \rangle$ is equal on the two sides of the junction, due to the $\mathbb{Z}_2$ symmetry. However, in the presence of a non-vanishing $h_x > 0$, the chain acquires an initial macroscopic energy imbalance between the left ("cold") part and the right ("hot") part. In particular, the latter may be viewed as a "false vacuum" whose energy lies in the middle of the many-body spectrum, and may thereby be expected to decay into a finite density of traveling

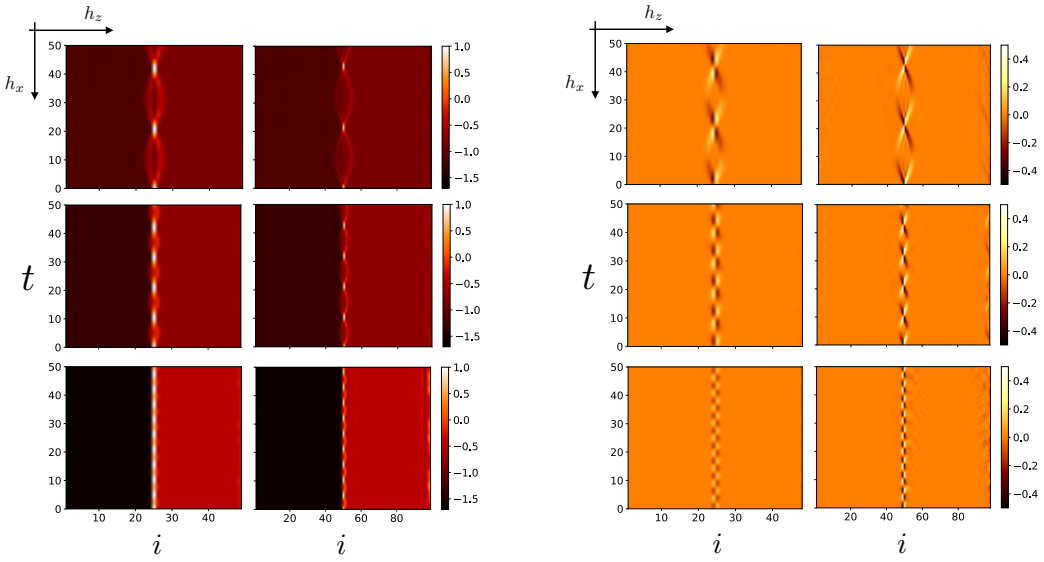

Figure 2.5: Evolution of the energy density $\langle \mathcal{H}_i(t) \rangle$ (left panel) and of the energy current density $\langle \mathcal{J}_i(t) \rangle$ (right panel) profiles, governed by the Hamiltonian (2.1) starting from the inhomogeneous domain-wall state (2.8), obtained from TEBD simulations, for a range of increasing field values $h_z = 0.2$ ($L = 50$), 0.4 ($L = 100$) and $h_x = 0.15, 0.3, 0.6$, varying as indicated by the axes. (Units are fixed such that $J = 1$.) The same qualitative behavior as that illustrated here persists up to long times $t = 10^3$. Note the oscillations of the profiles around the junction, with spatial amplitude $\propto h_z/h_x$ and frequency $\propto h_x$, while there is no evidence for the activation of transport.

excitations upon activating the transverse field $h_z \neq 0$, leading to a meltdown of the initial imbalance after a transient [80]. We shown, that actually this expectation is, surprisingly, unfulfilled. In order to explore numerically the non-equilibrium evolution of the chain, we employ matrix product state techniques, in particular TEBD simulations. It turns out that the entanglement grows slowly[2] up to moderate values of the field $h_z < 0.4J$. This fact, in particular, allows us to extend the simulations to long times $t_{\rm M} = 10^3 J^{-1}$ with modest computational efforts, because the maximum bond dimension of the MPS representation of the time-evolved state, remains low, see Fig. (2.6). We further investigate the behavior of $\langle \mathcal{H}_j(t) \rangle$ [see Eq. (2.9)] and of the associated current $\langle \mathcal{J}_j(t) \rangle$, with

$$\mathcal{J}_j = J h_z \left(\sigma^x_{j-1} \sigma^y_j - \sigma^y_j \sigma^x_{j+1} \right), \tag{2.10}$$

for various values of $h_{x,z}$. The results of the simulations are illustrated in Figs. (2.5,2.6) for different fields and times. As it is possible to see, in both the "strong" ($h_x \gg h_z$) and "weak" ($h_x < h_z$) confinement regime, energy transfer between the two halves of the chain is *suppressed* even at late times. The main dynamical

[2] We will quantify precisely the entanglement entropy growth in a successive section of this chapter.

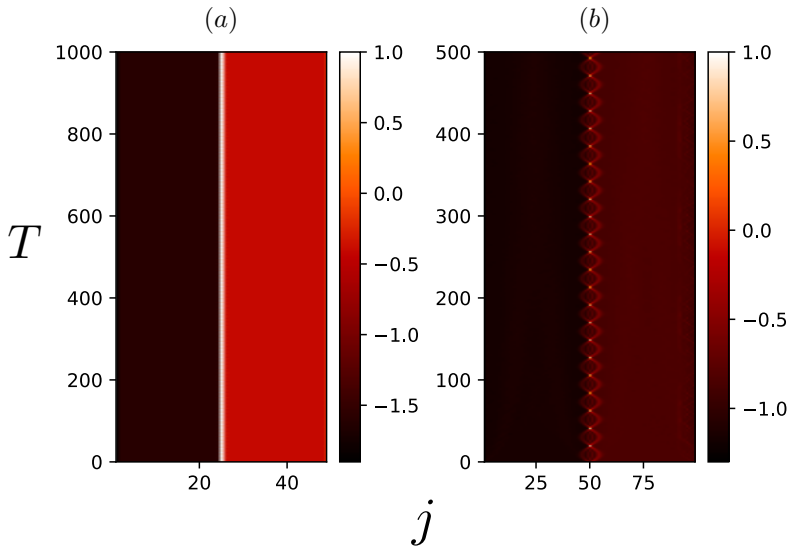

Figure 2.6: Evolution of the energy density for long times. Until moderate high times $t = 10^3 J^{-1}$ and $t = 5 \cdot 10^2 J^{-1}$ nothing happens. This means that the time scales associated with the thermalization, in this setup are extremely long. In panel (a) $L = 50$, $h_z = 0.2$, $h_x = 0.6$, in panel (b) $L = 100$, $h_z = 0.4$, $h_x = 0.15$.

effect of switching on h_z is given by pronounced oscillations of the profiles around the position $j = L/2$ of the junction, with characteristic emergent amplitudes and frequencies which depend on the values of the fields. In particular, the energy current density is zero everywhere apart around the junction, where it oscillates between positive values (aligned with the energy gradient) and negative values (against the energy gradient). We emphasize that, within our protocol, an increase in the energy gradient between the two halves, caused by a stronger h_x, does not result in the activation of transport: on the contrary, it turns out that the oscillations at the junction acquire an even smaller amplitude (see Fig. (2.5) from top to bottom and panel (a) of Fig. (2.6)).

The oscillations of the profiles shown in Figs. (2.5,2.6) may be interpreted as the quantum motion of the isolated kink initially localized at the junction, triggered by the transverse field $h_z \neq 0$. In fact, the kinetic energy associated with this motion has a finite bandwith $\sim h_z$ on the lattice, and therefore, because of energy conservation, the kink quasi-particle can travel, in the linear confining potential $V(l) \sim -h_x l$, at most a distance $l_{\text{conf}} \sim h_z/h_x$ (confinement length scale), before bouncing back and oscillating. This phenomenon is analogous to the Wannier-Stark localization of electrons in a one-dimensional crystal subject to a constant electric field [81]. In order to rationalize the above intuition and make a quantitative treatment of the evolution of the profiles, we propose a simple analytical approach based on dressing the meson quasi-particles perturbatively

in the transverse field $h_z \ll J$, with arbitrary h_x[3]. We stress, again, that this regime differs from the one $h_x \ll J$, $h_z < J$, of validity of the semiclassical technique of Ref. [76]. The approximation consists in neglecting the creation of new quasi-particles, which, in our setup, only affect the quantum fluctuations in the two homogeneous bulks away from the junction, as recognized in Refs. [77, 76]. In fact, we show that the dynamics at the junction is very well captured within this scheme up to moderate values of h_z. In the spirit of an effective quasi-particle description of mesons [82], we map the motion of the isolated kink onto the problem of a *single quantum particle* hopping on a one-dimensional lattice, by projecting the many-body Hilbert space onto the single-kink linear subspace. This $L-1$-dimensional subspace is spanned by the states $\{|n\rangle\}$ with a single domain-wall located between sites n and $n+1$, with $n = 1, 2, \ldots, L-1$., i.e.,

$$|n\rangle = \bigotimes_{i=1}^{n} |\uparrow\rangle_i \bigotimes_{i=n+1}^{L} |\downarrow\rangle_i \quad \text{with} \quad n = 1, 2, \ldots, L-1. \tag{2.11}$$

For simplicity we assume $h_x > 0$, such that the single "meson" in the state $|n\rangle$ is given by a block of $L-n$ spins reversed with respect to the longitudinal field direction x. Note that the initial state $|\Psi_0\rangle$ in Eq. (2) of the main text corresponds to $|L/2\rangle$. These states are eigenstates of the Hamiltonian $H(0, h_x)$,

$$H(0, h_x)|n\rangle = [2J + 2(L-n)h_x + E_{\rm GS}]|n\rangle, \tag{2.12}$$

where the ground state energy $E_{\rm GS} = -J(L-1) - h_x L$ of $H(0, h_x)$ is an additive constant which we neglect in what follows. The transverse field h_z provides a kinetic energy to the kinks and, as a matter of fact, it allows transitions from the state $|n\rangle$ to states $|n \pm 1\rangle$: since $\sigma_j^z|\uparrow\rangle_j = |\downarrow\rangle_j$ (and $\sigma_j^z|\downarrow\rangle_j = |\uparrow\rangle_j$), one has

$$(V)_{nm} = -h_z \delta_{n,m+1} - h_z \delta_{n,m-1}, \tag{2.13}$$

where as V here we denote the perturbation proportional to h_z, i.e. $V = -h_z \sum_{i=1}^{L} \sigma_i^z$ in (2.1). Therefore, the effective Hamiltonian $H^{\rm eff}$ governing the evolution of the system in the single-kink subspace reads

$$\left(H^{\rm eff}\right)_{nm} = [2J + 2(L-n)h_x]\, \delta_{n,m} - h_z(\delta_{n,m+1} + \delta_{n,m-1}), \tag{2.14}$$

This Hamiltonian can be exactly diagonalized in terms of Bessel functions (see Appendix (A)). Let us note that the off-diagonal perturbation produces an effective hopping amplitude for the kink quasi-particle. Accordingly, this effective

[3]Note, however, that resonances occur at particular values of h_x, commensurate with $2J$. Correspondingly, it costs no energy to break a single meson into multiple mesons by flipping individual spins. These transitions cause quantitative but not qualitative modifications to the evolution of the energy profile, which are not captured by the single-kink subspace projection discussed here. Evidence of this aspect will be discussed later.

Hamiltonian $H^{\rm eff}$ describes the dynamics in terms of a single particle hopping in a one-dimensional lattice in the presence of a linear potential, where the state of the particle is described by a vector $\{\psi_n\}$ with $n = 1, 2, \ldots, L-1$. The absolute value squared of the n-th component of the wavefunction $\psi_n(t)$ is equal to the probability that the particle is at site n at time t. Within this picture, the initial state in Eq. (2.8) maps to $\psi_n(0) = \delta_{n,L/2}$, corresponding to a particle completely localized at the junction between the two chains. Similarly, the magnetization $\langle\sigma^x_j(t)\rangle$ at site j and time t can be expressed within this single-particle picture as

$$m_j(t) \equiv 1 - 2\sum_{n=1}^{j-1} |\psi_n(t)|^2, \tag{2.15}$$

where $\psi_n(t) = \sum_m (\exp(-iH^{\rm eff}t))_{nm}\psi_m(0)$ is the time evolved state within the projected space. In order to test the accuracy of our approximation, we compare the dynamics obtained from the above effective single-particle problem with the exact dynamics generated by H (see Eq. (2.1)) in the full many-body Hilbert space, starting from the domain-wall initial state $|\Psi_0\rangle$ of Eq. (2.8) as obtained via both exact diagonalization (ED) and TEBD techniques [4]. The comparison between $m_{L/2}(t)$ and $\langle\sigma^x_{L/2}(t)\rangle$ is shown in Fig. 2.7. In particular, we observe that the agreement is fairly good up to moderate values of the transverse field $h_z < 0.4J$. Similarly, the relevant non-equilibrium profiles of the energy and energy current densities can be studied within the above effective single-particle description. This is achieved by projecting the energy density $\mathcal{H}_j$ at site j in Eq. (2.9) onto the single-kink subspace,

$$\begin{aligned}\left(\mathcal{H}^{\rm eff}_j\right)_{nm} = \frac{1}{2}\left[J(2\delta_{j,n}-1) - h_x \mathrm{sgn}(n-j)\right]\delta_{n,m} \\ - \frac{h_z}{2}\left(\delta_{j,m+1} + \delta_{j+1,m+1}\right)\delta_{n,m+1} + (m \leftrightarrow n),\end{aligned} \tag{2.16}$$

where the sign function $\mathrm{sgn}(x)$ equals 1 for $x > 0$, -1 for $x < 0$ and 0 for $x = 0$. From the continuity equation

$$\frac{d\mathcal{H}^{\rm eff}_j}{dt} = i[H^{\rm eff}, \mathcal{H}^{\rm eff}_j] = \mathcal{J}^{\rm eff}_j - \mathcal{J}^{\rm eff}_{j+1}, \tag{2.17}$$

we can infer the corresponding effective expression for the energy current density operator $\mathcal{J}_j$ at site j, i.e.,

$$\begin{aligned}\left(\mathcal{J}^{\rm eff}_j\right)_{nm} = 2iJh_z\delta_{n,m+1}\,\delta_{m,j-1} \\ - \frac{i}{2}h_z^2\delta_{m,j-2}\,\delta_{n,m+2} - \frac{i}{2}h_z^2\delta_{m,j-1}\,\delta_{n,m+2} \\ - (m \leftrightarrow n)\end{aligned} \tag{2.18}$$

[4] In this case, the simulations based on exact diagonalization of the Hamiltonian can be pushed until unexpected long times because finite-size effects such as revivals are suppressed, due to the fact that excitations are confined [77]

Note that the energy current $\mathcal{J}_j^{\text{eff}}$ obtained in this way differs from the one which would have been obtained by projecting directly the current operator in Eq. (2.10) on the single-kink subspace, with an analogous prescription as the one followed above for $\mathcal{H}_j^{\text{eff}}$. In fact, this procedure would have led to

$$(\widetilde{\mathcal{J}}_j)_{nm} = 2iJh_z\delta_{n,m+1}\delta_{m,j-1} + \text{h.c.}, \tag{2.19}$$

which differs from $\mathcal{J}_j^{\text{eff}}$ in Eq. (2.18) by terms of order h_z^2. However, in the regime of validity of our approximation scheme, corresponding to $h_z \ll J$, terms of order h_z^2 are negligible and there is actually no difference in using both definitions. The time-dependent expectation value of the energy density at site j within this single-particle picture can therefore be written as

$$e_j(t) \equiv \sum_{n,m} \psi_n^*(t) \left(\mathcal{H}_j^{\text{eff}}\right)_{nm} \psi_m(t), \tag{2.20}$$

with an analogous expression for the current $j_j(t)$, in terms of $\mathcal{J}_j^{\text{eff}}$.

In Figs. (2.8,2.9) we compare the time evolution of $e_{L/2}(t)$ and $j_{L/2}(t)$ with the corresponding exact quantities $\langle \mathcal{H}_{L/2}(t)\rangle$ and $\langle \mathcal{J}_{L/2}(t)\rangle$ as obtained from the TEBD simulations. (One can show that the spectrum of the effective Hamiltonian (2.14) consists of multiples of $2h_x$, which results in exactly periodic behavior of the blue lines in Figs. (2.8,2.9). It is remarkable that, in spite of the simplicity of this approach, the agreement is excellent for small values $h_z = 0.2J$ of the transverse field, whereas for larger values $h_z = 0.4J$, small quantitative discrepancies appear, still retaining a fairly good qualitative agreement.

Let us briefly discuss the range of applicability of this single-kink approximation and the limitations of its quantitative predictability in some special *fractal* points that we call *resonances*. As outlined before, we focus on the dynamics generated by $H(h_z, h_x)$ in Eq. (2.1), within a perturbative expansion for $h_z \ll J$. Let us first discuss the structure of the spectrum of the unperturbed Hamiltonian $H(h_z = 0, h_x)$. Its eigenstates can be written in terms of the eigenvectors $|\uparrow\rangle = \frac{1}{\sqrt{2}}(1,1)$, $|\downarrow\rangle = \frac{1}{\sqrt{2}}(1,-1)$ of the Pauli matrix σ^x. Examples of these eigenstates are reported in Fig. (2.10), where the various arrows correspond to the lattice sites of the chain. In particular, the ground state $|GS\rangle$ of $H(0, h_x)$ is

$$|GS\rangle = |\uparrow\uparrow \ldots \uparrow\uparrow\rangle \tag{2.21}$$

for $h_x > 0$ (a similar analysis can be done for $h_x < 0$). The energy levels $E(k, l)$ of the excited states can be characterized by two quantum numbers, namely the total number k of kinks (or domain-walls) and the total number l of reversed spins (i.e., arrows pointing downward), as

$$E(k, l) = E_{\text{GS}} + 2Jk + 2h_x l, \tag{2.22}$$

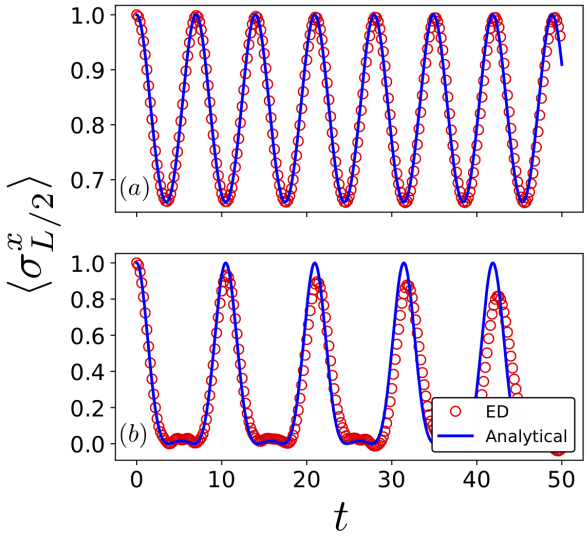

Figure 2.7: Comparison between the numerical results $\langle \sigma^x_{L/2}(t) \rangle$,(symbols), and the analytical predictions $m_{L/2}(t)$, for the magnetization at the junction $j = L/2$, as obtained from ED (with $L = 16$) and from the effective single-particle model, respectively. These curves refer to $h_x = 0.45$, $h_z = 0.2$ (top row), and $h_x = 0.3$, $h_z = 0.4$ (bottom row). (Units are fixed such that $J = 1$.) Note that discrepancies between symbols and solid lines appear as time increases, due to the neglected multi-kink processes. The associated time scale, however, increases upon decreasing h_z.

with $E_{\rm GS} = -J(L-1) - h_x L$. Note that the corresponding eigenspaces are highly degenerate, because energy is unchanged upon separately shifting each domain with consecutively reversed spins ("meson") by arbitrary distances, retaining the same number of kinks k. Given this structure, we can pictorially arrange the energy levels of the excited states in bands labelled, e.g., by the number k of kinks, as reported in Fig. (2.11). When the perturbation

$$V = -h_z \sum_{i=1}^{L} \sigma_i^z \tag{2.23}$$

is switched on, transitions between states $|k, l\rangle$ and $|k', l'\rangle$ become possible, where $|k, l\rangle$ ($|k', l'\rangle$) denotes a representative state in the eigenspace identified by k and l

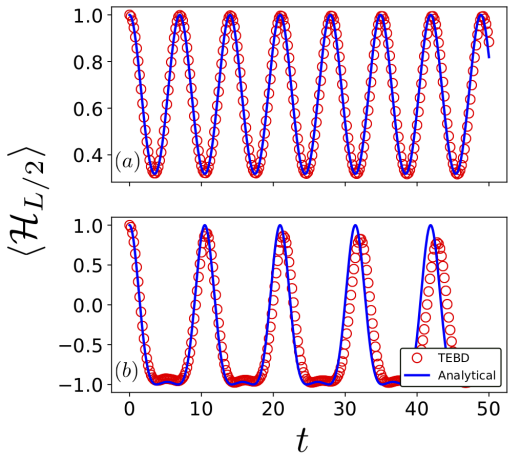

Figure 2.8: Comparison between the numerical results $\langle \mathcal{H}_{L/2}(t) \rangle$ (symbols), and the analytical predictions (solid lines). Same values of Fig.(2.7).

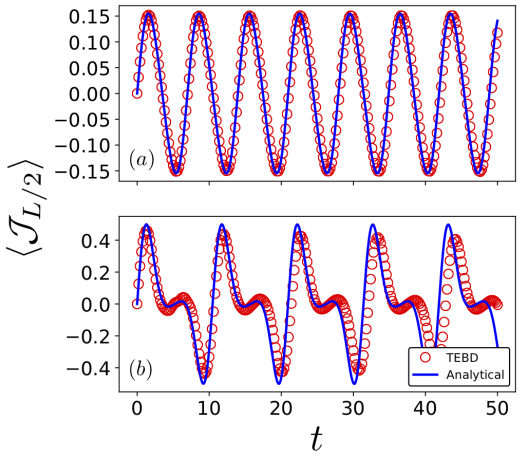

Figure 2.9: Comparison between the numerical results $\langle \mathcal{J}_{L/2}(t) \rangle$ (symbols) and the analytical predictions (solid lines). Same values of Fig.(2.7).

(k' and l'). For the single-kink ($k = 1$) initial states considered in the main text, the possible transitions occurring up to the first order in h_z are schematically shown in Fig. (2.11). In particular, they change l by one, while k can either remain constant or increase by two (in this discussion, for simplicity we disregard spin flips occurring at the boundary of the chain), i.e.,

1. $|k, l\rangle \to |k, l \pm 1\rangle$;
2. $|k, l\rangle \to |k + 2, l \pm 1\rangle$.

At the first order in perturbation theory, the associated long-time transition amplitudes are proportional to the matrix element $\langle k', l' \,|\, V \,|\, k, l \rangle$ of the perturbation

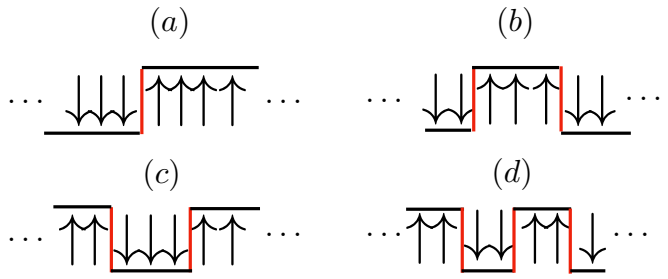

Figure 2.10: Schematic representation of some excited states of $H(h_z = 0, h_x)$, where the arrows indicate the eigenvectors $|\uparrow\rangle$, $|\downarrow\rangle$ of σ^x at the various lattice sites of the chain while the red vertical bars indicate the occurrence of domain-walls or kinks.

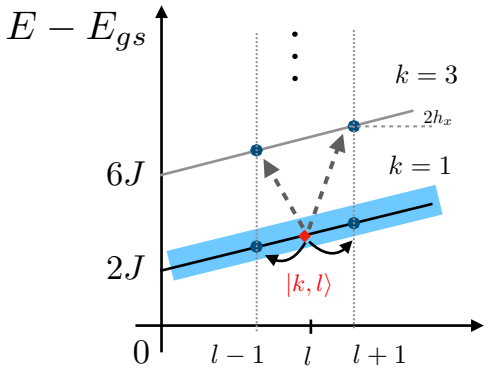

Figure 2.11: Energy spectrum $E - E_{\rm GS}$ of the excited states of $H(h_z = 0, h_x)$. From the initial state $|k, l\rangle$ marked in red, belonging to the single-kink ($k = 1$) band shaded in blue, the allowed transitions at first order in h_z are indicated by the various arrows and they correspond to single spin flips. If $h_x \ll J$, the transitions (dashed arrows) occurring outside the single-kink band are suppressed with respect to those (solid arrows) occurring within it.

between the two states divided by their energy difference $E(k', l') - E(k, l)$ (see, e.g., Ref. [21]), i.e., to

1. $h_z/(\pm 2h_x)$;
2. $h_z/(4J \pm 2h_x)$.

For $h_x \ll J$, the probability amplitude of process 1 above is much larger than that of process 2. Accordingly, transitions between single-kink states dominate the dynamics, which therefore can be conveniently projected onto the subspace spanned by these states (see Fig. 2.11). If the value of h_x is, instead, comparable to or larger than J, the transitions discussed above are generically suppressed as long as the corresponding energy denominators do not vanish.

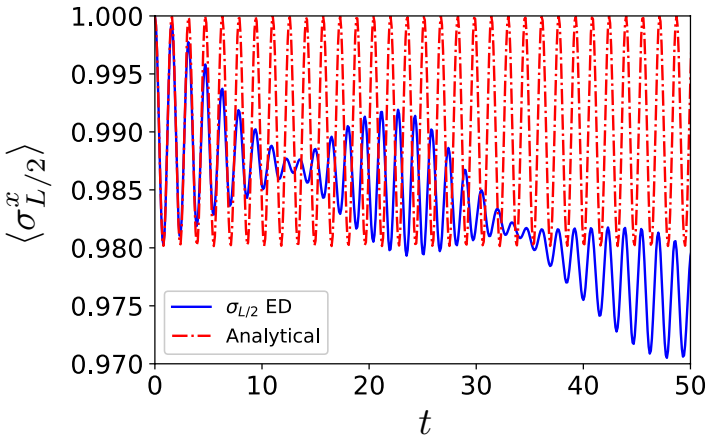

Figure 2.12: Comparison between the numerical data [determined by exact diagonalization (ED) with $L = 16$] of the magnetization $\langle \sigma^x_{L/2}(t) \rangle$ at the junction $j = L/2$ and the corresponding analytical prediction $m_{L/2}(t)$. At variance with what is observed in Fig. 2.7, a qualitative discrepancy emerge between the two curves, due to resonances at first order in perturbation theory. These curves refer to $h_x = 2$ and $h_z = 0.2$, where the units are fixed such that $J = 1$.

2.2.1 Resonant points

The agreement between the effective dynamics within the single-kink subspace discussed in the previous sections and the exact dynamics in the full many-body Hilbert space is fairly good for arbitrary values of h_x/J. However, if h_x and J are commensurable, degeneracies occur in the unperturbed energy spectrum in Eq. (2.22). In particular, this happens when the energies $E(k, l)$ and $E(k', l')$ of two states $|k, l\rangle$ and $|k', l'\rangle$, respectively, are equal, i.e., when

$$E(k, l) - E(k', l') = 2J(k - k') + 2h_x(l - l') = 0. \tag{2.24}$$

If two such states are connected by n spin flips, then resonances occur at the n-th order in perturbation theory, and therefore their effect becomes manifest only at a correspondingly long time scale. For instance, at the first order in h_z, the process 2 above is resonant when $h_x \simeq 2J$. In this case, it costs no energy to break the single initial meson into multiple mesons via single spin flips. During the evolution, a finite density of isolated reversed spins is thus generated, thereby lowering the average local magnetization. Since these states have $k > 1$, they no longer belong to the single-kink subspace and the effective single-particle description employed in the main text is therefore not expected to properly capture the resulting dynamics, as indeed demonstrated in Fig. (2.12). In order to understand if there are qualitative differences in the approach to relaxation and transport properties let us consider a more general initial state, namely a state with two reversed-domains of different length (we will refer often to these reversed

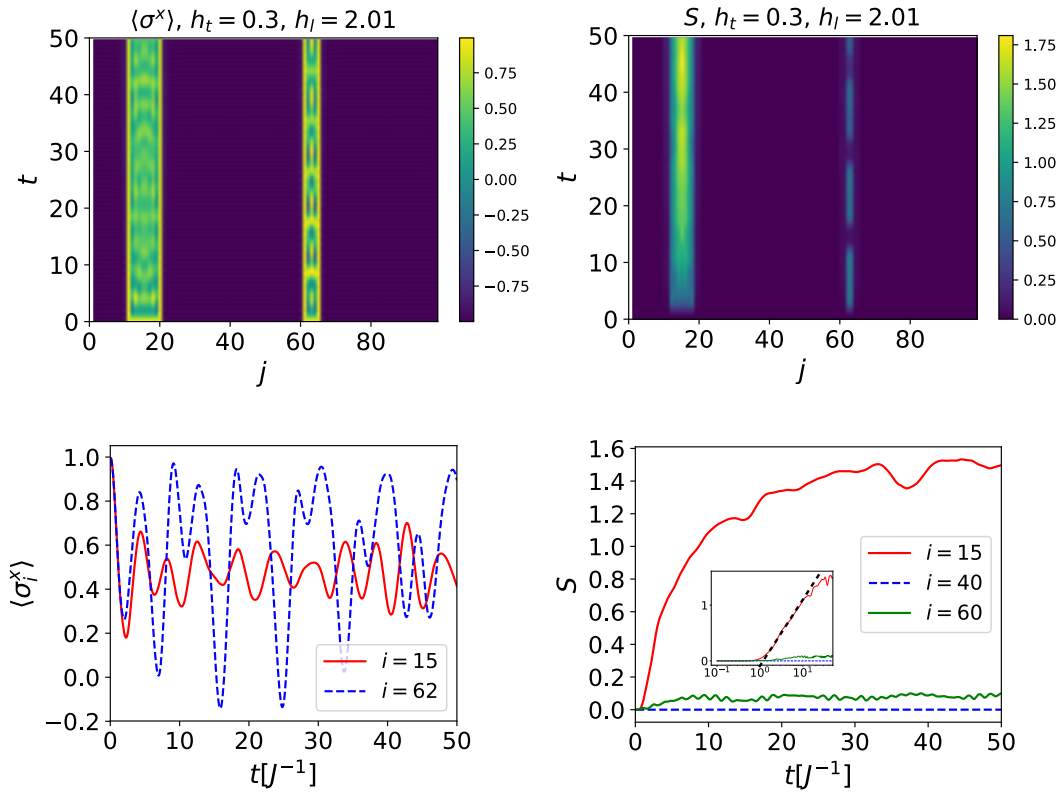

Figure 2.13: TEBD simulations for generic inhomogeneous initial state close to the first resonance $h_x = 2J$. First raw from left to right, density plot of the magnetization and of the bipartite entanglement entropy, the latter is obtained putting the cut on every bond. Second raw, details of the magnetization and of entanglement. In the inset we report the entanglement entropy growth in log-scale on the x axes, there are indications of logarithmic growth of entanglement entropy, this aspect will be treated in the next section.

domains as *strings*). As we can observe from a preliminary analysis in Fig. 2.13 in this case the reversed domains (in yellow) evolve because there is no energetical cost for flipping a spin. This fact implies that we have creation of particles which makes the strings unstable. This phenomenon resembles what usually in high energy theories is referred as *string breaking* connected to the *Schwinger effect* [83, 84, 85], that is the pair creation in the vacuum in the presence of an external field, recently studied numerical in similar setups [86]. This fact is not a coincidence, indeed, we can imagine that the decay of the false vacuum in our case happens in a similar way, through the creation of particles (kink) which lower the external field (linear potential in the string). We must keep in mind, however, that the Schwinger effect was introduced in field theories; the effect of discretization is usually absorbed in the coupling constants of the lattice models and this results in a hard quantitative comparison.

The fact that the strings are evolving is evidenced also by the value of entangle-

ment entropy inside the them which results to be higher with respect to outside. The surprising (and not yet understood) fact is that also in this case the transport is still *completely suppressed*. Therefore, although producing new particles has a zero cost in terms of energy, they do not propagate. This implies that the inhomogeneities of the initial state persist also when string breaking occurs.
The time evolution of this system at resonant points strongly depends on the initial state, in particular, there is a peculiar initial configuration in which it is no longer true that the dynamics is essentially *frozen*, nevertheless also in this case no thermalization is observed. Let us consider as initial state a Néel state that, in terms of the local spins is written as

$$|\Psi_0\rangle = \bigotimes_{i=1}^{L-1} |\uparrow\rangle_i |\downarrow\rangle_{i+1} \tag{2.25}$$

in this case the magnetization presents a weird time behavior, as reported in Fig. 2.14, in fact the only effect of the time evolution are coherent oscillations between the two Néel ordered states. This fact was observed for the first time

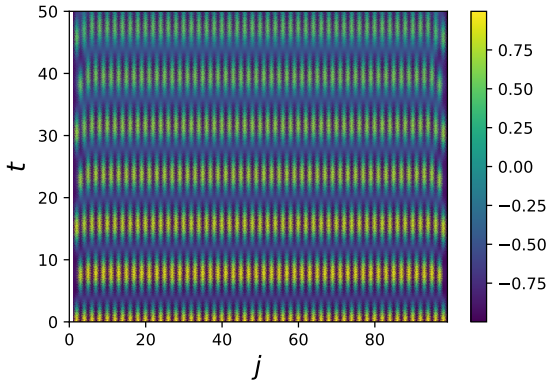

Figure 2.14: Time dependent magnetization starting from a Néel ordered state at the first resonance $h_x = 2J$. Coherent oscillations between Néel and anti-Néel states are observed, in this case the state is not frozen but there is still a lack of thermalization.

in an experiment in 2013 [87] but it has very recently drawn the attention of the community [88, 89]. It is, possible to show that Ising Hamiltonian (2.1) at the first resonance $h_x = 2J$ in the limit $h_z \ll 1$ can be mapped, using a Schrieffer-Wolf transformation, in the so-called *PXP-model* described by a *locally* constrained Hamiltonian

$$H = \sum_i P_i \sigma_i^x P_i, \qquad P_i = \frac{1 - \sigma_i^z}{2}, \tag{2.26}$$

that is a special case of the Fendley-Sachdev-Sengupta (FSS) model [90, 91]. In this case the mechanism behind the slow-thermalizaion is completely different

and it is related to the existence of a special band of states which violate ETH (*quantum scars*). This phenomenon can be actually viewed in a complementary way by means of gauge theories [92]. This topic will be extensively explored in the second part of this thesis, we decided to make a small anticipation in order to show how these two phenomena are inter-connected.

2.2.2 Generality of the phenomenon

Hitherto we have analyzed the effects of confining interactions in systems that can be described by Ising Hamiltonian in a longitudinal field (2.1), however, as we have stated at the beginning of this chapter, this phenomenon can be observed in large class of systems. In this section we report some results concerning the effects of confinement in anti-ferromagnetic XXZ chain in a longitudinal staggered magnetic field, described by the Hamiltonian

$$H_{XXZ} = \tilde{J}\sum_{i=1}^{L-1}(S_i^x S_{i+1}^x + S_i^y S_{i+1}^y + \Delta S_i^z S_{i+1}^z) - h\sum_{i=1}^{L}(-1)^i S_i^z, \tag{2.27}$$

where $S_i^\alpha = \frac{1}{2}\sigma_i^\alpha$. Let us note that in this case the magnetization is conserved, in fact we have

$$[H_{XXZ}, S_i^z] = 0.$$

Hamiltonian (2.27) has a phase transition when $\Delta/\tilde{J} = 1$, for $\Delta/\tilde{J} > 1$ the ground state has an anti-ferromagnetic axial order, instead for $-1 < \Delta/\tilde{J} < 1$ it presents planar order, this model for $h = 0$ was exactly solved by Yang and Yang using Bethe ansatz [93]. In the ordered phase[5] the excitations can be described by kinks, as the Ising model in the ordered ferromagnetic phase ($h_z < J$). The "Ising limit" is, in fact, recovered when $|\Delta| \gg 1$. As we have seen in the previous chapter, Hamiltonian (2.27) describes with a good approximation the intra-chain interactions in $SrCo_2V_2O_8$ crystals [67, 23], in this case the external staggered magnetic field is given by the average effect of the inter-chains interactions. In Refs. [94, 67], the masses of the first bound states are computed, using semi-classical and perturbative approximations, and an almost perfect match with the experimental data, obtained with neutron scattering, is found. However, we are interested in the investigation of the dynamical properties in non-equilibrium, as we have done for the Ising model in longitudinal field. For this purpose let us stick in the $\Delta > 1$ sector, where the ground state is Néel-ordered. In the limit $\Delta \gg 1$ the ground state, twofold degenerate, is well approximated by the Néel

[5] For $\Delta/\tilde{J}$<-1 the ground state has ferromagnetic order. We will discuss the anti-ferromagnetic case for experimental relevance [67, 23] however the same arguments apply for the ferromagnetic case without the staggerization of the external field.

($|N\rangle$) and the anti-Néel ($|AN\rangle$) states

$$|N\rangle = \bigotimes_{i=1}^{L/2} |\uparrow\rangle_i|\downarrow\rangle_{i+1} \qquad |AN\rangle = \bigotimes_{i=1}^{L/2} |\downarrow\rangle_i|\uparrow\rangle_{i+1}. \tag{2.28}$$

Kinks interpolate between these two vacua and for $h = 0$ they have no long-range interactions. If we switch-on an external staggered magnetic field the spectrum changes in a non-perturbative way. In particular, the two vacua are no longer degenerate, one is the true vacuum and the other the false vacuum laying in the middle of the spectrum. In this case the quasi-particle excitations feel a long-range confining potential, as sketched in Fig. **??**. In order to study the dynamics,

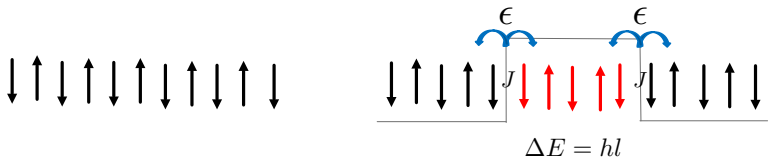

Figure 2.15: Sketch of the origin of confinement in XXZ Hamiltonian in a staggered external magnetic field, described by Eq. (2.27).

let us rewrite Hamiltonian (2.27), defining $J = \tilde{J}/\Delta$ and $\epsilon = 1/\Delta$, as

$$H_{XXZ} = J \sum_{i=1}^{L-1} S_i^z S_{i+1}^z + \epsilon(S_i^x S_{i+1}^x + S_i^y S_{i+1}^y) - h \sum_{i=1}^{L} (-1)^i S_i^z. \tag{2.29}$$

We fix $J = 1$ and we consider $\epsilon < 1$ in order to be in the anti-ferromagnetic phase. We consider as initial state a combination of Néel and anti-Néel states, we can define this as an "anti-ferromagnetic domain-wall"

$$|\Psi_0\rangle = \bigotimes_{i=1}^{L/2-1} |\uparrow\rangle_i|\downarrow\rangle_{i+1} \bigotimes_{i=L/2+1}^{L-1} |\downarrow\rangle_i|\uparrow\rangle_{i+1}, \tag{2.30}$$

and we study the evolution of the staggered magnetization, i.e. $S^z_{j,stagg} = (-1)^j S^z_j$. In Fig. 2.16 we report the space-time density plot of the staggered magnetization. As we can observe there is a radical change in the transport properties when the external staggered magnetic field is turned on. In particular, for $h = 0$ we can observe a diffusive transport between the two halves, but for $h \neq 0$ we have an oscillating behavior. This effect, analogously to what already observed in the Ising model, is caused by the confining nature of the long-range interaction. It is interesting to note that the frequency of oscillation ν, also in this case, is proportional to the external magnetic field strength $\nu \propto h$. The similarity with the Ising case can be pushed forward observing the dependence of the confinement length l_{conf} on the parameters of the Hamiltonian (2.29). In Fig. 2.17, in fact, we can observe

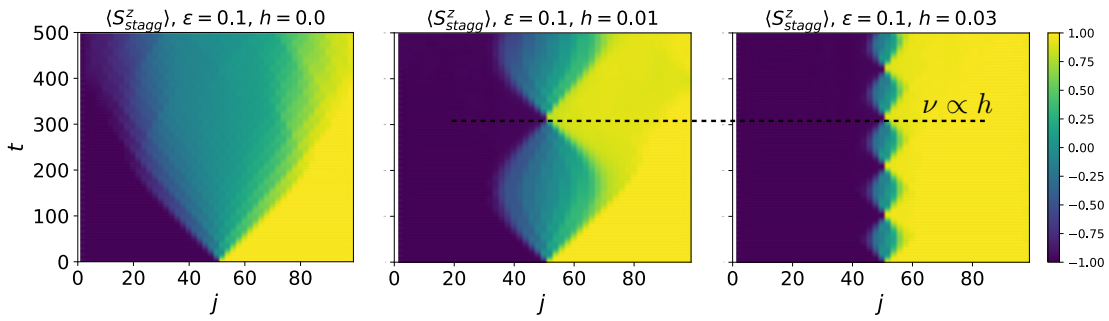

Figure 2.16: TEBD simulation of the staggered magnetization starting from an antiferromagnetic domain wall defined in Eq. (2.30). For $h = 0$, there is diffusion, as expected for interacting models. As soon as we switch an external confining field there is a strong change in the behavior of the system, we observe the same qualitative features already observed in the Ising model with longitudinal external field.

that $l_{conf} \propto \frac{\epsilon}{h}$, that is the same relation found earlier in the Ising case upon the substitution $h_x \to h$ and $h_z \to \epsilon$. We can observe as in this case the system is extremely sensitive to the parameter ϵ that is proportional to the inverse mass of the quasi-particles. Indeed, as we increase ϵ toward the Heisenberg isotropic limit ($\epsilon = 1$), the false vacuum becomes more unstable and the thermalization process is enhanced. We expect that in the planar phase ($|\epsilon| > 1$), in which the excitation are massless, the effect of the confinement disappears, however numerical simulations in this regime are extremely computationally demanding. The effect of the confinement can be also quantified investigating the entanglement entropy growth. In particular from the average time-dependent entanglement entropy, defined as $S_{avg} = \sum_i S_i/L$ with S_i the entanglement entropy computed across the boundary at site i, for several values of h, we can observe (Fig. 2.18) as until a given t^* there is essentially no difference in the time evolution of the system, as evidenced by the fact that the curves are almost perfectly overlapped. This time t^* is related to the confinement length, indeed $t^* = l_{conf}/v_{max}$, where v_{max} is the maximum velocity of the quasi-particles excitations. Also in this case the oscillations of the kink in the middle can be viewed as Bloch-oscillations and studied analytically considering an effective Hamiltonian obtained projecting (2.29) onto the one-kink subspace (see Appendix (A)).

2.3 General characterization of slow-dynamics

In this section we want to analyze some general features about slow dynamics in the class of systems with confinement, and we characterize it quantitatively by giving a lower bound on the thermalization time and predictions concerning entanglement entropy growth [95]. We will furthermore discuss (in the last sec-

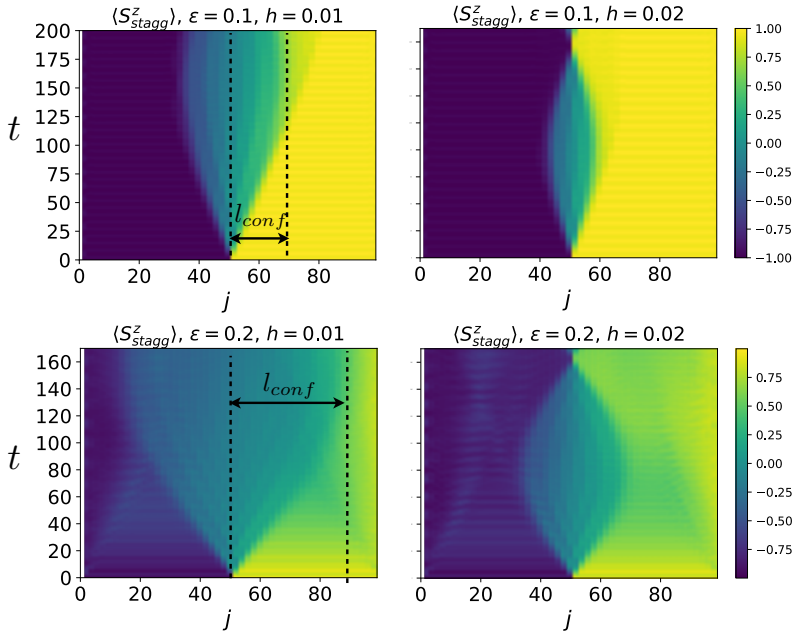

Figure 2.17: Dependence of the confinement length on the parameters h and ϵ of Hamiltonian (2.29).

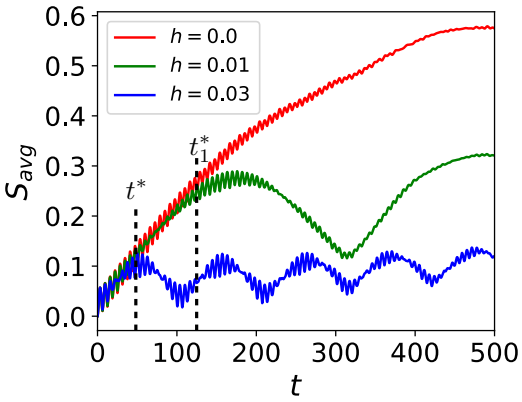

Figure 2.18: Average entanglement entropy growth, starting from initial state defined in Eq. (2.30) and evolving with Hamiltonian (2.29), for different values of h.

tion of Chapter 4) how this problem can be related exactly with *string-breaking* phenomena in lattice gauge theories (LGTs); it is possible to show how, in one-dimension, statistical models with confining potential can be viewed as matter-integrated abelian LGTs. For this reason we will refer henceforth to kinks as particles, bound states of kinks as *mesons*, and long domain of reversed spins as *strings*.

Let us preliminarly show a quite remarkable fact concerning the time-evolution of the "false-vacuum" of Hamiltonian (2.1). The problem of the false vacuum

decay in such systems was already treated in Ref. [80] in the scaling regime, i.e. ($h_x \approx 1$), however, the dynamics of the bipartite entanglement entropy has never been investigated. In particular, what happens in the long transient phase in which the false vacuum is stable and how it depends on the size of the system. These questions are of relevant importance because the false vacuum lies in the middle of the spectrum of the Hamiltonian (2.1), therefore it is a *high-temperature* state in a non-integrable system so we expect that it should behave as a thermal state. We thus consider time evolution starting from $|\Psi_0\rangle = \bigotimes_{i=1}^{L} |\uparrow\rangle_i$ and we let it evolve with the Hamiltonian (2.1) with, $h_x < 0$. In this case the initial

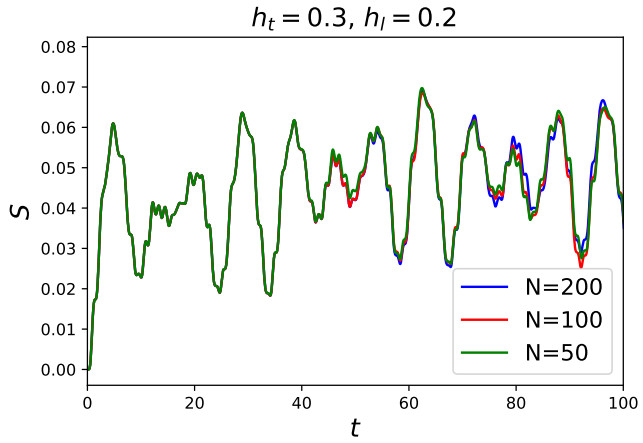

Figure 2.19: Time evolution of the bipartite entanglement entropy in the false vacuum. It is possible to see how the constant value reached is system size independent, at least for a very long transient time. This fact seems to suggest the existence of *area-law* high energy states also in this system.

state is very close to the false vacuum of the theory and it can be written as superposition of high energy states. In Fig. 2.19 we report the result of TEBD simulations for different sizes of the system. It is possible to observe that the value of the entanglement entropy is constant and independent of the system size, this means that there is at least one high-energy state of (2.1) which shows area-law of entangelement entropy. Physically it is clear why this happens: the quasi-particles produced during the quench do not propagate, and the only contribution to the entanglement growth is given by the ones produced close to the cut of the system. An interesting point is understanding whether the stability of these states is something that survives at infinite time [96, 97], thus representing a violation to eigenstate thermalization hypothesis, or if it is possible to associate a time-scale for thermalization in this setup.

In order to rationalize this concept let us be more quantitative and let us consider separately all the different processes that could eventually lead to thermalization.

There essentially three different processes that take part to the thermalization of the system: *string breaking* and production of mobile mesons, *quantum diffusion* of small mesons, scattering processes between the particles which lead to the creation of mobile mesons. Each of this process is dominant for a given range of parameters. The Hamiltonian of a generic spin system with confinement can be cast in the following form:

$$H = m \cdot H_{\text{mass}} + g \cdot H_{\text{motion}} + h \cdot H_{\text{int}}, \tag{2.31}$$

the precise meaning of every term in (2.31) will be clearer after that we will have explained the relation with LGTs. However for the Ising model with longitudinal field (2.1) we have

$$m \cdot H_{\text{mass}} = J \sum_{i=1} \sigma_i^x \sigma_{i+1}^x \tag{2.32}$$

$$g \cdot H_{\text{motion}} = h_z \sum_i \sigma_i^z \tag{2.33}$$

$$h \cdot H_{\text{int}} = h_x \sum_i \sigma_i^x. \tag{2.34}$$

In what follows we will focus our attention on two type of initial states, namely, "string-states" that are states with a string of length l in the middle and "many-particle states" that are states in which there is a particle every l sites, in the latter case $p = 1/l$ can be interpreted as a chemical potential for the kinks. Furthermore, for sake of simplicity, we will hencefort consider the prototypical case of Ising model in longitudinal field (2.1), however, the results hold in general. It is important to point out that the parameter p is of primary importance in the thermalization, in fact for $p > 0.5$ states with many particles close to each other are no longer "rare-states" and scattering processes eventually take the system toward an equilibrium state smoothing out any initial inhomogeneity, as shown in Fig. 2.20. The value of the chemical potential at which thermalization starts to occur in the usual way is related to the confinement length. In fact, when the average distance among the particles $l_{avg} = 1/p$ is comparable with the confinement length $l_{conf} \approx g/h$ we observe thermalization. In order to avoid to be in such situation, in which the thermalization process is trivially explained, when we will deal with multi-particles states we will consider the parameters such that $l_{conf} \gg l_{avg}$, that is in the Ising case $ph_z \gg h_x$.

Let us first analyze first the *string-breaking* mechanism which is the way through which states with big strings, as the one reported in Fig. 2.1, may thermalize. We are interested in the regime in which the mass term is the biggest scale of the system, i.e. $m \gg h, g$. In this regime the effect of string breaking is suppressed and it is possible to perturbatively expand the Hamiltonian in series

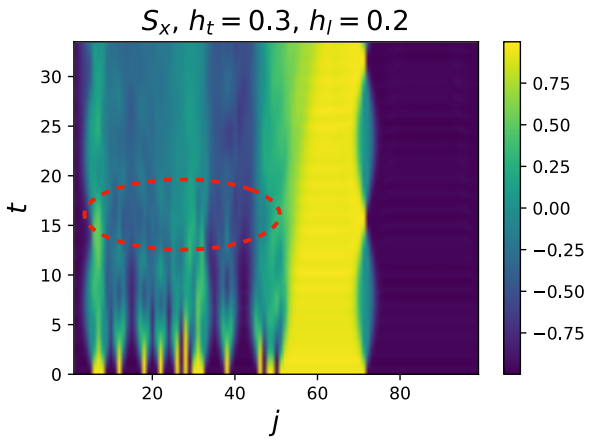

Figure 2.20: Example of thermalization by scattering with $p \approx 0.5$. In the circled region we see how the initial inhomogeneity is rapidly smoothed out.

of $1/m$. Ergodicity would prescribe the meltdown of the inhomogeneity by means of creation of particles inside the string. However, in order to occur, this process must be energetically possible, meaning that, since the configurational energy in a string is proportional to its length $E_n = hl_{str}$, it can happen only if it is possible to convert this energy (that is nothing but the energy of the gauge field) into a particle-antiparticle pair. This process takes place when $h\dot{l}_{string} \geq 2m$. We assert that strings can break up, but the time-scale with which this happens is *exponentially long* in the parameters of the model. This fact can be rigorously proven by sistematically constructing the effective Hamiltonian governing string dynamics in perturbation theory in the parameter $1/m$. Before doing this let us understand why this phenomenon is slow, as we have already stated, in order to conserve energy, the two particles produced in string breaking must be separated to a distance d such that $hd \approx 2m$, this is a process at the d^{th} order in perturbation theory, therefore if $m \gg h$ we have $d \gg 1$ and the process is unlikely to occur.
Let us now prove this, for this purpose let us split Hamiltonian (2.31) in two parts, H_0, the dominant one proportional to the mass term m, and a potential V. The H_0 part has a block-diagonal structure, each block is labelled by the number of particles and is highly degenerate. The perturbation term V can be further split in $V_{\text{diag}} = H_1$, which accounts for the motion of the particle without creating or destroying them and $V_{\text{offdiag}} \equiv R_1$, that connects different blocks. The off-diagonal term can be eliminated using a proper unitary transformation e^{S_1} that transforms the Hamiltonian as

$$H' = e^{S_1} H e^{-S_1} = H_0 + H_1 + R_1 + [S_1, H_0] + \text{second order}, \quad (2.35)$$

S_1 is an anti-hermitian operator such that $R_1 + [S_1, H_0] = 0$. The resulting effective Hamiltonian $H^{(1)}_{\text{eff}} = H_0 + H_1$ describes the intra-blocks motion until a time that is quadratic in m. This procedure can be generalized to an arbitrary order n upon defining a unitary transformation $e^{S_{\leq n}}$, with $S_{\leq n} = -S^\dagger_{\leq n} = S_1 + S_2 + \cdots + S_n$ which transform the Hamiltonian as

$$H' = e^{S_{\leq n}} H e^{-S_{\leq n}} = H_0 + H_1 + \cdots + H_n + R_{>n} \equiv H^{(n)}_{\text{eff}} + V_{>n}, \quad (2.36)$$

with $[H_j, H_0] = 0$, $\forall j = 1, \ldots, n$. In other words, also in this case $H^{(n)}_{\text{eff}}$ describes motion of particles within each block up to order n dressing the hopping. The operators V_n can be explicitly written in terms of S_k [95].

The crucial point illustrated by Abanin et al. in Ref. [98] is that the magnitude of the term H_n is bounded by $n!$ and that there is an *optimal* point n^* where the truncation of the perturbation series minimizes the error. At this order the inverse of the error gives us an *exponential* bound for the thermalization time in the perturbation strength, for the Ising model in a longitudinal field this can be estimated as

$$h_z t_{\text{sb}} \sim \exp(J/\sqrt{h_x^2 + h_z^2}). \quad (2.37)$$

This is perhaps the most important result of this section, it says that, upon tuning appropriately the parameters, we can ignore string-breaking effects on thermalization up to exponentially long times.

The explicit computation of the effective Hamiltonian order by order is computationally extremely hard because the complexity of all the commutators increases rapidly. For the Ising in longitudinal magnetic field, we report the first two orders that have been manually computed

$$H_0 = -J \sum_j \sigma^z_j \sigma^z_{j+1} \quad (2.38)$$

$$H_1 = -h \sum_j \sigma^z_j - g \sum_j P^\uparrow_{j-1} \sigma^x_j P^\downarrow_{j+1} + P^\downarrow_{j-1} \sigma^x_j P^\uparrow_{j+1} \quad (2.39)$$

$$H_2 = \frac{g^2}{4J} \sum_j + P^\uparrow_{j-1} (\sigma^-_j \sigma^+_{j+1} + \sigma^+_j \sigma^-_{j+1}) P^\uparrow_{j+2} \quad (2.40)$$

$$+ P^\downarrow_{j-1} (\sigma^-_j \sigma^+_{j+1} + \sigma^+_j \sigma^-_{j+1}) P^\downarrow_{j+2} \quad (2.41)$$

$$- P^\uparrow_{j-1} (\sigma^+_j \sigma^+_{j+1} + \sigma^-_j \sigma^-_{j+1}) P^\downarrow_{j+2} \quad (2.42)$$

$$- P^\downarrow_{j-1} (\sigma^+_j \sigma^+_{j+1} + \sigma^-_j \sigma^-_{j+1}) P^\uparrow_{j+2} \quad (2.43)$$

$$- \sigma^z_j \sigma^z_{j+1}. \quad (2.44)$$

$$(2.45)$$

We have seen that if we consider in Eq. (2.31) $m \gg, g, h$ we have a very-long time until which string-breaking processes can not occur and the motion of particles is

controlled by an effective Hamiltonian H_{eff}. Let us characterize the dynamics of the system in this regime, for this purposes let us consider states with only one string, i.e. a particle and an antiparticle. As we have reported in Appendix (A), the single-particle wave function for a particle localize around the site n reads

$$\Psi_j^{(n)} = J_{j-n}(l_{conf}), \tag{2.46}$$

where J_{j-n} is a Bessel function of the first kind. An initial state with many particles localized on different sites can be written as product states of single-particle state. Since the Bessel's functions decay very fast for $|n-j| \gg l_{conf}$, if the average distance between the kinks is greater than the confinement length, i.e. $1/p \gg l_{conf}$, particles keep oscillating around their initial position and thermalization and transport are completely hindered. If instead the average distance between the particles is of the same order of the confinement length the situation is more intriguing. In fact, in this case, the overlap between the orbitals of the particles is no-longer negligible and they interact. Our aim is to quantitatively describe the effects of this interaction. It is important to point out that we are not treating the case in which $1/p \leq l_{conf}$, indeed in that case we would need a scattering theory that we currently lack and whose implementation is not easy. Let us project Hamiltonian (2.1) onto the Hilbert space with only one string, i.e. with a particle on the site n_1 and an antiparticle on the site n_2, the lowest order Hamiltonian, can be split in two parts, diagonal (configurational) and off-diagonal (hopping), also in this case

$$(H_{\text{diag}})_{n_1 n_2, m_1 m_2} = h_x(n_2 - n_1)\, \delta_{n_1,m_1}\delta_{n_2,m_2} \tag{2.47}$$

and

$$\begin{aligned}(H_{\text{hop}})_{n_1 n_2, m_1 m_2} = h_z(&\delta_{n_1+1,m_1}\delta_{n_2,m_2} + \delta_{n_1-1,m_1}\delta_{n_2,m_2} \\ &+ \delta_{n_1,m_1}\delta_{n_2+1,m_2} + \delta_{n_1,m_1}\delta_{n_2-1,m_2}).\end{aligned} \tag{2.48}$$

It is convenient to adopt the relative and center of mass coordinates,$n_\pm = n_1 \pm n_2$. The Schrödinger equation, $H\Psi = E\Psi$, with the ansatz wave function $\Psi_{n_+,n_-}(K) = e^{iKn_+}\psi_{n_-}(K)$, reduces simply to the single particle Wannier-Stark lattice problem, since the dependence from the center of mass coordinate can be factored out,

$$h_x n_- \psi_{n_-} + 2h_z \cos K(\psi_{n_- -1} + \psi_{n_- +1}) = E\psi_{n_-} \tag{2.49}$$

with the condition that $\psi_{n_-=0} \equiv 0$, because $n_- > 0$. The presence of this boundary is of utmost importance in this problem, in fact, particles very distant among each other are not affected by this constraint. In this case the energy levels

are independent of K and hence their band is *flat*, $E_l(K) = h_x l$. This means that large strings, for which $n_- \gg l_{conf}$ do not diffuse, because the motion of the center of mass is related with the group velocity $v_g = \partial E(K)/\partial K = 0$, this fact can be interpreted as these particles are too massive to diffuse. However, for strings whose length is comparable with the confinement length we have a non-zero band curvature. This can be estimated by considering that the modification of the bulk Wannier-Stark wave function around a site $l \geq l_{conf}$ induced by the presence of the hard-wall, is proportional to the wave-function amplitude, i.e.

$$J_l(2g/h) \sim \frac{1}{l!}(g/h)^{2l}. \tag{2.50}$$

This result agrees with the perturbative calculation which states that, in order to move a string of length l we have to destruct and reconstruct the whole string, it is, therefore, a process which occur at the l^{th} order in perturbation theory. The quantum diffusion time-scale, i.e. the time-scale in which the string starts to move as whole, is the inverse of the band curvature, therefore for a general many-particle state with chemical potential p, in which the average particle-particle distance is $1/p$ we have that

$$h_z t_{\text{diff}}(p) \sim \Gamma(1/p)\left(\frac{h}{g}\right)^{2/p}. \tag{2.51}$$

We note that $t_{\text{diff}} \ll t_{\text{sb}}$, therefore, in this regime, this is the most relevant dynamical time-scale of the problem.

We have seen that the single-particle wave functions $J_l(l_{conf})$ are highly localized objects. This picture is extremely similar to what is observed in many-body localization problems (See Chapter 1) it is therefore natural to ask whether the same features concerning suppressed growth of entanglement entropy are observed. Applying straightforwardly the procedure of Ref. [55] we find that the prediction for the time growth of entanglement entropy in a state with chemical potential p, should be

$$S(t) \sim p \log\left(\frac{g^2 t}{h \log(gt)}\right), \tag{2.52}$$

in the regime in which $p \geq h_z$. The correctness of (2.52) is still under numerical investigation a preliminary result is reported in Fig. 2.21. We observe how there is a clear dependence of the slope on p, however relation (2.52) seems to hold only in one case, the reason is that the regime in which it is derived is quite peculiar we must have that $p > h_z$, but $p \ll p^*(h_z, h_x)$ at which the confinement length is of the order of the $1/p$.

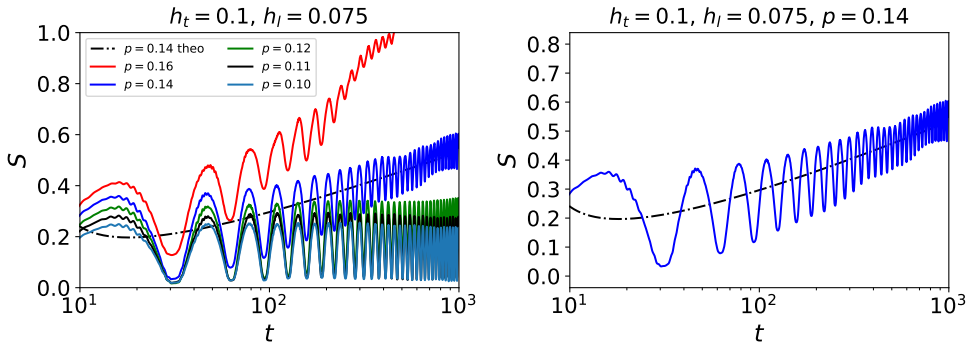

Figure 2.21: Average entanglement entropy for different chemical potential values p. In this case only "regular realizations" are considered, i.e. one particle every $1/p$ sites. In the left panel the comparison between several values of p, in the right panel the comparison between the theoretical prediction of Eq. (2.52) and the simulation for one realization, the only one in this regime in which it works.

CHAPTER 3

SLOW DYNAMICS IN RYDBERG ATOMS CHAINS

In this chapter we introduce the second main topic of this thesis, i.e. slow dynamics arising from energetic constraints that restrict the Hilbert space. As we have pointed out in the previous chapter, in this case we do not observe a *frozen* dynamics that maintains the initial inhomogeneities for extremely long times, but we rather see coherent *long-lived* oscillations between some accessible states. This fact is highly unexpected because the effective theories that describe thesw constrained models are usually non-integrable, i.e. they do not have explicit conservation laws that could give an easy interpretation of non-thermal behavior. Henceforth we will focus the anomalous dynamics observed in some Rydberg atoms setups [88, 87] with the so-called "blockade" constraints, that prevent two contiguous atoms to be both in the Rydberg (excited) state. We show how the effective theoretical model which describe the system, i.e. the "massless" FSS model, sometimes called *PXP*, presents some intriguing properties connected with the recently studied phenomenon of the *quantum scars* [99, 100, 101, 102]. In this chapter we give a brief overview of the last two years of investigation of this model both from experimental and theoretical perspective, in the next one we will show how these phenomena can be connected with some prototypical features of high-energy physics.

3.1 Anomalous dynamics in Rydberg atom chains

Let us start by describing an experiment concerning anomalously slow dynamics observation. The first relevant observation of this phenomenon has been done in 2016 by H. Bernien et al. [88] in Harvard. They prepared a chain of strongly interacting Rydberg atoms trapped in an optical lattice by means of

optical tweezers. This kind of technology is of extreme importance because it enables to construct the setup atom-by-atom and therefore to have an extreme control on it. In Ref. [88] 51 ^{87}Rb atoms, called "qubits" since they mimic a two-levels system, are loaded in a trapping potential, they interact with a repulsive Van-Der-Walls interaction, the Hamiltonian governing the dynamics of the system is a long-ranged Ising one, i.e.

$$\frac{H}{\hbar} = \sum_i \frac{\Omega_i}{2}\sigma_x^i - \sum_i \Delta_i n_i + \sum_{i<j} V_{i,j} n_i n_j \tag{3.1}$$

where, $V_{i,j} = V/|i-j|^6$, $\sigma_x^i = |g_i\rangle\langle r_i| + |r_i\rangle\langle g_i|$ is the operator which connects the ground states and Rydberg states of the atoms, Δ_i is a detuning (mass) term, which is set to zero, $n_i = |r_i\rangle\langle r_i|$ counts the number of excitations (i.e. atoms in the Rydberg state) and Ω_i is the Rabi frequency.

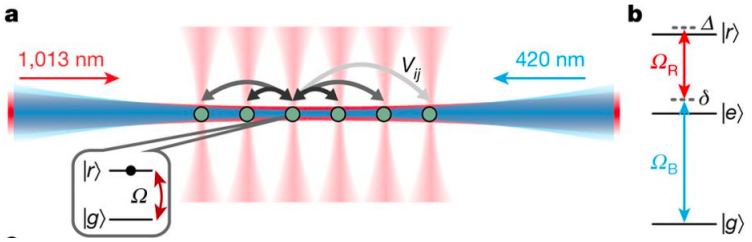

Figure 3.1: Figure from Ref. [88]. Experimental setup, using optical tweezers it is possible to have control at the level of single atom.

The aspect that makes the experiment relevant from our purposes is that the atoms in the trap are strongly interacting, this means that

$$V_{i,i+1} \gg \Delta \gg \Omega \gg V_{i,i+2} \tag{3.2}$$

this regime is formally called "Rydberg blockade". The energetic constraint (3.2) has deep consequences on the dynamics of the system, in fact it *reduces* the number of states that can be explored during the time evolution thus limiting the accessible Hilbert space to the states in which there are no contiguous excitations, i.e. $n_i n_{i+1} = 0$ (see Fig. 3.2). The dynamics of the system in this regime

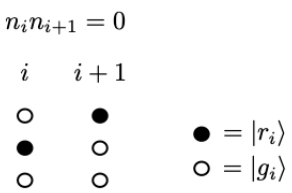

Figure 3.2: Local Hilbert space in the strongly interacting regime (3.2), no contiguous excitations are allowed.

results to be initial-state dependent, meaning that, starting from Néel ordered ($\mathbb{Z}_2$ symmetric) initial states, i.e.,

$$|\Psi_0\rangle = |rgrgrgrgr\ldots\rangle \tag{3.3}$$

persistent oscillations in local observables are observed. In particular in Ref. [88] the number of *defects*, i.e. the number of contiguous atoms in the ground state $|\Psi(t)\rangle = |\ldots gg\ldots\rangle$, as a function of time have been counted. We can clearly

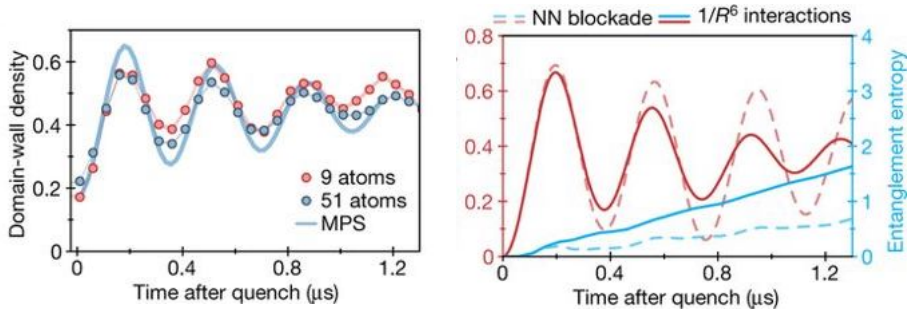

Figure 3.3: Figure from Ref. [88]. Left panel: experimental data for different system sizes. Right panel: numerical simulation both for a *realistic* system, with full interactions and a fully constrained one.

observe (see Fig. 3.3) persistent oscillations and a damping, however the damping in the actual experimental data is given by the fact that it is not possible to set $V_{i,i+j} = 0\ \forall j \geq 1$. It is possible to isolate this effect, in fact the damping time-scale τ is related to the inverse of the next-to-nearest neighbours interaction strength $\tau \propto V_{i,i+2}^{-1}$. Performing numerical simulations, as reported in the right panel of Fig. 3.3, it is possible to see how a pure constrained model, i.e. $V_{i,i+j} = 0$ $\forall j \geq 1$ does not show signs of damping. This, together with the suppressed (but still linear) temporal growth of the entanglement entropy, is a sign of slow dynamics.

It is important to stress that this effect can be observed only starting from a Néel ordered state, in fact as reported in Fig. 3.4, considering as initial state

$$|\Psi\rangle = |gggggggggg\rangle,$$

in which all the atoms are set in the ground state, we see that either evolving with the fully constrained model or with the real strong interacting Hamiltonian, no persistent oscillations are observed and the entanglement entropy saturates to its usual thermal value.

The Hamiltonian (3.1) can be rewritten in terms of the Pauli matrices σ_j^α

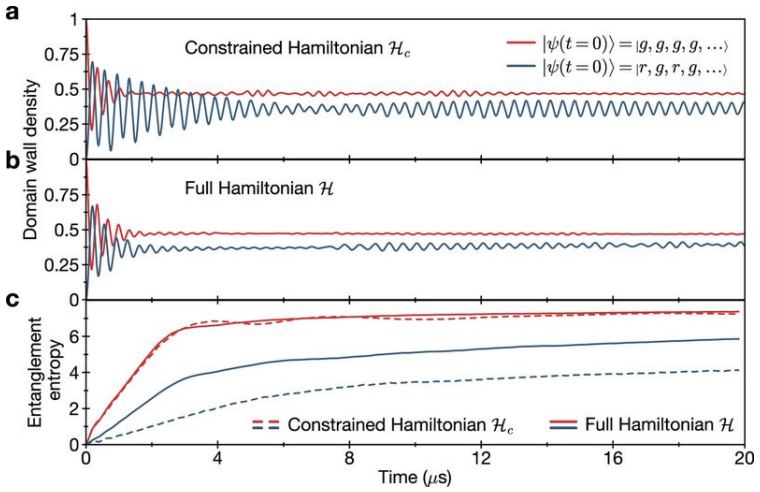

Figure 3.4: Figure from Ref. [88]. Difference in the time evolution for homogeneous and Néel ordered initial states either for the full Hamiltonian and the constrained one. It is possible to observe how persistent oscillations are observed only starting from $|\Psi_0\rangle = |rgrgrg-\ldots\rangle$. This fact is signaled also by an appreciable difference in the entanglement entropy growth.

defining $\sigma_i^z = 2n_i - 1$, we have

$$H = \sum_{j=1}^{L} \frac{\Omega}{2}\sigma_j^x - \Delta\frac{\sigma^z + 1}{2} + \sum_{i<j} V_{i,j}\left(\frac{\sigma_i^z + 1}{2}\right)\left(\frac{\sigma_j^z + 1}{2}\right). \tag{3.4}$$

In the blockade regime of the experiment we have $\Delta = 0$ and $V_{i,i+1} \gg V_{i,i+2}$, therefore we can cast Eq. (3.4) in the following form

$$H = \sum_{j=1}^{L} \frac{\Omega}{2}\sigma_j^x + \frac{V}{2}\sigma_i^z + \frac{V}{4}\sum_{i=1}^{L-1}\sigma_i^z\sigma_{i+1}^z, \tag{3.5}$$

let us note that this Hamiltonian is identical to Eq. (2.1) upon setting $h_x = 2J$ that is exactly the first resonant point. In Fig. 2.14 we observed persistent oscillations between the two Néel states, as we have already pointed out in chapter 2, this phenomenon is exactly the same observed in the experiment [88]. The effective Hamiltonian governing the dynamics can be further simplified, defining $\epsilon = \Omega/2V$, in the blockade regime we have $\epsilon \ll 1$, therefore we can rewrite (3.5) as

$$H = H_0 + \epsilon H_1 = \sum_{i=1}^{L-1}(\sigma_i^z + 1)(\sigma_{i+1}^z + 1) + \epsilon\sum_{j=1}^{L}\sigma_j^x, \tag{3.6}$$

performing a Schrieffer-Wolf transformation we obtain, at the first order, Hamiltonian (2.26), i.e.,

$$H = \sum_i \sigma_i^x \qquad \text{with} \qquad n_i n_{i+1} = 0. \tag{3.7}$$

Hamiltonian (2.26), is a the massless case of the FSS Hamiltonian

$$H_{\mathrm{FSS}} = \sum_i \sigma_i^x + U n_i + V n_i n_{i+2}, \tag{3.8}$$

where $n_i = (\sigma_i^z + 1)/2$, U is the mass term and V is the next-to-nearest neighbours interaction strength. The FSS model was introduced in Ref. [90] as a possible description of tilted Mott insulators. Its ground state phase-diagram is very rich from physical point of view: there are first-order and second-order (in the same class of universality of the Ising model) critical lines, Kosterlitz transition zones, and even some regions in which the nature of the phase phase transition is still not clear. In Fig. 3.5, in particular, it is possible to observe how there are two

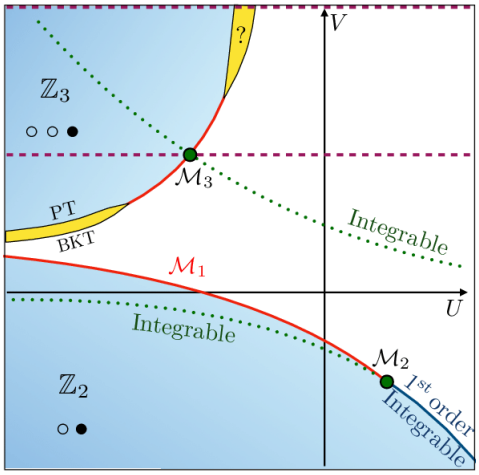

Figure 3.5: Figure from Ref. [91]. Phase diagram of the ground state of the FSS model.

lines of integrability and two different ordered phases ($\mathbb{Z}_2$ and $\mathbb{Z}_3$). In particular for $V = 0$, that is the regime in which we work, it is possible to note that there are two phases, a Néel ordered one for $U < U^*$ and a paramagnetic one, these are separated by an Ising-like second order phase transition.

3.2 Quantum scars and proximity to integrability

The observation of coherent oscillations in the FSS model have raised some doubts concerning the validity of ETH. In fact, this model is non-integrable, non-disordered, therefore, the natural expectation would be to observe a fast relaxation toward a thermal state; especially because in this case there are no physical reasons (e.g. confining interactions) for a slowdown of the dynamics. The proper way to attack this problem is studying the full spectrum of the system. This procedure, however, is not always very informative because in order

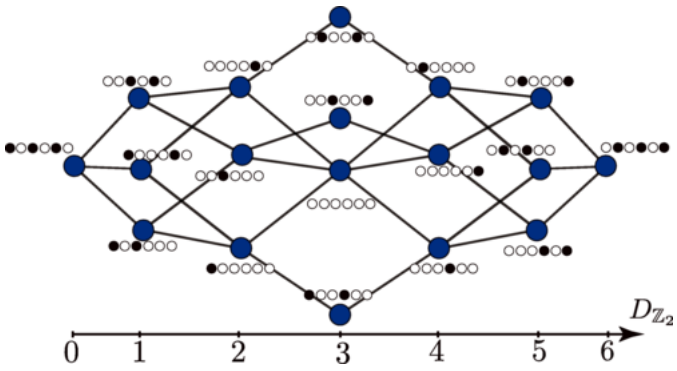

Figure 3.6: Figure from Ref. [100]. Fibonacci graph for $L = 8$, at the two extreme of the graph there are the two Néel ordered states.

to study the spectrum one has to diagonalize huge matrices and this results in a strong limitations on the accessible sizes of the system. In this case it could be difficult to distinguish between truly physical effects and finite size ones. The PXP model, however, as already discussed, presents a reduced Hilbert space due to the presence constraint. In fact, a spin system of L sites usually has an exponentially growing Hilbert space in L, i.e., $\dim\mathcal{H} = 2^L$. For the PXP model, instead, the Hilbert space grows according to the Fibonacci sequence. This fact can be demonstrated counting recursively the allowed states: the last spin in such states can either be in the ground state $|\ldots g\rangle$ or in the Rydberg state $|\ldots r\rangle$. In the first case the state can be obtained by adding g or r to a state with $L-1$ sites, but in the second one it is possible to obtain it only adding a couple gr to a state of $L-2$ sites. Accordingly, the Hilbert space with L sites is obtained, by adding the two contributions, as

$$d_L = d_{L-1} + d_{L-2} \tag{3.9}$$

with the conditions that $d_0 = 1$ and $d_1 = 2$, this is exactly the Fibonacci series. In particular, for open bounday conditions the Hilbert space of the PXP coincides with the $(L-2)^{\text{th}}$ term of the sequence, for periodic conditions we have to add a corrective term, but behavior is the same. As it has been studied in Ref. [100] the constrained dynamics can be viewed as a path a on subgraph of an hypercube, this graph is known in the computer science literature as Fibonacci's graph. In Fig. 3.6 is schematically reported how this graph looks for $L = 8$. The two Néel states between which coherent oscillations are observed are in the edge of it. These two states seem to play a fundamental role in the dynamics of the model, for this reason in Refs. [99, 100] the overlap between them and the eigenstates of the PXP have been studied. As it has been reported in Fig. 3.7, it is possible to observe how there is a special band of eigenstates, equally separated in energy, that has a considerably higher overlap with the $\mathbb{Z}_2$ ordered states. More-

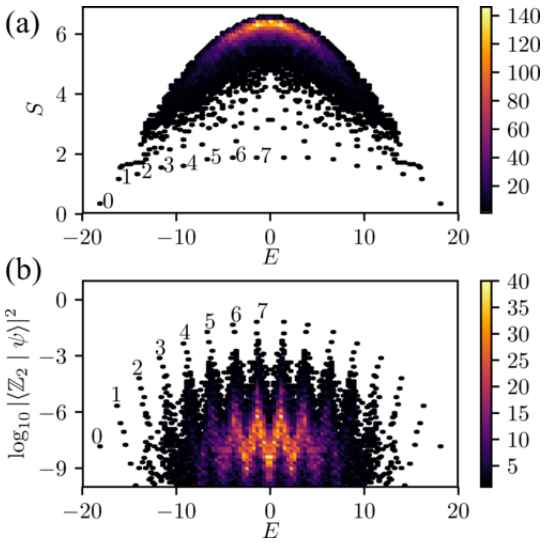

Figure 3.7: Figure from Ref. [100]. Overlap between Néel ordered states and eigenstates of the PXP (bottom panel). Entanglement entropy of the eigenstates (upper panel).

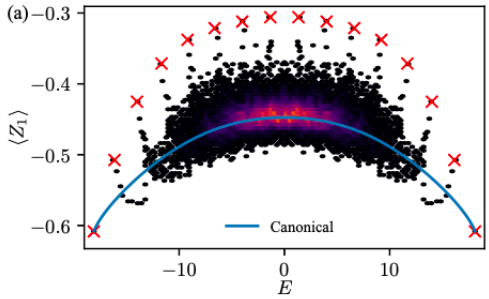

Figure 3.8: Figure from Ref. [100]. Expectation value of the magnetization on the eigenstates of the PXP model.

over, these states have a non-thermal behavior as signaled by the fact that the entanglement entropy has a smaller value with the respect the other states. The strong violation of ETH is evident in the fact that the local magnetization $\langle Z_1\rangle$, measured on the special band of eigenstates, is clearly out from the thermal cloud around the canonical expectation value, as reported in Fig. 3.8. These states are thus responsable for the critical slowdown of the thermalization process. In analogy to what happens in the single-particle chaotic biliards [103], they have been named *many-body quantum scars*. In fact, in the semiclassical quantization of single-particle chaotic billiards, scars represent an enhancement of eigenfunction density along the trajectories of classical periodic orbits.

It is important to stress that the number of this ETH-violating states scales lineraly with the system size L, therefore the ratio between the Hilbert space dimension and the number of these special states goes to zero in thermodynamic

limit. The crucial point is that for some initial states they play a fundamental role in the dynamics. Similar phenomena have been recently observed also in other models, e.g. Ref. [104], while it is not clear whether an akin circumstance occurs also in Ising model with longitudinal field [96].
Quantum scars' argument gives a detailed description of the mechanism behind the slow-dynamics in this model, however it does not clarify the reason of the existence of this special band of ETH-violating states. A step toward this direction has been done by Khemani et al. in Ref. [102]. In this work the authors built a suitable deformation of the Hamiltonian (2.26), preserving its symmetries, which reads

$$H = H_{PXP} + \sum_i h_{XZ}(P_{i-1}\sigma_i^x P_{i+1}\sigma_{i+1}^z + \sigma_{i-2}^z P_{i-1}\sigma_i^x P_{i+1}) + h_{YZ}(P_{i-1}\sigma_i^y P_{i+1}\sigma_{i+2}^z + \sigma_{i-2}^z P_{i-1}\sigma_i^y P_{i+1}), \quad (3.10)$$

where, as usual, $P_i = \left(\frac{1-\sigma_i^z}{2}\right)$. This deformed Hamiltonian represents an expansion up to the fourth order of Eq. (2.26). Studying the $r-$parameter, that we introduced in Chapter (1), averaged over the middle-third of the spectrum (in order to capture the infinite temperature properties of the system) they realized that for a particular value of the couplings there is a drop of r from $r = 0.6$ typical of gaussian unitary ensemble (GUE) random matrices (or $r = 0.53$ when $h_{YX} = 0$ typical of gaussian orthonormal ensemble (GOE)) to $r = 0.39$, a typical value of poissonian statistics of energy level that is observed in integrable systems in which there is not level repulsion. As reported in Fig. 3.9, for $h_{YZ} = 0$ and $h_{XZ} \approx -0.02$, the system seems to have a truly poissonian statistics. The fact that the averaged value of r tends to rise increasing the system size is the signal that integrability is not fully restored at the fourth order in the expansion, and further terms are necessary. We can see how for both h_{XZ} and h_{YX} set to zero, restoring thus the PXP limit, the average value of r is still not completely thermal, at least for finite L. This means that the proximity to integrability could influence the dynamics of the system. In other words, some of the conserved charges that should be present in the actual integrable model could affect the dynamics slightly away from this special point. In this perspective the observed slow dynamics observed in the experiment [88], could be seen as a *prethermal* effect, this is in strong opposition with what reported in Refs. [99, 100]. The argument concerning the "proximity to integrability" seems to have some pitfalls, first of all it has been shown in earlier works in the Affleck-Kennedy-Lieb-Tasaki (AKLT) model [105, 106], that it is possible to construct ETH-violating states with low entanglement entropy and arbitrary energy even when the spectrum is fully thermal. Secondly, in Ref. [101], it has been reported the possibility of

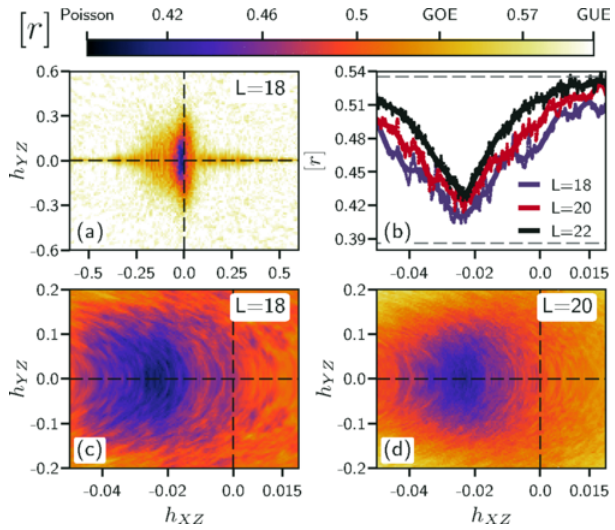

Figure 3.9: Figure from Ref. [102]. Level statistics as a function of the parameters of the deformation (3.10). In panel (b) the average value of r is reported for $h_{YX} = 0$ as a function of h_{XZ} and L. It is possible to observe that although the constraints, the average value of r is almost everywhere GOE, thus signaling fast thermalization.

constructing suitable deformations of the PXP model that, not only keep the spectrum thermal, as signaled, again, by the average value of the r parameter, but show *enhanced* (or *perfect*) scars. This means that the dynamics starting from a $\mathbb{Z}_2$ ordered state returns *exactly* to it after one period. In other words, the Loschimdt echo (or *fidelity*) is periodically almost one (see Fig. 1 in [101]). Let us be slightly more specific, the deformations added in Ref. [101] are, again, fourth-order deformations, but, in this case, they are longer-ranged perturbations, i.e. the R-sites deformation reads

$$\delta H_R = -\sum_i \sum_{d=2}^{R} h_d \mathcal{C} \sigma_i^x \mathcal{C} (\sigma_{i-d}^z + \sigma_{i+d}^z), \tag{3.11}$$

where $\mathcal{C} = \prod_i [1 - (1+\sigma_i^z)(1+\sigma_{i+1}^z)/4]$. The coupling constant h_d is numerically optimized in order to maximize the fidelity. It turns out that this optimal value is

$$h_d^* = h_0 (\phi^{d-1} - \phi^{-(d-1)})^{-2}, \tag{3.12}$$

in which $\phi = (1+\sqrt{5})/2$ is the golden ratio. It is interesting to note that the coupling strength decreases exponentially with the distance.

As we have observed in this brief chapter, the arising of slow dynamics in this simple model is convoluted and still not completely understood. If, on the one hand, the description of the phenomenon seems to be under control and well explained by the existence of this band of atypical states, on the other we still lack a satisfying motivation of why these states arise and especially why they play

a crucial role in the dynamics of particular initial states (i.e. $\mathbb{Z}_2$ ordered). This phenomenon may be connected with the Shiraishi-Mori mechanism [107] which permits to build non-integrable models that sistematically violates strong-ETH. In the next chapter we will explain in detail our interpretation of the phenomenon, we will show in particular, how this can be connected to the dynamics of lattice gauge theories.

CHAPTER 4

A LATTICE GAUGE THEORY PERSPECTIVE

In this chapter we will take stock of some arguments that we touched on in the previous chapters. In particular we will see how it is possible to interpret the Rydberg Blockade constraints as an effect of *gauge* symmetry and thus how the anomalous dynamics can be understood in terms of *pair production* and *string-breaking* phenomena [108, 109]. The core of the discussion lies in the fact that in one spatial dimension Rydberg blockade systems can be *exactly* mapped to a $U(1)$ gauge theory in which we have integrated out the matter field exploiting the *Gauss' law* constraint. This re-interpretation is twofold important, in fact, on the one side it enables us to see the slow dynamics occurring in these systems under a new light, and thus to use the machinery developed in high-energy contexts to tackle this problem. On the other side it could open the door to simulations of lattice gauge theory in *large* systems, thing that so far has been elusive. After our work [92] (on which is mainly based this chapter), successive papers have attempted to generalize and adapt the argument also in higher dimensions [110, 111], thus demonstrating the interest of the community in reaching the task of performing simulations of lattice gauge theories in large (and scalable) systems. We will furthermore show how some phenomena reported in Chapter 2 can be interpreted in matter-integrated-out gauge theory language, and we will highlight the similitudes between frozen dynamics in Ising model with longitudinal field and the Schwinger model in the presence of confinement. Before explaining the details of our work, let us review briefly the concept of gauge theory and its *staggered fermions* version on lattice made by Kogut and Susskind [112], we will, for sake of simplicity, consider only the Abelian case.

4.1 Reminds of gauge invariance

In classical field theory the electromagnetic field is described by a four-vector A_μ, with $\mu = 0, 1, \ldots$ space-time indices, $A_0 = \phi$ the electric potential and $A_i = \vec{A}$ the vector potential, for which $\vec{\nabla} \times \vec{A} = \vec{B}$ and $\vec{E} = \vec{\nabla}\phi$. The field strength tensor is defined as

$$F_{\mu\nu} = \partial_\mu A_\nu - \partial_\nu A_\mu, \tag{4.1}$$

the quadratic lagrangian of the free electromagnetic field is

$$\mathcal{L} = -\frac{1}{4} F_{\mu\nu} F^{\mu\nu}. \tag{4.2}$$

From it we can derive the Maxwell's equations written in covariant form, the first two are given by the equations of motion

$$\partial_\mu F^{\mu\nu} = 0, \tag{4.3}$$

which can be rewritten in the more common form as $\vec{\nabla} \cdot \vec{E} = 0$ and $\vec{\nabla} \times \vec{B} = \partial_0 \vec{E}$. Defining $\tilde{F}^{\mu\nu} = \frac{1}{2}\epsilon^{\mu\nu\rho\sigma} F_{\rho\sigma}$ we obtain the second pair of Maxwell's equations

$$\partial_\mu \tilde{F}^{\mu\nu} = 0, \tag{4.4}$$

obtained by the contraction of an antisymmetric tensor $\epsilon^{\mu\nu\rho\sigma}$ with a symmetric one $\partial_\mu \partial_\rho$. A crucial aspect of Lagrangian (4.2) is that it is, by construction, invariant under a $U(1)$ local symmetry, i.e. it is invariant upon redifining the vector potential as:

$$A_\mu \to A_\mu - \partial_\mu \theta. \tag{4.5}$$

Free fields are described by the Dirac lagrangian

$$\mathcal{L} = \bar{\Psi}(i\gamma^\mu \partial_\mu - m)\Psi, \tag{4.6}$$

in which Ψ is a four-components Dirac spinor and $\bar{\Psi} = \gamma_0 \Psi^\dagger$, with γ_0 the Dirac matrix. In order to consider matter field interacting with gauge fields we need to make it gauge invariant, i.e. invariant under the transformation

$$\Psi \to \mathrm{e}^{iq\theta(x)}\Psi \qquad \bar{\Psi} \to \mathrm{e}^{-iq\theta(x)}\bar{\Psi}. \tag{4.7}$$

From (4.5), which describe how A_μ changes under the action of gauge transformation, it is straightforward to see that this task is achieved by redifining the derivative as

$$D_\mu = \partial_\mu + iqA_\mu, \tag{4.8}$$

in which q, the only parameter of the Abelian group $U(1)$, is the charge. The introduction of the covariant derivative is the standard way through which the interaction between gauge fields and matter is described. The resulting Lagrangian

can be quantized using the covariant quantization that enables us to identify *particles* and *anti-particles* [113].
The discretization of a gauge theory is not an easy task, in fact, a naive approach can lead to problems that make the lattice lagrangian unphysical, as for example the fermion doubling problem [114]. There are essentially two different ways of proceed: using the Wilson approach [115], or by means of the Kogut staggered fermions technique [112]. In the last case, that is the one in which we are interested in since it is more straightforward to be implemented with cold atoms, the four-component Dirac spinor is divided in its Weyl components $\psi_{L/R}$, the left part ψ_L is placed on the even (odd) sites of the lattice and the right one ψ_R on the odd (even) ones.

4.1.1 Discretization of a gauge theory

Let us briefly summarize how to build a discrete version of a lattice gauge theory. For this purpose, henceforth, we will focus on the prototypical Schwinger model which describes the electromagnetic interaction in $(1+1)$-dimensions [83, 84]. This model, despite its simplicity, captures some non-trivial aspects of a gauge theory, in particular it can describe the physics of confinement. In order to discretize a gauge theory we have to introduce a length scale a, the lattice spacing. This length-scale can be seen as an ultraviolet cut-off at energies of the order $1/a$, this means that gauge theory on the lattice is not useful if one wants to describe high-energy properties of the model under examination. However, this aspect is not a problem in our case since we are interested in studying the dynamical effects of confinement and these are *low-energy* properties of the system; meaning that they appear only at a length scales much bigger than the lattice spacing. In order to study high-energy features of the system, thanks to the *asymptotic freedom*, which essentially tells us that at very short distance the system behaves as a free one, it is possible to use perturbative methods directly on the continuum theory.
In $(1+1)$-dimensions the vector potential A_μ has only two components $\mu = 0, 1$ and the electric field has only one component, i.e[1].

$$F^{01} = \hat{E} = -\partial_0 \hat{A}^1(x), \tag{4.9}$$

$\hat{E}$ represents the conjugate momentum to $\hat{A}^1(x)$. In the abelian case we have the following commutation relations

$$[\hat{A}^1(x), \hat{E}(y)] = -i\delta(x-y). \tag{4.10}$$

[1] In this case both $\hat{A}(x)$ and $\hat{E}(x)$ are operators living on a given Hilbert space

Choosing a time-like axial gauge, i.e. $A^0 = 0$, the Hamiltonian of the Schwinger model can be written as:

$$\hat{H} = \int dx \left[-i\bar{\Psi}(x)\gamma^1(\partial_1 + ig\hat{A}^1(x))\Psi(x) + m\bar{\Psi}(x)\Psi(x) + \frac{1}{2}\hat{E}^2(x)) \right], \quad (4.11)$$

in which, again, $\bar{\Psi}(x) = \Psi(x)^\dagger\gamma^0$, with $\gamma^0 = \hat{\sigma}^z$ and $\gamma^1 = i\hat{\sigma}^y$ and $\Psi(x) = \left(\Psi_{e^-}(x), \Psi^\dagger_{e^+}(x)\right)$ is a spinor field. In order to discretize Hamiltonian (4.11) we consider fermionic matter fields on the sites of a lattice and bosonic gauge fields on the links (or on the dual lattice), absorbing the lattice spacing in the renormalization of the couplings. In $(1+1)$-dimensions the description in terms of both matter and gauge field is redundant, because of the constraint given by the Gauss' law, which in the continuum can be cast in the following way

$$\partial_1 E = g\bar{\Psi}(x)\Psi(x). \quad (4.12)$$

Before showing in detail how to define the fermionic fields on the lattice, let us introduce the most important object which encodes gauge symmetry in a LGT. When a lattice gauge theory is regularized on the lattice it is of fundamental importance to maintain its invariance, in the continuum the vector potential transforms according to the (4.5), and thus involves an infinitesimal neighborhood of a point x due to the presence of the derivative. In the discrete, it is therefore natural to integrate the continuum gauge field along the link which connects two sites x and y, however this must be done in the proper way. Following Wilson's work [115] we can construct the parallel transporter

$$U_{xy} = \exp\left[ig \int_x^{x+a=y} dz A_1(z) \right], \quad (4.13)$$

which is a $U(1)$ object. Under the action of the gauge group we have

$$A^{'}(z) = A_1(z) - \partial_1\alpha(z), \quad (4.14)$$

where α_z is an arbitrary regular function, therefore,

$$U^{'}_{xy} = \exp\left[ig \int_x^{x+a=y} dz A^{'}_1(z) \right] = \exp\left[ig \int_x^{x+a=y} dz (A_1(z) - \partial_1\alpha(z)) \right] \quad (4.15)$$

$$= \exp\left[ig \int_x^{x+a=y} dz A_1(z) - \alpha(y) + \alpha(x) \right] \quad (4.16)$$

$$= \Omega_x U_{xy} \Omega^\dagger_y, \quad (4.17)$$

where we have introduced the lattice gauge transformation operator

$$\Omega_x = \exp[ig\alpha(x)] \in U(1). \quad (4.18)$$

The parallel transporter is the truly gauge degree of freedom on the lattice from which we can can derive the vector potential operator $\hat{A}_{xy}$ living on the link

as $\hat{U}_{xy} = \exp[iag\hat{A}_{xy}]$. The electric field operator on the link $\hat{E}_{xy}$, being the conjugate operator to the vector potential, can be defined as

$$\hat{E}_{xy} = -i\frac{\partial}{\partial(ag\hat{A}_{xy})}. \tag{4.19}$$

This gives rise to the following commutation relations

$$[\hat{E}_{xy}, \hat{U}_{rs}] = \delta_{xr}\delta_{ys}\hat{U}_{xy} \qquad [\hat{E}_{xy}, \hat{U}^{\dagger}_{rs}] = \delta_{xr}\delta_{ys}\hat{U}^{\dagger}_{xy}, \tag{4.20}$$

we note how on the lattice the gauge degrees of freedom of an Abelian gauge theory have an $SU(2)$ algebra.

At this point we are ready to write the Hamiltonian on the lattice, let us slightly change notation, we define

$$\hat{L}_n = \frac{1}{g}\hat{E}_{x_n,x_n+a} \qquad \hat{\theta}_n = -ag\hat{A}_{x_n,x_n+a}. \tag{4.21}$$

The staggered matter fields are

$$\hat{\Phi}(x_n) = \sqrt{a}\hat{\Psi}_{e^-}(x_n) \qquad \text{even sites} \tag{4.22}$$

$$\hat{\Phi}(x_n) = \sqrt{a}\hat{\Psi}^{\dagger}_{e^+}(x_n) \qquad \text{odd sites.} \tag{4.23}$$

We see how the two Weyl components are fictitiously separated, this is done in order to ensure the continuity of the Dirac equation when the limit $a \to 0$ is performed. The Hamiltonian can be written as:

$$\hat{H} = -iw\sum_{n=1}^{N-1}\left[\hat{\Phi}^{\dagger}_n\hat{U}_{n,n+1}\hat{\Phi}_{n+1} - \text{h.c.}\right] + m\sum_{n=1}^{N-1}(-1)^n\hat{\Phi}^{\dagger}_n\hat{\Phi}_n + J\sum_{n=1}^{N-1}\hat{L}^2_n, \tag{4.24}$$

where N is the number of sites, m is the mass of the fermions and we have defined $w = \frac{1}{2a}$ and $J = \frac{g^2a}{2}$. Using the natural units ($\hbar = c = 1$) w, J, m and g have the dimensions of the inverse of a mass. In this representation the Gauss' law operator becomes

$$\hat{G}_n = \hat{L}_n - \hat{L}_{n-1} - \hat{\Phi}^{\dagger}\hat{\Phi} + \frac{1}{2}[1-(-1)^n], \tag{4.25}$$

by construction the Hamiltonian (4.24) commutes with $\hat{G}_n$. The operator defined in Eq. (4.25) is the generator of an infinitesimal gauge transformation, a general Ω_x can be represented by

$$\hat{V} = \prod_x \exp(ig\alpha(x)\hat{G}_x) \tag{4.26}$$

such that $\hat{V}^{\dagger}\hat{\Psi}(x)V = \Omega_x\Psi(x)$. Hamiltonian (4.24) can be rewritten, using a Jordan-Wigner transformation and integrating out the gauge fields, as a long-range interacting spin model [116]. For this purpose, we first rewrite the fermion operator $\hat{\Phi}_n(x)$ in terms of Pauli's spin operators

$$\hat{\Phi}_n(x) = \prod_{l<n}[i\hat{\sigma}^z_l]\hat{\sigma}^-_n, \tag{4.27}$$

secondly, we eliminate the operators $\hat{\theta}_n$ performing a gauge transformation

$$\hat{\sigma}_n^- \rightarrow \left[\prod_{l<n} \mathrm{e}^{-i\hat{\theta}_l}\right] \hat{\sigma}_n^- \tag{4.28}$$

which essentially rotates every Pauli operator by a phase depending on the gauge fields on the previous links. Finally we obtain

$$H = w \sum_{n=1}^{N-1} \left[\hat{\sigma}_n^+ \hat{\sigma}_{n+1}^- + h.c.\right] + \frac{m}{2} \sum_{n=1}^{N} \hat{\sigma}^z + J \sum_{n=1}^{N-1} \hat{L}_n^2, \tag{4.29}$$

in this formulation the Gauss' law takes the form $\hat{L}_n - \hat{L}_{n-1} = \frac{1}{2}[\hat{\sigma}_n^z + (-1)^n]$, from which we obtain $\hat{L}_n = \epsilon_0 + \frac{1}{2}\sum_{l=1}^{n}(\hat{\sigma}_l^z + (-1)^l)$, ϵ_0 is a background electric field, this term can be rewritten as $\epsilon_0 = \frac{\theta}{2\pi}$, where θ is called topological angle [117]. Using this we can rewrite the last term in (4.29) in terms of spin operators. In writing the Gauss' law using the spin formalism we have assumed to be in the zero charge subspace, i.e., for the physical states $\hat{G}_n|\Psi_{Phys.}\rangle = 0$, this assumption will be valid henceforth.

4.1.2 Quantum-Link models

The electric field on the link in Hamiltonian (4.24) can take every integer value

$$\hat{L}_n = 0, \pm 1, \pm 2, \ldots \tag{4.30}$$

therefore the dimension of the Hilbert space is infinite on every link. This fact makes the model (4.24) of poor practical use, especially in the perspective of quantum simulating a gauge theory using cold atoms (usually bosons-fermions mixtures). In order to tackle this problem we can "cut" the dimension of the gauge field on the links by choosing a finite dimensional representation of the algebra. As we have seen in the Abelian case the gauge fields follow an $SU(2)$ algebra (see Eq. (4.20)), therefore we can use a *spin representation* in order to decrease the degrees of freedom. This is clearly an approximation, in fact, doing this we lose some configurations of the electric field, but we have still a good agreement with the actual theory, especially if we choose a high S-spin representation, but the basic features of the theory are captured also in small S-representation. This can be achieved by simply defining

$$\hat{U}_{xy}^\dagger = S_{xy}^1 - iS_{xy}^2 = S_{xy}^- \qquad \hat{U}_{xy} = S_{xy}^1 + iS_{xy}^2 = S_{xy}^+ \tag{4.31}$$

$$\hat{E}_{xy} = S_{xy}^3, \tag{4.32}$$

where $S^\alpha = \frac{1}{2}\sigma^\alpha$ in the case of $S = 1/2$ quantum link models.

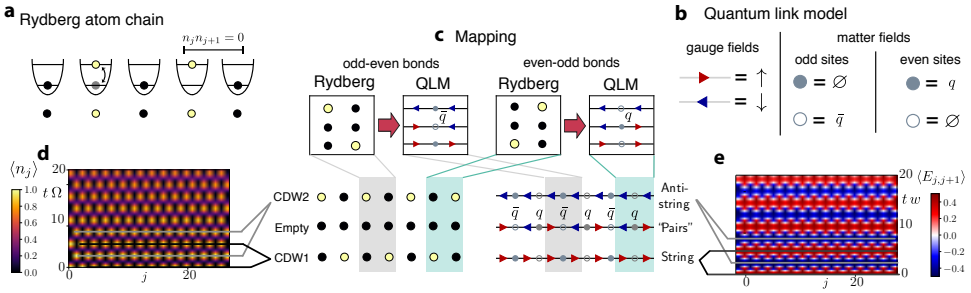

Figure 4.1: Gauge-theory interpretation of Rydberg-atom quantum simulations. **a**: Schematics of a Rydberg atom chain. Each potential well of the optical lattice hosts a single atom, which can be either in the ground (black) or excited Rydberg (yellow) state. The two levels are coupled by a laser field. The Rydberg blockade prevents the simultaneous excitations of neighboring atoms. **b**: Degrees of freedom of a $U(1)$ LGT in the spin-1/2 quantum link model (QLM) formulation. Gauge fields are represented by spin variables residing on links. Matter fields are represented by Kogut-Susskind fermions: an occupied site corresponds to the vacuum on odd sites, and to a quark q on even sites. An empty site, instead, to the vacuum on even sites and to an anti-quark $\bar{q}$ on odd sites. **c**: Mapping between Rydberg-blockaded states and configurations of the electric field constrained by the Gauss law in the QLM. Due to the staggered electric charge, the allowed configurations of the electric field depend on the link, as illustrated. The two so-called charge-density wave configurations "CDW1" and "CDW2" of the Rydberg-atom arrays are mapped onto the "string" and "anti-string" states, respectively, characterized by uniform rightward or leftward electric fluxes. The empty configuration with all Rydberg atoms in their ground state is mapped to a state filled by adjacent particle-antiparticle pairs. **d**: Time evolution of the Rydberg array governed by the effective Hamiltonian $H_{\rm FSS}$ in Eq. (4.34), starting from the CDW1 state. The plot shows the space and time resolved population $\langle n_j \rangle$ of the excited Rydberg atoms. **e**: Evolution of the expectation value of the electric field operator $\hat{E}_{j,j+1}$ in the QLM. These dynamics map exactly onto the ones shown in panel **d** via the mapping illustrated in panel **c**. The thin lines highlight the oscillation between CDW1, CDW2 (left, bottom of panel **c**) or string and anti-string (right) states. In these simulations, $L = 24$ and $\delta = m = 0$.

4.2 Lattice gauge theories and string dynamics

In this section we show that $(1 + 1)$-dimensional LGTs akin to quantum electrodynamics are naturally realized in state-of-the-art experiments with Rydberg atom arrays [88, 118], building the bridge between the slow dynamics described in Chapter 3. In particular, we show how the dynamics of Rydberg excitations in these chains is exactly mapped onto a spin-1/2 quantum link model (QLM), a $U(1)$ LGT where the gauge fields span a finite-dimensional Hilbert space, equivalent to a lattice Schwinger model in the presence of a topological term [117], what has been reported in this section can be found in Ref. [92]. The key element of our mapping, which is schematically illustrated in Fig. 4.1, is that gauge invariance has a natural counterpart in the Rydberg blockade mechanism, which constrains the Hilbert space in the same way as Gauss law does in gauge theories. This

provides an immediate interpretation of the recent experiment with Rydberg-blockaded atom arrays in Ref. [88] as the first large-scale quantum simulation of a LGT at the edge of classical computational methods [119].

From a theoretical viewpoint, the mapping offers a hitherto unexplored perspective on the anomalously slow relaxation recently observed in experiments: the long-lived oscillations in the population of excited Rydberg atoms correspond to a string inversion, a phenomenon which is directly tied to string breaking [120, 121, 122] prototypical of gauge theories including dynamical matter (cf. Fig. 4.1**d** and (4.1)**e**). The mapping indicates that this phenomenon has a natural interpretation in the LGT framework, and suggests the occurence of slow dynamics in other $U(1)$ gauge theories, such as higher-spin QLMs [123], Higgs theories [124], and the Schwinger model [84, 112]. These theories have been widely discussed in the context of Schwinger pair production taking place at high-intensity laser facilities, thus providing a highly unexpected, direct link between apparently unrelated experimental platforms [108, 122, 125, 86, 126].

We discuss the generality of this type of quantum evolution by extending our analysis to other relevant instances of "slow dynamics", characterized by the absence of relaxation on all time scales corresponding to any microscopic coupling present in the system. As initial states, we focus on those consisting of particle-antiparticle pairs, corresponding to regular configurations of the Rydberg-atom arrays with localized defects, which are accessible within the setup of Ref. [88]. We show that these defects propagate ballistically with long-lived coherent interference patterns. This behavior is found to be governed by special bands of highly excited eigenstates characterized by a regularity in the energy-momentum dispersion relation. These findings open up a novel perspective which complements and extends towards gauge theories recent approaches to slow relaxation in Rydberg-blockaded atomic chains [99, 100, 82, 127, 101, 102].

4.2.1 Rydberg atom arrays

We are interested in the dynamics of a one-dimensional array of L optical traps, already introduced in the previous chapter, each of them hosting a single atom, as schematically illustrated in Fig. 4.1**a**. The atoms are trapped in their electronic ground state (black circle), denoted by $|\downarrow\rangle_j$, where j numbers the trap. These ground states are quasi-resonantly coupled to a single Rydberg state, i.e., a highly excited electronic level, denoted by $|\uparrow\rangle_j$. The dynamics of this chain of qbits $\{|\uparrow,\downarrow\rangle_j\}_{j=1,\dots,L}$ is governed by Ising-type Hamiltonian already introduced

in Chapter 3, [128, 129]:

$$\hat{H}_{\text{Ryd}} = \sum_{j=1}^{L} (\Omega\, \hat{\sigma}_j^x + \delta\, \hat{\sigma}_j^z) + \sum_{j<\ell=1}^{L} V_{j,\ell} \hat{n}_j \hat{n}_\ell, \tag{4.33}$$

where $\hat{\sigma}_j^\alpha$ are Pauli matrices at site j, the operator $\hat{n}_j = (\hat{\sigma}_j^z + 1)/2$ signals the presence of a Rydberg excitation at site j, 2Ω and 2δ are the Rabi frequency and the detuning of the laser excitation scheme, respectively, and $V_{j,\ell}$ describes the interactions between atoms in their Rydberg states at sites (j, ℓ). For the cases of interest here, this interaction is strong at short distances and decays as $1/|j-\ell|^6$ at large distances. The dynamics described by $\hat{H}_{\text{Ryd}}$ has already been realized in several experiments utilizing either optical lattices or optical tweezers [118, 130, 88]. In particular, Ref. [88] investigated, as we have seen, the case in which $V_{j,j+1}$ is much larger than all other energy scales of the system, resulting in the so-called Rybderg *blockade effect*: atoms on neighboring sites cannot be simultaneously excited to the Rydberg state, hence the constraint $\hat{n}_j \hat{n}_{j+1} = 0$.

In this regime, the resulting Hamiltonian, again, is

$$\hat{H}_{\text{FSS}} = \sum_{j=1}^{L} \left(\Omega\, \hat{\sigma}_j^x + 2\delta\, \hat{n}_j \right), \tag{4.34}$$

where we neglect longer-range terms which do not affect qualitatively the dynamics. $\hat{H}_{\text{FSS}}$ acts on the constrained Hilbert space without double occupancies on nearest-neighbor sites, as illustrated in Fig. 4.1**a**. As we show below, the direct connection between Rydberg atomic systems and gauge theories is indeed provided by this constraint at the level of the Hilbert space.

4.2.2 Rydberg blockade as a gauge symmetry constraint

We establish here the exact mapping between the FSS Hamiltonian in Eq. (4.34) governing the dynamics of the Rydberg atom quantum simulator in Ref. [88] and a $U(1)$ LGT. The latter describes the interaction between fermionic particles, denoted by $\hat{\Phi}_j$ and residing on the lattice site j, mediated by a $U(1)$ gauge field, i.e., the electric field $\hat{E}_{j,j+1}$, defined on lattice bonds, as depicted in Fig. 4.1**b**. We use here Kogut-Susskind (staggered) fermions [112], with the conventions that holes on odd sites represent antiquarks $\bar{q}$, while particles on even sites represent quarks q. Their dynamics is described by:

$$\hat{H} = -w \sum_{j=1}^{L-1} (\hat{\Phi}_j^\dagger \hat{U}_{j,j+1} \hat{\Phi}_{j+1} + \text{h.c.}) + m \sum_{j=1}^{L} (-1)^j \hat{\Phi}_j^\dagger \hat{\Phi}_j + J \sum_{j=1}^{L-1} \hat{E}_{j,j+1}^2, \tag{4.35}$$

where the first term provides the minimal coupling between gauge and matter fields through the parallel transporter $\hat{U}_{j,j+1}$ with $[\hat{E}_{j,j+1}, \hat{U}_{j,j+1}] = \hat{U}_{j,j+1}$, the second term is the fermion mass, and the last one is the electric field energy. The generators of the $U(1)$ gauge symmetry are defined as

$$\hat{G}_j = \hat{E}_{j,j+1} - \hat{E}_{j-1,j} - \hat{\Phi}_j^\dagger \hat{\Phi}_j + \frac{1-(-1)^j}{2}, \tag{4.36}$$

and satisfy $[\hat{H}, \hat{G}_j] = 0$, so that gauge invariant states $|\Psi\rangle$ satisfy Gauss law $\hat{G}_j |\Psi\rangle = 0$ for all values of j. Restricting the dynamics to their subspace is by far the most challenging task for quantum simulators.

Different formulations of $U(1)$ LGTs are obtained for different representations of gauge degrees of freedom $\hat{E}_{j,j+1}$. While in the standard Wilsonian formulation (i.e., the lattice Schwinger model) they span infinite-dimensional Hilbert spaces, here we first focus on the $U(1)$ QLM formulation [123, 131], where they are represented by spin variables, i.e., $\hat{E}_{j,j+1} = \hat{S}^z_{j,j+1}$ and $\hat{U}_{j,j+1} = \hat{S}^+_{j,j+1}$, so that $[\hat{E}_{j,j+1}, \hat{S}^+_{j,j+1}] = \hat{S}^+_{j,j+1}$. As noted in Ref. [132], this formulation is particularly suited for quantum simulation purposes.

In the following, we consider the QLM with spin $S = 1/2$, in which all the possible configurations of the electric field have the same electrostatic energy, rendering the value of J inconsequential; we anticipate that this model is equivalent to the lattice Schwinger model in the presence of a θ-angle with $\theta = \pi$ [2]. The Hilbert space structure following Gauss law is particularly simple in this case [132]: as depicted in Fig. 4.1**c**, for each block along the chain consisting of two electric fields neighbouring a matter field at site j, there are only three possible states, depending on the parity of j. In fact, in a general (1+1)-dimensional $U(1)$ LGT, the configuration of the electric field along the chain determines the configuration of the charges via the Gauss law. Accordingly, $\hat{H}$ in Eq. (4.35) can be recast into a form in which the matter fields $\hat{\Phi}_j$ are integrated out.

We now provide a transformation which maps exactly the latter form into the FSS Hamiltonian (4.34). The correspondence between the two Hilbert spaces is realized by identifying, alternately on odd and even lattice sites, the computational basis configurations of the atomic qubits allowed by the Rydberg blockade with the classical configurations of the electric field allowed by the Gauss law (see Fig. 4.1**c**). In terms of the two Hamiltonians (4.34) and (4.35), this unitary transformation consists in identifying the operators

$$\hat{\sigma}^x_j \leftrightarrow 2\hat{S}^x_{j-1,j} \tag{4.37}$$

$$\hat{\sigma}^{y,z}_j \leftrightarrow (-1)^j 2\hat{S}^{y,z}_{j-1,j} \tag{4.38}$$

[2] The similarity between the phenomenology of the two models was pointed out in Ref. [132]. Here, we are instead interested in establishing an exact relation.

and the parameters

$$\Omega = -w \tag{4.39}$$

$$\delta = -m. \tag{4.40}$$

This mapping overcomes the most challenging task in quantum simulating gauge theories, by restricting the dynamics directly within the gauge-invariant Hilbert space. The only states that would violate Gauss law are nearest-neighbor occupied sites which are strongly suppressed by the Rydberg blockade and can be systematically excluded via post-selection of the configurations. Beyond providing a direct link between Gauss law and the Rydberg blockade mechanism, the most important feature of the mapping is that, differently from other remarkable relations between $\hat{H}_{\mathrm{FSS}}$ and lattice models with gauge symmetries [133, 134], it provides an immediate connections between Rydberg experiments and particle physics phenomena, as we describe below.

4.2.3 Gauge-theory interpretation of slow dynamics

The exact description of Rydberg-blockaded chains in terms of a $U(1)$ LGT allows us to shed a new light on the slow dynamics reported in Ref. [88], by interpreting them in terms of well-studied phenomena in high-energy physics, related to the production of particle-antiparticle pairs after a quench akin to the Schwinger mechanism.

In the experiment, as we discussed in chapter 3, the system was initialized in a charge density wave state (CDW1 in Fig. 4.1**c**), and subsequently, the Hamiltonian was quenched, inducing slowly-decaying oscillations between CDW1 and CDW2. As shown in Fig. 4.1**c**, CDW1 and CDW2 are mapped onto the two states of the $S = 1/2$-QLM with uniform electric field $\hat{S}^z_{j,j+1} = \pm 1/2$. The experimental results in Ref. [88] may thus be interpreted as the evolution starting from one of the two degenerate bare particle vacua $|0_\pm\rangle$ (i.e, the vacua in the absence of quantum fluctuations, $w = 0$) of the gauge theory. In Fig. 4.1**d** and in the first column of Fig. 4.2, we illustrate these dynamics as it would be observed in the excitation density $\langle n_j \rangle$ along the Rydberg-atom quantum simulators ("Rydberg") and compare it with that of the electric field $\langle E_{j,j+1} \rangle$ within its gauge-theory description ("QLM") in Fig. 4.1**e** and in the second column of Fig. 4.2, respectively, utilizing exact diagonalization.

The qualitative features of this evolution are strongly affected by quantum fluctuations, whose impact is quantified by the ratio between the coupling constant w and the particles mass m. For small values of m/w (first two lines in Fig. 4.2), production of particle-antiparticle pairs occurs at a finite rate. We

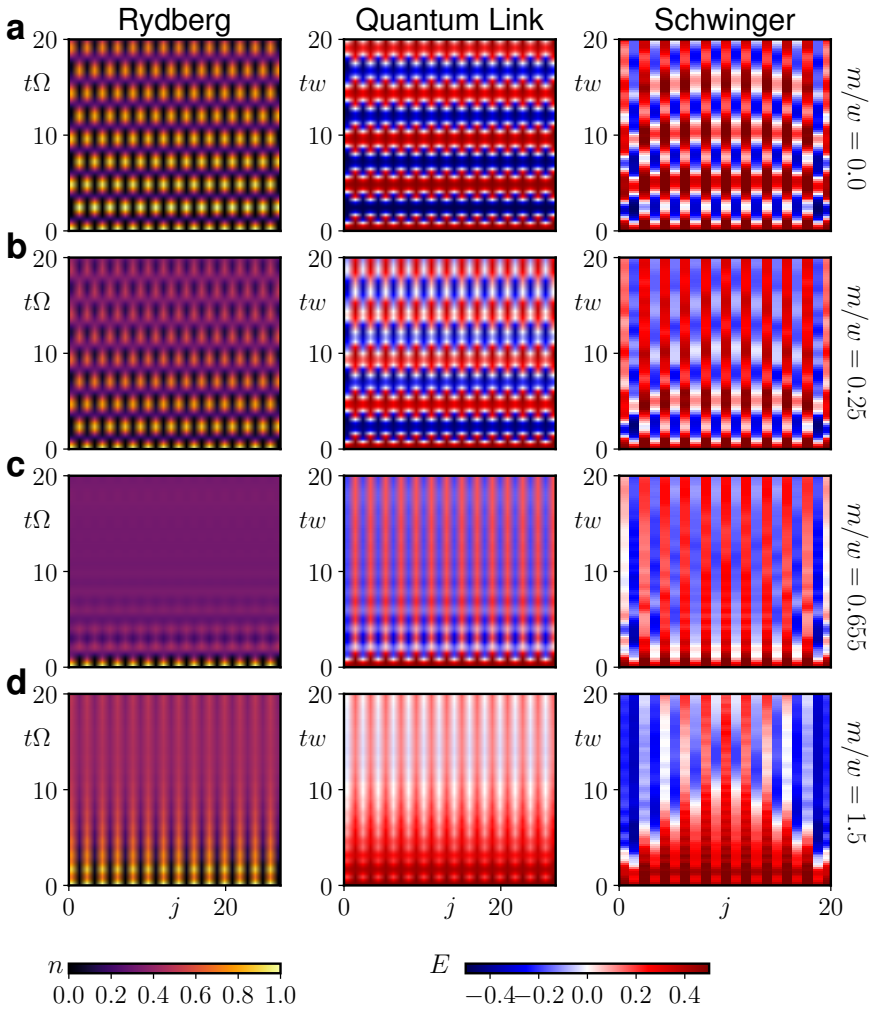

Figure 4.2: Slow dynamics in Rydberg atoms, $U(1)$ quantum link model (QLM), and the lattice Schwinger model. Coherent quantum evolution of (first column) the local Rydberg excitation density profile $n_j(t) = \langle \hat{n}_j(t) \rangle$ in the FSS model [see Eq. (4.34)], starting from a charge-density wave, of the local electric field profile (second column) $E_{j,j+1}(t) = \langle \hat{S}^z_{j,j+1}(t) \rangle$ in the QLM, and (third column) $\langle \hat{L}_{j,j+1}(t) - \theta/(2\pi) \rangle$ (see further below in the main text) in the lattice Schwinger model [see Eq. (4.35)] with $J/w = 1.5$ and $\theta = \pi$. The four rows correspond to increasing values of the detuning δ (Rydberg) or, equivalently, of the particles mass $m = -\delta$ (QLM and Schwinger model). Figures (4.1)**d** and (4.1)**e** correspond to the first two plots in panel **a** here. Data in the first and second columns are connected by a unitary transformation, while a remarkable similarity is manifest between the second and third column despite the larger Hilbert space of the gauge degrees of freedom in the Schwinger model. The persistent string inversions observed within the symmetric phase with $m < m_c = 0.655|w|$ (first two lines) are suppressed as the quantum critical point is approached. The dynamics in the third column feature edge effects due to the imposed open boundary conditions.

remark that this effect is reminiscent of the Schwinger mechanism [120], which however concerns pair creation from the true (and not the bare) vacuum. These

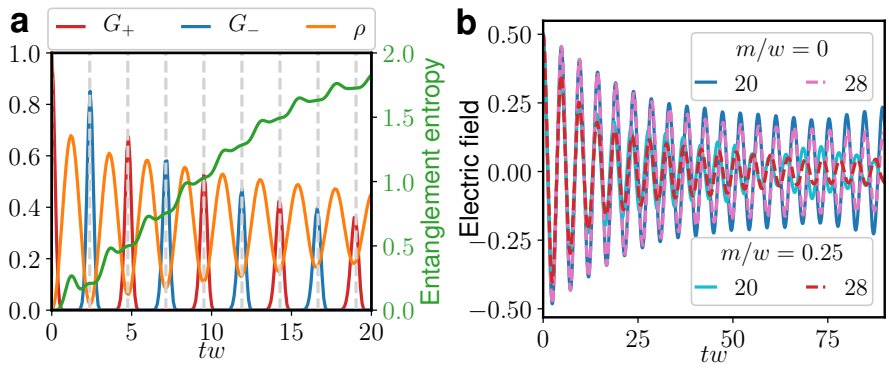

Figure 4.3: Characterization of slow dynamics in the FSS model. **a:** Hilbert space characterization of the persistent string inversions ($m = 0$, $L = 28$): alternating strong revivals of the overlaps $G_\pm(t) = |\langle 0_\pm|e^{-i\hat{H}t}|0_+\rangle|^2$ with the two bare vacuum states $|0_\pm\rangle$, corresponding to the two charge-density wave configurations of Rydberg-atom arrays. Both the total density $\rho = \langle\hat{\rho}_j\rangle$ of particle-antiparticle pairs, with $\hat{\rho}_j = (-1)^j\hat{\Phi}_j^\dagger\hat{\Phi}_j + [1-(-1)^j]/2$ and the half-chain entanglement entropy (see the supplementary information) have regularly-spaced maxima between the peaks. **b:** Persistent oscillations of electric field for two values of the mass and of the system size.

particles get accelerated by the electric field and progressively screen it, until coherent pair annihilation takes place and eventually brings the system to a state with opposite electric flux. This process, referred to as *string inversion*, occurs several times in a coherent fashion, causing a dramatic slowdown of thermalization and of quantum information scrambling. As a further evidence, we compute both the total electric flux and the vacuum persistence amplitude (or Loschmidt echo), defined as $G_+(t) = |\langle 0_+|e^{-i\hat{H}t}|0_+\rangle|^2$, whose large value $\simeq 1$ was already noted in Ref. [135]. The anomalous long-lived oscillations of these quantities experimentally detected with Rydberg atom arrays in Ref. [88] show a clear analogy with several previous numerical studies of the real-time dynamics of higher-spin QLMs [86] as well as of the Schwinger model [108, 136, 125] and Higgs theories [124]. In addition, as noted in Ref. [132], the dynamics discussed here describes the coherent oscillations of the parity-symmetric order parameter (in our case, $\langle\hat{E}_{j,j+1}\rangle$) as a function of time, reminiscent of the decay of a chiral condensate in QCD [126]. We thus provide here a bridge among all these observations.

However, if fermionic particles are sufficiently heavy, with m/w exceeding a critical threshold, pair production is a virtual process and string inversion cannot be triggered, as shown in the third and fourth line of Fig. 4.2. We find that this behavior is related to the quantum phase transition occurring in the FSS model at $\delta_c = -0.655|\Omega|$ [90]. This transition corresponds to the spontaneous breaking of the chiral symmetry in the LGT (4.36) at $m_c = 0.655|w|$ [137]. Let us observe

that this transition occurs in the ground state of the FSS model, while here we are studying the dynamics of the excited states. The fact that the properties of the ground state influence also the dynamics of excited states is not a trivial aspect. The four rows in Fig. 4.2 show the temporal evolution of the same initial uniform flux configuration (CDW or "string" in Fig. 4.1**c**) upon increasing values of the mass $m/w = 0, 0.25, 0.655, 1.5$ corresponding to the dynamics (**a**, **b**) at $m < m_c$, (**c**) at the quantum critical point $m = m_c$, and (**d**) at $m > m_c$.

Figure (4.3) further illustrates the appearance of string inversions for $m < m_c$ and the corresponding slow dynamics. Panel **a** shows the long-lived revivals of the many-body wavefunction in terms of the evolution of the probability $G_{\pm}(t)$ of finding the system at time t in the initial bare vacuum state $|0_+\rangle$ or in the opposite one $|0_-\rangle$, corresponding to G_+ or G_-, respectively, as well as in terms of the time-dependent density ρ of particle-antiparticle pairs. The entanglement entropy of half system also displays an oscillatory behavior (see supplementary information). Panel **b** shows the scaling of the collective oscillations of the electric field with respect to the system size L, as well as their persistence with a small but non-vanishing fermion mass $m < m_c$.

4.2.4 Slow dynamics in the Schwinger model

The above phenomenology is not restricted to QLMs, but is expected to be a generic feature of LGTs including dynamical matter. We show this in the context of a Wilsonian LGT, i.e., the lattice version of the Schwinger model in Eq. (4.35). In this case, $\hat{U}_{j,j+1} = e^{i\hat{\vartheta}_{j,j+1}}$ are $U(1)$ parallel transporters with vector potential $\hat{\vartheta}_{j,j+1}$, the corresponding electric field operator is $\hat{E}_{j,j+1} = \hat{L}_{j,j+1} - \theta/(2\pi)$, where $\hat{L}_{j,j+1}$ have integer spectrum and $\theta/(2\pi)$ represents a uniform classical background field parameterized by the θ-angle. Canonical commutation relations for the gauge degrees of freedom read $[\hat{\vartheta}_{j,j+1}, \hat{L}_{p,p+1}] = i\delta_{jp}$. In our numerical simulations, we utilize the spin formulation of the model obtained upon integration of the gauge fields under open boundary conditions [85, 138].

We consider the case of a θ-angle with $\theta = \pi$, such that two uniform field configurations have equal electrostatic energy. In the limit $J/w \to \infty$, the lattice Schwinger model is equivalent to the spin-1/2 QLM discussed above. We find evidence that the corresponding behaviour persists qualitatively down to $J \simeq w$, when the electrostatic energy competes with the matter-field interaction, as shown in the third column of Fig. 4.2. Despite the strong quantum fluctuations allowed in principle by the exploration of a locally infinite-dimensional Hilbert space, a qualitative similarity (which becomes a quantitative correspondence concerning the relationship between the coupling and the period of oscillation) with

the case of the locally finite-dimensional Hilbert space of the QLM is manifest in the second column of Fig. 4.2, related to the observed dynamics in Ref. [88].

The generality of the occurrence of oscillations which do not decay on time scales immediately related to the microscopic couplings points to a rather robust underlying mechanism. In fact, we suggest here that this behavior may arise from a universal field-theoretical description of the nonequilibrium dynamics of states possessing a well-defined continuum limit. Concerning the $U(1)$ LGTs discussed in this work, the reference continuum field-theory description is provided by the Schwinger model, representing quantum electrodynamics in one spatial dimension. In the massless limit $m = 0$, this model can be exactly mapped by bosonization to a free scalar bosonic field theory (see Appendix B), described in terms of the canonically conjugate fields $\hat{\Pi}$ and $\hat{\phi}$ by the integrable Hamiltonian [120]

$$\hat{H}_{\mathrm{B}} = \int \mathrm{d}x \left[\frac{1}{2}\hat{\Pi}^2 + \frac{1}{2}(\partial_x \hat{\phi})^2 + \frac{1}{2}\frac{e^2}{\pi}\hat{\phi}^2 \right]. \tag{4.41}$$

Within this bosonized description, the field $\hat{\phi}(x,t)$ represents the electric field, and all its Fourier modes $\tilde{\phi}(k)$ correspond to decoupled harmonic oscillators. The evolution starting from a false vacuum with a uniform string of non-vanishing electric field $\langle \hat{\phi}(x, t = 0) \rangle = \mathrm{const} \neq 0$ represents an excitation of the single uniform mode with $k = 0$, and hence the electric field will show uniform periodic string inversions around zero, with a frequency $\omega_0 = e/\sqrt{\pi}$, where e is the charge of the fermion. A non-vanishing value of m leads to the additional potential term $-cm\omega_0 \cos(2\sqrt{\pi}\hat{\phi} - \theta)$ in the integrand in Eq. (4.41), such that the resulting total potential shows a transition from a shape with a single minimum for $m < m_c$ to two symmetric minima for $m > m_c$. This weak local non-linearity introduced by a small m couples the various Fourier modes and hence induces a weak integrability breaking. In this case, the uniform string inversions of the electric field evolving from a false vacuum configuration with $\langle \tilde{\phi}(k = 0) \rangle \neq 0$ are expected to be superseded by slow thermalization processes at long times (see, e.g., Ref. [139]).

We suggest that a remnant of this slow dynamics induced by the underlying integrable field theory may persist in lattice versions of this gauge theory as long as initial states with a well-defined continuum limit are considered. With the latter, we mean states whose field configuration is smooth at the level of the lattice spacing: for our case here, the two Néel states represent the smoother ones, as they correspond to the bare vacuum of the fermionic fields, and no electric field excitations. At a qualitative level, the effect of integrability-breaking induced by lattice effects is expected to be much weaker in the small Hilbert space sector involving uniform excitations with $k = 0$ only, where the long-lived string

inversion dynamics take place. The number of states in this sector grows linearly with the lattice size L and their energy spans an extensive range, in agreement with the characteristics of "many-body quantum scars", see Ref. [99] and Sec. 4.2.6 below.

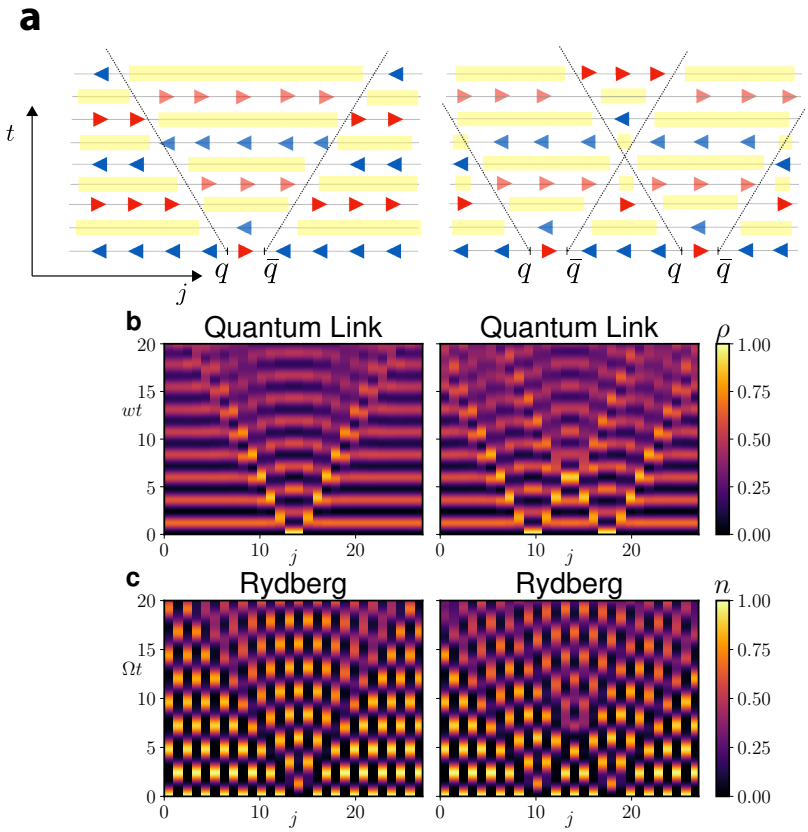

Figure 4.4: Slow dynamics of particle-antiparticle pairs. **a**: Cartoon states representing the propagation of particle-antiparticle pairs q-$\bar{q}$. The notation is the same as in Fig. 4.1**c**, while the yellow stripes denote regions of space with largest particle density and therefore $\langle \hat{E}_{j,j+1} \rangle \simeq 0$. **b**: Evolution of the particle density in the QLM starting from a bare vacuum or "string" state, see Fig. 4.1**c**, with initial particle-antiparticle pairs. **c**: Same as in panel **b**, but in the Rydberg excitation density representation. Left column: the oscillations observed in the light-cone shaped region originating from the particles is expected to be out of phase with respect to those of the bare vacuum. Right column: In the presence of two q-$\bar{q}$ pairs, an additional change of periodicity is expected in correspondence of elastic scattering. In these simulations, $m = \delta = 0$.

4.2.5 Propagation of particle-antiparticle pairs

States of the QLM corresponding to particle-antiparticle pairs in the bare vacuum can be constructed in Rydberg-atom quantum simulators by preparing two or more defects in a charge-density wave configuration, each corresponding to pairs of adjacent non-excited Rydberg atoms.

As an illustration, we discuss how the time-evolution of one or two particle-antiparticle pairs for $m < m_c$ features the emergence of slow dynamics. In Fig. 4.4, we show the time evolution of both the particle density in the QLM and the corresponding density of excitations in the Rydberg chain, fixing for simplicity $m = 0$. The pairs in the initial state break and ballistic spreading of quark and antiquark takes place. The string inversion dynamics induced by this propagation shows coherent interference patterns with long-lived oscillations. Due to retardation effects induced by the constrained dynamics, these oscillations are shifted by half a period with respect to the vacuum oscillation, as captured by second-order perturbation theory.

These unusual dynamics turn out to be robust under experimentally realistic conditions: In Fig. 4.5 we consider the evolution of a particle-antiparticle pair, the simulated dynamics of which is not constrained to the subspace satisfying $\hat{n}_j\hat{n}_{j+1} = 0$ and includes the effect of the long-range Rydberg interactions between atoms. The evolution is performed via Krylov subspace techniques in the unconstrained Hilbert space with the Hamiltonian in Eq. (4.33), with $\delta = 0$ and $V_{j,k} = V_1|j-k|^{-6}$. The value of $V_1/\Omega = 25.6$ is the same as considered in Ref. [88]. The dynamics displayed Fig. 4.5 is similar to the constrained one in Fig. 4.4**b**,**c** at short times, after which the effects of having realistic interactions gradually kick in.

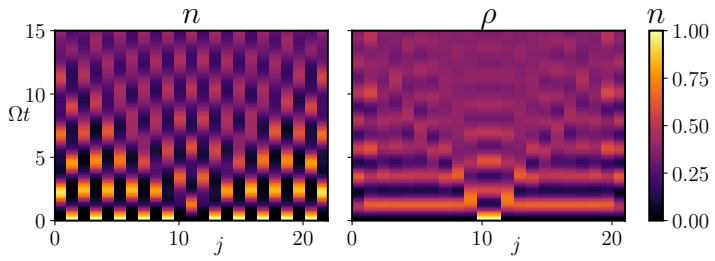

Figure 4.5: Propagation of a particle-antiparticle pair q-$\bar{q}$ with realistic Rydberg interactions. Left panel: density of Rydberg excitations. Right panel: density of particles/antiparticles (ρ in the QLM language). Results are obtained for a chain of $L = 23$ sites governed by the realistic Hamiltonian (4.33) with $V_{ij} = V_1 r_{ij}^{-6}$ and no constraints in the Hilbert space. Parameters: $\delta = 0$, $V_1/\Omega = 25.6$. We checked explicitly that the violation of Rydberg blockade is always small, $\langle n_j n_{j+1}\rangle < 10^{-2}$.

4.2.6 Spectral properties and bands of non-thermal states

We characterize the anomalous ballistic spreading of particle-antiparticle pairs discussed in the previous Section in terms of the emergence of corresponding

anomalous spectral properties of the FSS model, which generalize those recently observed [99] in the special case $m = 0$, involving families of special energy eigenstates referred to as "many-body quantum scars". The latter are constituted by towers of regularly-spaced states in the many-body spectrum with alternating pseudo-momentum $k = 0$ and $k = \pi$, characterized by non-thermal expectation values of local observables as well as by anomalously large overlaps with the charge-density wave initial states. The long-lived coherent oscillating behavior has been attributed in Ref. [99] to the existence of these "scarred" eigenstates.

Fig. 4.6**a** shows that the modulus of the overlap between the energy eigenstate $|\psi\rangle$ with energy E and the above described inhomogeneous states $|\phi_{q\bar{q}}\rangle$ with momentum k clearly identifies a number of special bands of highly-excited energy eigenstates characterized each by an emerging functional relationship $E(k)$. As shown in Fig. 4.6**d** some of the states in these bands strongly deviate from the thermal value $\langle n_j \rangle_{th} \simeq 0.276$. This fact has already been observed in the previously studied quantum-scarred eigenstates, which coincide with the extremal points of these bands at momenta $k = 0$ and $k = \pi$. A closer inspection of these energy-momentum relations, presented in Fig. 4.6**b**, shows that they are close to cosine-shaped bands, suggesting the emergence of single-particle excitations in the middle of the many-body energy spectrum.

We further characterize this spectral structure by constructing a quasi-particle variational ansatz $|\chi_k\rangle$ on top of the exact matrix-product-state zero-energy eigenstate of the Hamiltonian (4.34) with $\delta = 0$, recently put forward in Ref. [82]. In order to obtain physical intuition on the emergence of regular energy-momentum bands in highly-excited states which govern the non-equilibrium evolution of localized defects, we propose the following wavefunction

$$|\chi_k\rangle = \sum_{j=1}^{L} e^{-ikj} \hat{O}_{j-1,j,j+1} |\Phi_{k=0}\rangle \,, \tag{4.42}$$

where $|\Phi_{k=0}\rangle$ is the exact eigenstate found in Ref. [82] with momentum $k = 0$ and energy 0, and $\hat{O}_{j-1,j,j+1}$ is a three-site operator depending on a number of variational parameters. Due to the constraints, the space where this operator acts is reduced from dimension 2^3 to 5. The inversion symmetry with respect to site j reduces the number or free variational parameters in $\hat{O}_{j-1,j,j+1}$ to 11. We choose a basis of operators $\{\hat{M}^{\alpha}_{j-1,j,j+1}\}_{\alpha=1}^{11}$ for parameterizing $\hat{O}_{j-1,j,j+1}$ and define

$$|\phi^{\alpha}_{k}\rangle = \sum_{j=1}^{L} e^{-ikj} \hat{M}^{\alpha}_{j-1,j,j+1} |\Phi_{k=0}\rangle \,. \tag{4.43}$$

For each k, we minimize the energy variance in the space spanned by the states $|\phi^{\alpha}_{k}\rangle$. To this aim, we compute the three matrices $N^{k}_{\alpha\beta} = \langle \phi^{\alpha}_{k} | \phi^{\beta}_{k} \rangle$, $P^{k}_{\alpha\beta} =$

$\langle\phi_k^\alpha|\hat{H}|\phi_k^\beta\rangle$, $Q^k_{\alpha\beta} = \langle\phi_k^\alpha|\hat{H}^2|\phi_k^\beta\rangle$. In order to prevent numerical issues in the minimization, we diagonalize the matrix of the norms N_k and we compute the (rectangular) matrix U^k whose columns are the eigenvectors of N^k having non-zero eigenvalues. We then find the vector $\boldsymbol{c_k} = (c_k^1, \ldots, c_k^m)$ that minimizes

$$\sigma^2_{\hat{H}} = \frac{\boldsymbol{c_k}^\dagger U^{k\dagger} Q^k U^k \boldsymbol{c_k}}{\boldsymbol{c_k}^\dagger U^{k\dagger} N^k U^k \boldsymbol{c_k}} - \left(\frac{\boldsymbol{c_k}^\dagger U^{k\dagger} P^k U^k \boldsymbol{c_k}}{\boldsymbol{c_k}^\dagger U^{k\dagger} N^k U^k \boldsymbol{c_k}}\right)^2 . \tag{4.44}$$

Note that by introducing the matrix U^k we restrict the minimization to states with non-zero norms, thus further reducing the number of variational parameters to $m(k) \leq 11$. The optimal wavefunction is then obtained as

$$|\chi_k\rangle = \sum_{\alpha=1}^{11} \sum_{\beta=1}^{m} U^k_{\alpha\beta} c_k^\beta \, |\phi_k^\beta\rangle \, . \tag{4.45}$$

As shown in Fig. 4.6**c**, the optimal quasi-particle ansatz has the largest overlap with the states on the energy-momentum bands of special eigenstates closest to zero energy, thus reinforcing the above emergent quasi-particle picture.

4.2.7 Tuning the topological θ-angle in Rydberg experiments

So far, our discussion has focused exclusively on the relation between Rydberg experiments and the Schwinger model with topological angle $\theta = \pi$. A natural question to ask is whether, within the present setting, it is possible to realize genuinely confining theories, i.e., generic values of the topological angle $\theta \neq \pi$.

This is possible within the strong coupling limit upon introducing a linear term in the electric field. To see this, with reference to the lattice Schwinger model introduced in chapter 3, let us introduce the parameter $\epsilon = \theta/\pi - 1$ which quantifies the deviation of the topological angle from π. For $|\epsilon| \ll 1$, the two lowest energy states of the electric field have $L_{j,j+1} = 0, +1$ on each bond. In order to keep the structure of the Hilbert space compatible with the FSS model, one requires the energy gap $\Delta = 2J(1+\epsilon)$ of the next excited state (either $L_{j,j+1} = 2$ or $L_{j,j+1} = -1$ depending on the sign of ϵ) to be much larger than that separating the first two, i.e., $\sigma = J\epsilon$. Accordingly, the lattice Schwinger model with strong $J \gg \Omega, m$ and with a topological angle $\theta = \pi(1 + \sigma/J)$ is efficiently approximated by the QLM with an additional term linear in the electric field and proportional to σ. The confining nature of the potential can be intuitively understood as follows: starting form the bare vacuum (the "string" state in Fig. 4.1), creating and separating a particle-antiparticle pair at a distance ℓ entails the creation, between the two, of a string of length ℓ with opposite electric field. The corresponding energy cost is proportional to $\ell\sigma$, signalling the confining nature of the potential.

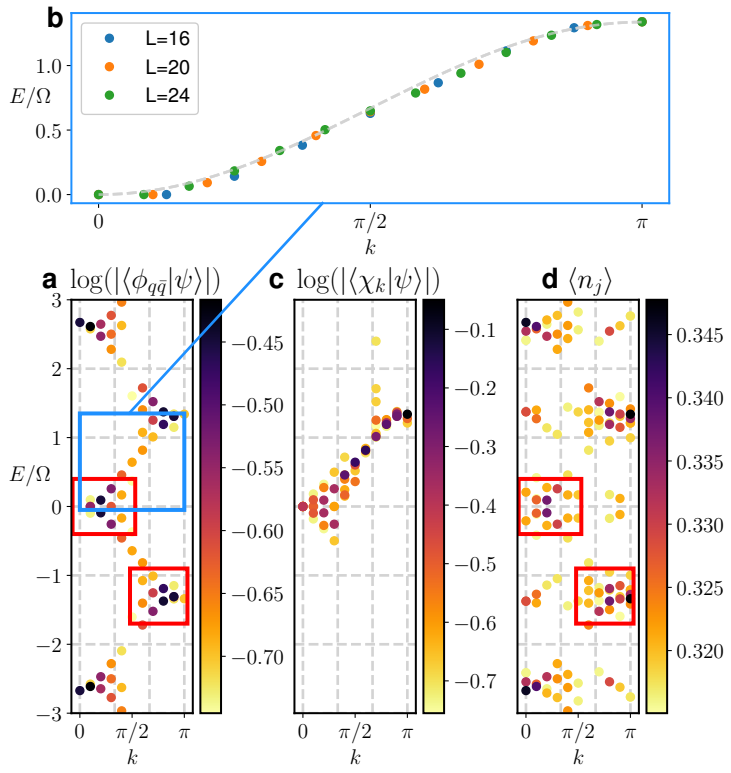

Figure 4.6: Emergent quasi-particle description of highly-excited states. **a**: Largest overlaps of the initial state $|\phi_{q\bar{q}}\rangle$ with a localized defect in a charge-density wave configuration of the Rydberg-atom chain with the energy eigenstates $|\psi\rangle$ of the FSS Hamiltonian ($\delta = 0, L = 20$) in Eq. (4.34), as a function of their corresponding momentum and energy. Within the gauge-theory description, the initial state corresponds to having a localized particle-antiparticle pair q-$\bar{q}$. **b**: The eigenstates with the largest overlaps display a regular functional dependence of energy on momentum that is remarkably close to a simple cosine band. **c**: The largest overlaps of the optimal matrix-product state quasi-particle ansatz $|\chi_k\rangle$ built on an exact eigenstate with zero energy (see the main text) accurately reproduce the corresponding emergent quasi-particle band of panel **a**. **d**: Anomalous (non-thermal) expectation values of a local observable in energy eigenstates. The red boxes highlight the correspondence between the most relevant eigenstates building up $|\phi_{q\bar{q}}\rangle$ (panel **a**) and the most non-thermal eigenstates (panel **d**). The emergent spectral structure illustrated in this picture underlies the clean ballistic spreading of particle-antiparticle pairs displayed in Fig. 4.4.

In turn, within the exact mapping outlined in Sec. 4.2.2 and illustrated in Fig. 4.1, this $\theta-$angle term corresponds to an additional staggered field in the FSS model, leading to the Hamiltonian:

$$\hat{H}_{\text{Ryd}} = \sum_{j=1}^{L} (\Omega\, \hat{\sigma}_j^x + \delta\, \hat{\sigma}_j^z) + \sum_{j=1}^{L} (-1)^j \frac{\sigma}{2} \sigma_j^z. \tag{4.46}$$

The new term can be experimentally realized, e.g., by utilizing a position dependent AC Stark shift or, alternatively, a space-dependent detuning on the

transition between ground and Rydberg states.

In Fig. 4.7, we show the effect of the $\theta-$angle on the evolution of the total electric field in the QLM starting from a uniform string state. As data clearly show, while in the symmetric phase with $m < m_c$, the explicit symmetry breaking caused by the electric field energy imbalance leads to damping of the string inversions, in the broken-symmetry (chiral) phase with $m > m_c$ the effect of confinement is dramatic, causing the persistence of the initial electric string, with small long-lived oscillations. Focusing on the latter phase, in Fig. 4.8 we show the dynamical evolution of a finite electric string generated by a particle-antiparticle pair (left panels), at the deconfined point $\theta = \pi$ (top) and in the confined phase with $\theta \neq \pi$ (bottom). The right panels show the same evolution as it would appear in terms of measurements of Rydberg atom excitations. While for $\sigma = 0$ nothing prevents the initially localized bare particles to propagate along the chain (top panels), the presence of a linear confining potential proportional to σ between them stabilizes the electric string, leading to effective Bloch oscillations of the edges and to a surprisingly long lifetime [79] (bottom panels). This effect signals that confinement can dramatically affect the non-equilibrium dynamics, potentially slowing it down as observed in both gauge theories [140] and statistical mechanics models [77, 96].

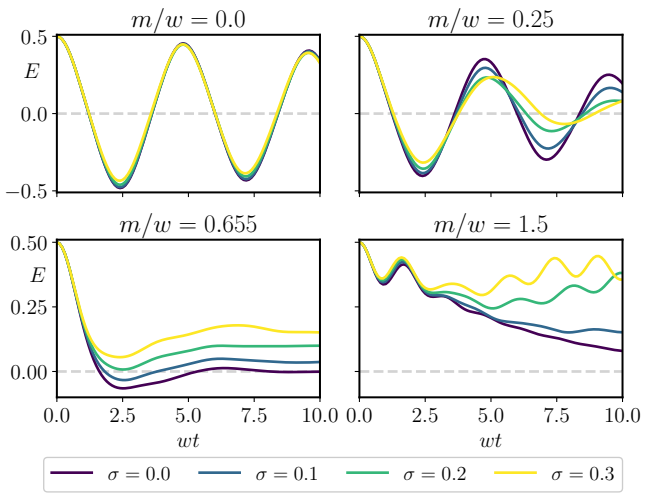

Figure 4.7: Effect of the $\theta-$angle on the dynamics of the electric field from uniform string states of the QLM. Data are shown for a chain of $L = 28$ sites, for increasing values of the particle mass m/w and of the parameter σ, quantifying the deviation of the $\theta-$angle from π (see the main text). Dynamics for $\sigma = 0$ correspond to the second column of Fig. 4.2.

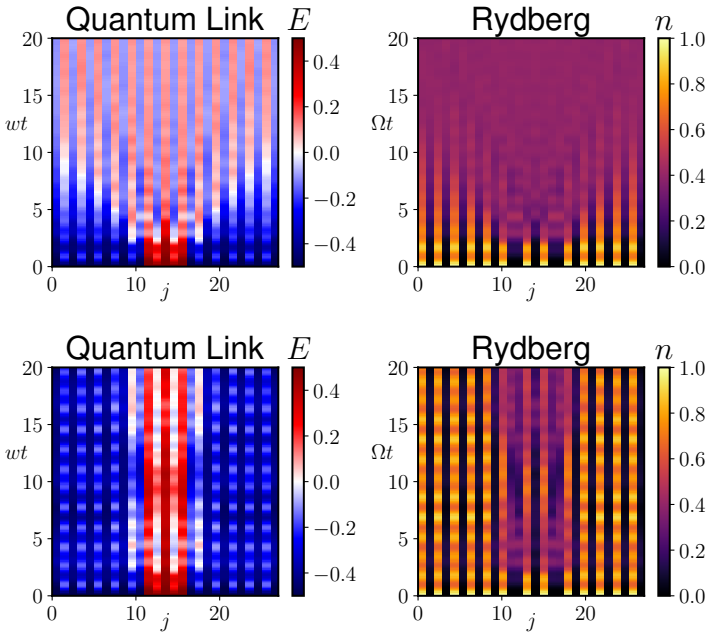

Figure 4.8: $\theta-$angle and string-breaking dynamics. Evolution of a bare particle-antiparticle pair state is displayed in terms of space- and time-dependent electric field in the QLM (left panels) and of the density of excited atoms in the Rydberg array (right panels), with $m = -\delta = 1.5\Omega$ and $L = 28$. Simulations in the top row have $\sigma = 0$, corresponding to the deconfined field theory with $\theta = \pi$. Effects of confinement emerge in the second row, where a non-vanishing $\sigma = 0.3\Omega$ stabilizes the electric string.

4.3 Similarities between Ising model and Schwinger model

In this section we report some results which show how the confinement observed in the lattice Schwinger model (4.29) causes similar effects in the dynamics of string states of the linear interaction among the quasi-particles excitations in the Ising model with longitudinal field (2.1). For this purpose let us consider "string" initial states, in which we have a particle q and an anti-particle $\bar{q}$ at a distance d, and let us measure the electric field on site, $\langle \hat{L}_n \rangle$, defined as

$$\hat{L}_n = \frac{1}{2} \sum_{l=1}^{n} (\hat{\sigma}_l^z + (-1)^l). \tag{4.47}$$

In this case we consider $\theta = 0$. As we can observe in Fig. 4.9, the bare vacuum evolves creating many pairs of particle and antiparticles, as signaled by the fast oscillations of the electric field. However, *inside* the string, the dynamics is essentially frozen, this fact is reminiscent of the dynamics in multiple-kink states observed in Chapter 2. The similitude is not only qualitative, but also quantitative. It is in fact possible to interpret the Ising model with longitudinal field

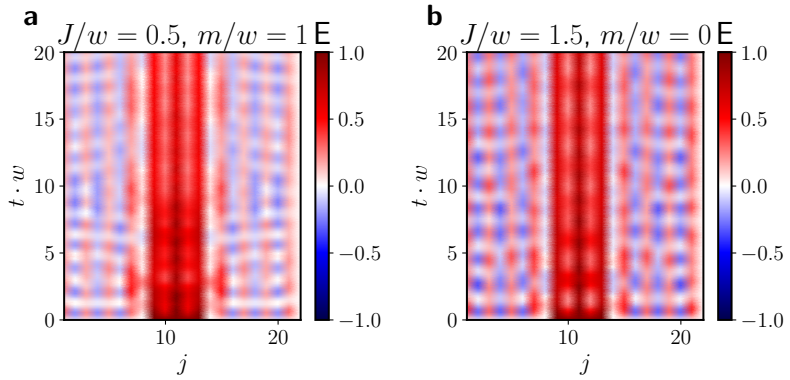

Figure 4.9: Space-time dependence of the electric field starting from initial states with one e^+e^- pair, for different values of the coupling J/w and of the mass m/w in Hamiltonian (4.29).

as a matter-integrated-out gauge theory [95]. In order to show this aspect let us rewrite Hamiltonian (2.1) changing notation,

$$H = -J \sum_j \sigma_j^z \sigma_{j+1}^z - h \sum_j \sigma_j^z - g \sum_j \sigma_j^x. \tag{4.48}$$

Let us introduce two species of fermions (+ and −) living on the bond of the lattice. The corresponding operators $(c^+_{j,j+1})^\dagger$ and $(c^-_{j,j+1})^\dagger$ create an anti-particle $\bar{q}$ or a particle q at the bond $(j, j+1)$, respectively. Denoting the occupancy numbers $n^\pm_{j,j+1} = (c^\pm_{j,j+1})^\dagger c^\pm_{j,j+1}$, we can write

$$H_{U(1)} = H_{\text{matter}} + H_{\text{gauge}} + H_{\text{int}} \tag{4.49}$$

where

$$H_{\text{matter}} = m \sum_j (n^+_{j,j+1} + n^-_{j,j+1}) + U \sum_j n^+_{j,j+1} n^-_{j,j+1} \tag{4.50}$$

$$H_{\text{gauge}} = \frac{\tau}{2} \sum_j \sigma_j^z \tag{4.51}$$

$$H_{\text{int}} = w \sum_j (c^+_{j-1,j})^\dagger \sigma_j^- c^+_{j,j+1} + \text{ h.c. } + \tag{4.52}$$

$$(c^-_{j-1,j})^\dagger \sigma_j^+ c^-_{j,j+1} + \text{ h.c. } + \tag{4.53}$$

$$(c^+_{j-1,j})^\dagger \sigma_j^+ (c^-_{j,j+1})^\dagger + \text{ h.c. } + \tag{4.54}$$

$$(c^-_{j-1,j})^\dagger \sigma_j^- (c^+_{j,j+1})^\dagger + \text{ h.c.} \tag{4.55}$$

We must to point out that in order to obtain an exact correspondence with the Ising chain, it is necessary to prevent that particles and antiparticles to occupy the same place; this can be enforced with a strong Hubbard interaction $U \to \infty$. Gauge-invariance of interactions is expressed, as usual, by the local conservation laws

$$[H, G_j] = 0 \tag{4.56}$$

with

$$G_j = \frac{\sigma^z_{j+1}}{2} - \frac{\sigma^z_j}{2} - (n^+_{j,j+1} - n^-_{j,j+1}), \tag{4.57}$$

which give rise to the Gauss law constraints within the neutral gauge sector $G_j \equiv 0$. The redundant matter degrees of freedom may be thereby eliminated using these constraints. It is possible to check that all matrix elements of the Hamiltonian (4.55) coincide with the corresponding matrix elements of the quantum Ising chain, upon identifying $m = 2J$, $\tau = 2h$, $w = g$.

CHAPTER 5

CONCLUSIONS

In this thesis we have analyzed the extremely fascinating topic of dynamics in isolated constrained quantum statistical systems. We have shown how this class of systems shows peculiar dynamical properties. In fact, although being non-integrable and non-disordered, they present an extremely slow dynamics, unrelated to any microscopical parameter of the Hamiltonian, which prevents a relaxation toward a thermal ensemble.

In the first original part of this thesis, reported in chapter 2, we focused on a general class of spin systems which, in the presence of an external field, has a linear confining potential between the excitations. Motivated by some recent results concerning the spreading of the correlation in these systems, we have shown that the transport properties are strongly affected by the presence of this kind of interaction. Despite its simplicity, this interaction may deeply influence the dynamics of the system for an unexpected long time-scale, unaccessible in any state-of-the-art experimental setup. In particular, we considered the prototypical case of the Ising model with a longitudinal field and we studied the dynamics starting from inhomogeneous initial states with energy imbalance. Contrary to the common expectation of seeing these inhomogeneities being smoothed out by the time evolution for some, easily realizable, initial states, we observed a persistence of them, resulting in a freezing of the dynamics. We argued that this phenomenon is expected to occur in a general class of spin systems and that it is also relevant for experimental purposes, being some actual crystals effectively described by similar Hamiltonians. We discussed, in particular, the example of the antiferromagnetic XXZ model with a staggered magnetic field. In addition, we have tried to tackle this problem in a general way by giving a lower bound

on the ultimate thermalization time that turned out to be exponentially long in the parameters J and h_z/x of the Hamiltonian (2.1). By studying the temporal growth of the entanglement entropy, starting from multiple-kink states, we have shown that in some regimes this growth is logarithmic in time, thus confirming a physical picture that, at least on long time scales, is similar to what is observed in many-body localized systems.

In the second part of the thesis we focused on another type quantum systems, i.e., systems that have some energetic constraint (Rydberg atom chains in the blockade regime) which prevent them from fully exploring the Hilbert space during the non-equilibrium time evolution. Also in this case, as witnessed by recent experiments, an anomalously slow dynamics is observed if the system is prepared in certain initial states. These strongly interacting systems can be described by simple effective Hamiltonians. In particular, we analyzed the case of Rydberg atoms chain in the blockade regime that is described by the Fendley-Sachdev-Sengupta (FSS) model. Our major contribution to this topic has been to establish a connection between the FSS model and an abelian lattice gauge theory, namely the $S = 1/2$ quantum link model (QLM), which can mimic the electrodynamics in $(1 + 1)$-dimensions described by the Schwinger model. This enabled us to interpret the observed persistent oscillations as a consequence of string breaking processes. Another interesting aspect of the mapping between the FSS model and the $S = 1/2$-QLM is that it shown the possibility of performing large scale experiments in lattice gauge theory with the state-of-the-art-technology, although many steps have still to be done in this direction to simulate more complex theories.

The two parts of the thesis, as we emphasized in several occasions in the main text, are connected. This aspect has been highlighted, in particular in the last section of Chapter 4, in which we shown some phenomenological similarities between the dynamics of string states in the Schwinger model and in the Ising model with longitudinal field, and, furthermore, how the latter can be interpreted as $U(1)$ lattice gauge theory in which we have integrated out the gauge fields.

It would be relevant to understand whether the mapping between the FSS model and the $S = 1/2$-QLM can provide some insight concerning the origin of quantum scars (see chapter 3).

A possible interpretation is based on the fact that the continuum Schwinger model with $m = 0$ is integrable, as it can be shown using bosonization techniques (see Appendix B). This fact suggests us that for certain initial states, namely those for which the field configuration is *smooth* in space, the discretization procedure does not completely hide the effects of integrability. In this perspective, quantum scars could be seen as an effect of an underlying integrable field theory. This idea,

although fascinating, at the moment has not been tested. It would be interesting in the future to investigate further this issue by performing a also comparison with other models.

Another possible line of research would be to understand whether it is possible to engineering some cold atom systems with constraints that mimic a non-abelian gauge theory: this would represent a further step towards the "Holy Grail" of performing quantum simulations of non-abelian gauge theories in higher dimensions.

Concerning both part of the thesis it would be of extreme interest to perform experiment for testing the results discussed here. In particular, new initial states, with particles and antiparticles in the presence of a θ term slightly different from π, could be already created with the present technology and could be used to mimic very easy "scattering processes" with cold atoms quantum simulators.

APPENDIX A
EFFECTIVE HAMILTONIAN

In this appendix we discuss the solution of the effective Hamiltonian (2.14) introduced in chapter (2). This Hamiltonian is obtained once that we project the Ising long range Hamiltonian (2.1), or the XXZ in a staggered field Hamiltonian (2.29), onto the one-kink Hilbert space. It thus describes the oscillatory motion of a single particle on a lattice in the presence of a constant force, caused by the Bloch's band structure. Under the action of a constant force, the moment of the quasi-particle grows linearly in time $k(t) = k(0) + Ft/\hbar$ until it reaches the boundary of the Bloch's band and it is "reflected". This phenomenon was discovered and studied in the early days of the quantum mechanics during the twenties [141, 142]. A recent review about Bloch's dynamics in periodic potentials can be found in [143].

A.1 Ising with longitudinal field

Let us consider a tight-binding Hamiltonian described in terms of the Wannier states $|n\rangle$ which represent "a particle" localized on the site n:

$$H = -\frac{\Delta}{4}\sum_n (|n\rangle\langle n+1| + |n+1\rangle\langle n|) + dF\sum n|n\rangle\langle n|, \tag{A.1}$$

where F is the force's intensity and d is the periodicity of the potential, in our case, the lattice spacing. Let us note that Hamiltonian (A.1) is equivalent to (2.14) upon replacing $\Delta/4 \to h_z$ and $dF \to -2h_x$. In order to find the eigenstates of (A.1) let us move to the Fourier space defining the Bloch's waves functions

$$|\kappa\rangle = \sum_n |n\rangle\langle n|\kappa\rangle = \sqrt{\frac{d}{2\pi}}\sum_n |n\rangle e^{in\kappa d} \tag{A.2}$$

that satisfy the Bloch condition $\langle n+1|\kappa\rangle = \mathrm{e}^{ikd}\langle n|\kappa\rangle$. The quasi-momentum κ is confined in the Brillouin zone $-b/2 \leq \kappa \leq b/2$ with $(b = 2\pi/d)$. In this basis Hamiltonian (A.1) is diagonal $\langle \kappa^{'}|H|\kappa\rangle = \delta(\kappa^{'} - \kappa)H(\kappa)$ with

$$H(\kappa) = -\frac{\Delta}{2}\cos(\kappa d) + iF\frac{d}{d\kappa}. \tag{A.3}$$

Hamiltonian (A.3) is diagonalized, solving a first order differential equation, by the Wannier-Stark states $|\Psi_m\rangle$

$$-\frac{\Delta}{2}\cos(\kappa d)\Psi(\kappa) + iF\frac{d\Psi(\kappa)}{d\kappa} = E\Psi(\kappa), \tag{A.4}$$

which satisfy periodic boundary conditions $\Psi(\kappa + b) = \Psi(\kappa)$. We thus obtain

$$\Psi_m(\kappa) = \sqrt{\frac{d}{2\pi}}\mathrm{e}^{-i(m\kappa d + \gamma\sin(\kappa d))} \qquad m = 0, \pm 1, \ldots, \tag{A.5}$$

with $\gamma = \Delta/2dF$, and $E_m = mdF$. In real space the description is a little bit more elaborate, in fact a Fourier transformation leads to

$$\begin{aligned}\Psi_m(n) = \langle n|\Psi_m\rangle &= \int_{-b/2}^{b/2} d\kappa\langle n|\kappa\rangle\langle\kappa|\Psi_m\rangle = \\ &= \frac{d}{2\pi}\int_{-b/2}^{b/2} d\kappa \mathrm{e}^{i[(n-m)\kappa d - \gamma\sin(\kappa d)]} = \\ &= \frac{1}{2\pi}\int_{-\pi}^{+\pi} du \mathrm{e}^{i[(n-m)u - \gamma\sin u]} = J_{n-m}(\gamma),\end{aligned} \tag{A.6}$$

where $J_{n-m}(\gamma)$ is a Bessel function. Therefore the Wannier-Stark states in the Wannier representation are written in terms of the Bessel functions

$$|\Psi_m\rangle = \sum_n J_{n-m}(\gamma)|n\rangle. \tag{A.7}$$

The time evolution operator is periodic with period equal to the Bloch period $T_B = 2\pi\hbar/(dF)$, the propagator in the basis of the Wannier states is

$$\begin{aligned}U_{nm} = \langle n|U(t)|m\rangle = \sum_l \langle n|\Psi_l\rangle \mathrm{e}^{-iE_l t/\hbar}\langle\Psi_l|m\rangle = \\ J_{n-m}\left(2\gamma\sin\frac{\omega_B t}{2}\right)\mathrm{e}^{i(n-m)(\pi-\omega_B t)/2 - im\omega_B t},\end{aligned} \tag{A.8}$$

where $\omega_B = 2\pi/T_B$. Therefore for the time evolution of generic state we have

$$|\Psi(t)\rangle = \sum_n c_n(t)|n\rangle, \qquad \sum_n |c_n|^2 = 1, \tag{A.9}$$

assuming an extreme localized initial condition (that is the one in which we are interested) $c_n(0) = \delta_{n0}$ we obtain

$$c_n(t) = U_{n0}(t) = J_n\left(2\gamma\sin\frac{\omega_B t}{2}\right)\mathrm{e}^{in(\pi-\omega_B t)/2} \tag{A.10}$$

The eigenfunctions of the Hamiltonian (2.14) can be therefore written as

$$|\Psi_m\rangle = \sum_n J_{n-m}\left(\frac{h_z}{h_x}\right)|n\rangle, \tag{A.11}$$

with $m = 1, \ldots, L$, L number of sites, is the site where the kink is localized. Indeed in our problem the eigenvalues can be labelled with the position of the kinks because the state with a kink localized at site n has energy $E_n = (L-n)h_x$. Let us note as the argument of the eigenfunction is exactly the confinement length l_{conf} and that when $|n-m| \gg l_{conf}$ the wave function decays *faster* than exponential. At this point we can obtain the analytical expressions for the quantities that we have discussed in chapter (2). A domain-wall initial state (2.8) in this picture corresponds to having one particle localized in the middle of the chain, therefore

$$\psi_n(0) = \delta_{n,L/2}. \tag{A.12}$$

Time-dependent magnetization at a site j, defined in (2.15) can be thus be cast in the following form

$$m_j(t) = 1 - 2\sum_{n=1}^{j-1}|c_n(t)|^2 = 1 - 2\sum_{n=1}^{j-1} J^2_{n-\frac{L}{2}}(2l_{conf}\sin(h_x t)). \tag{A.13}$$

Similar calculations can be carried out for the computation of the energy density and energy current.

A.2 XXZ with staggered external field

For the antiferromagnetic XXZ chain defined in Eq. (2.27) similar calculations can be done, however there is an important difference, because in this case the quantum fluctuations term, i.e. $h_i^{QF} = (S_i^x S_{i+1}^x + S_i^y S_{i+1}^y)$, allows for a hop of the kink of *two* sites. In order to understand this fact let us rewrite (2.27) applying the so-called *staggered inversion* operator defined as

$$I = \prod_{j=1}^{L/2} \mathrm{e}^{i\pi S_{2j}^x} \qquad I^\dagger = I^{-1}, \tag{A.14}$$

we have

$$I^\dagger H_{XXZ} I = -\sum_{j=1}^{L-1}(S_i^x S_{i+1}^x - S_i^y S_{i+1}^y - \Delta S_i^z S_{i+1}^z) - hS_i^z. \tag{A.15}$$

In the limit $\Delta > 1$, in this case, the ground state is ferromagnetic ordered. If we consider a state with a kink at position n, i.e. $|\psi\rangle = \bigotimes_{i=1}^{n}|\uparrow\rangle \bigotimes_{i=n+1}^{L}|\downarrow\rangle = |n\rangle$,

assuming $h > 0$, we have

$$\left(-\Delta \sum_{j=1}^{L-1} S_i^z S_{i+1}^z - \sum_{j=1}^{L} S_j^z\right) |n\rangle = [E_{GS} + 2\Delta + 2(L-n)h]|n\rangle \tag{A.16}$$

for the diagonal part,

$$\sum_{i=1}^{L-1} S_j^x S_{j+1}^x |n\rangle = |n \pm 2\rangle \tag{A.17}$$

for the off-diagonal one. At this point, we can straightforwardly repeat the same procedure done for the Ising chain in longitudinal field, upon substituting $h_z \to J$, $h_x \to h$ and $J \to J\Delta$, obtaining

$$H_{XXZ}^{eff} = \sum_n \left[(J\Delta + (l-n)h)|n\rangle\langle n| + J(|n\rangle\langle n+2| + |n+2\rangle\langle n|)\right], \tag{A.18}$$

we see how the odd and even sectors are disconnected, i.e. if we initialize a particle on odd (even) site it will hop only on odd (even) sites. Also in this case the Hamiltonian (A.18) can be diagonalized in terms of Bessel functions and accordingly all the quantities (magnetization...) can be analytically computed.

APPENDIX B

CONTINUUM LIMIT OF THE MASSIVE SCHWINGER MODEL

The massive Schwinger model (4.11) describes the quantum electrodynamics of fermions of mass m and charge e in $1+1$ dimensions. Its Lagrangian density is

$$\mathcal{L} = -\frac{1}{4}F_{\mu\nu}F^{\mu\nu} + \bar{\psi}(i\partial - eA - m)\psi \tag{B.1}$$

where $F_{\mu\nu} = \partial_\mu A_\nu - \partial_\mu A_\nu$. The indices $\mu, \nu = 0, 1$ indicate respectively the time and space directions, and the slash notation indicates contraction with the Dirac matrices γ_μ. This model can be formulated in terms of a bosonic field ϕ [85]. We briefly recall here the main points of the derivation of the bosonic Hamiltonian obtained in Ref. [117].

In the Coulomb gauge ($A_1 = 0$), the Euler-Lagrange equation for A_0 yields

$$\partial_1^2 A_0 = -ej_0 \tag{B.2}$$

where $j_0 = \psi^\dagger\psi$ is the charge density. Integrating Eq. (B.2), we obtain the continuum version of the Gauss' law (4.25),

$$F_{01} = -\partial_1 A_0 = e\partial_1^{-1} j_0 + F \tag{B.3}$$

where F is a number, representing a classical background field. The Hamiltonian density obtained from the Lagrangian (B.1) has the form

$$\mathcal{H} = \bar{\psi}(i\gamma_1\partial_1 + m)\psi + \frac{1}{2}{F_{01}}^2. \tag{B.4}$$

The interacting Hamiltonian for the fermions can be formulated using Eq. (B.3) to integrate out the gauge fields. Integrating by parts in the zero charge sector,

i.e., $\int dx\ j_0(x) = 0$, we obtain

$$H = \int dx\ \bar{\psi}(i\gamma_1\partial_1 + m)\psi - \frac{e^2}{4}\int dx\ dy\ j_0(x)j_0(y)|x-y| - eF\int dx\ x j_0(x). \quad \text{(B.5)}$$

Similarly to the lattice version of this model [cf. Eq. (4.29)], the resulting Hamiltonian contains the energy of massive free fermions, the Coulomb interaction between charges (which increases linearly in one spatial dimension) and the interactions between the charges and the background field. The method of bosonization can be applied, by noting that in $1+1$ dimensions the conserved vector field $j^\mu = \bar{\psi}\gamma^\mu\psi$ can be written as the curl of a scalar field ϕ

$$j_\mu = \pi^{-1/2}\epsilon_{\mu\nu}\partial^\nu\phi. \quad \text{(B.6)}$$

By substituting in Eq. (B.3) we get

$$F_{01} = e\pi^{-1/2}\phi + F, \quad \text{(B.7)}$$

and, from the results obtained for a free massive Dirac field [144], we know

$$\bar{\psi}(i\gamma_1\partial_1 + m)\psi \to N_m\left[\frac{1}{2}\Pi^2 + \frac{1}{2}(\partial_1\phi)^2 - cm^2\cos(2\pi^{1/2}\phi)\right]. \quad \text{(B.8)}$$

where $c = e^\gamma/(2\pi)$, $\gamma \simeq 0.577$ is the Euler constant and N_m indicates normal ordering with respect to the mass m. Inserting Eqs. (B.7) and (B.8) in Eq. (B.4), the Hamiltonian density reads

$$\mathcal{H} = N_m\left[\frac{1}{2}\Pi^2 + \frac{1}{2}(\partial_1\phi)^2 - cm^2\cos(2\pi^{1/2}\phi) + \frac{e^2}{2\pi}\left(\phi + \frac{\pi^{1/2}F}{e}\right)^2\right]. \quad \text{(B.9)}$$

By shifting the field $\phi \to \phi - \pi^{1/2}F/e$ and defining a new normal ordering with respect to the mass $\mu = \pi^{-1/2}e$, we finally obtain

$$\mathcal{H} = N_\mu\left[\frac{1}{2}\Pi^2 + \frac{1}{2}(\partial_1\phi)^2 - cm\mu\cos(2\pi^{1/2}\phi - \theta) + \frac{\mu^2}{2}\phi^2\right] \quad \text{(B.10)}$$

where $\theta = 2\pi F/e$.

BIBLIOGRAPHY

[1] R. Kubo and H. Ichimura. *Statistical Mechanics: An Advanced Course with Problems and Solutions*. North-Holland personal library. North-Holland, 1990.

[2] K. Huang. *Statistical mechanics*. Wiley, 1987.

[3] L. Boltzmann. *Vorlesungen über Gastheorie: Th. Theorie van der Waals'; Gase mit zusammengesetzten Molekülen; Gasdissociation; Schlussbemerkungen*. Vorlesungen über Gastheorie. J. A. Barth, 1898.

[4] George D. Birkhoff. Proof of a recurrence theorem for strongly transitive systems. *Proceedings of the National Academy of Sciences*, 17(12):650–655, 1931.

[5] George D. Birkhoff. Proof of the ergodic theorem. *Proceedings of the National Academy of Sciences*, 17(12):656–660, 1931.

[6] G. D. Birkhoff and B. O. Koopman. Recent contributions to the ergodic theory. *Proceedings of the National Academy of Sciences*, 18(3):279–282, 1932.

[7] J. v. Neumann. Proof of the quasi-ergodic hypothesis. *Proceedings of the National Academy of Sciences*, 18(1):70–82, 1932.

[8] M. Toda, R. Kubo, and N. Saito. *Statistical Physics I: Equilibrium Statistical Mechanics*. Springer Series in Solid-State Sciences. Springer Berlin Heidelberg, 2012.

[9] John H. Lowenstein. *Essentials of Hamiltonian Dynamics*. Cambridge University Press, 2012.

[10] K. Vogtmann, A. Weinstein, and V.I. Arnol'd. *Mathematical Methods of Classical Mechanics*. Graduate Texts in Mathematics. Springer New York, 1997.

[11] Edwin T Jaynes. Information theory and statistical mechanics. *Physical review*, 106(4):620, 1957.

[12] A N Kolmogorov. On conservation of conditionally periodic motions for a small change in Hamilton's function. *Dokl. Akad. Nauk SSSR*, 98:527–530, 1954.

[13] V. I. Arnol d. The stability of the equilibrium position of a Hamiltonian system of ordinary differential equations in the general elliptic case. *Dokl. Akad. Nauk SSSR*, 137:255–257, 1961.

[14] J Moser. On invariant curves of area preserving mappings of an annulus Nachr. Akad. Wiss. Gottingen, II Math.-Phys. Kl. pages 1–20, 01 1962.

[15] Thierry Dauxois. Fermi, Pasta, Ulam, and a mysterious lady. *Physics Today*, 61(1):55–57, 2008.

[16] Giovanni Gallavotti. *The Fermi-Pasta-Ulam Problem*, volume 728. 01 2008.

[17] T. Dauxois and S. Ruffo. Fermi-Pasta-Ulam nonlinear lattice oscillations. *Scholarpedia*, 3(8):5538, 2008. revision #91257.

[18] E. Fermi, P Pasta, S Ulam, and M Tsingou. Studies of the nonlinear problems. *Los Alamos report LA-1940*, 1955.

[19] Tomer Goldfriend and Jorge Kurchan. Equilibration of quasi-integrable systems. *Phys. Rev. E*, 99:022146, Feb 2019.

[20] J. v. Neumann. Beweis des ergodensatzes und desh-theorems in der neuen mechanik. *Zeitschrift für Physik*, 57(1):30–70, Jan 1929.

[21] J.J. Sakurai and J. Napolitano. *Modern Quantum Mechanics*. Addison-Wesley, 2011.

[22] Anatoli Polkovnikov, Krishnendu Sengupta, Alessandro Silva, and Mukund Vengalattore. Nonequilibrium dynamics of closed interacting quantum systems. *Rev. Mod. Phys.*, 83:863, 2011.

[23] Zhe Wang, Jianda Wu, Wang Yang, Anup Kumar Bera, Dmytro Kamenskyi, A.T.M. Nazmul Islam, Shenglong Xu, Joseph Matthew Law, Bella Lake, Congjun Wu, et al. "experimental observation of bethe strings". *Nature*, 554(7691):219, 2018.

[24] Sidney Coleman and Jeffrey Mandula. All possible symmetries of the s matrix. *Phys. Rev.*, 159:1251–1256, Jul 1967.

[25] Pasquale Calabrese, Fabian H L Essler, and Giuseppe Mussardo. Introduction to 'quantum integrability in out of equilibrium systems'. *Journal of Statistical Mechanics: Theory and Experiment*, 2016(6):064001, jun 2016.

[26] Fabian H L Essler and Maurizio Fagotti. Quench dynamics and relaxation in isolated integrable quantum spin chains. *Journal of Statistical Mechanics: Theory and Experiment*, 2016(6):064002, jun 2016.

[27] Lev Vidmar and Marcos Rigol. Generalized gibbs ensemble in integrable lattice models. *Journal of Statistical Mechanics: Theory and Experiment*, 2016(6):064007, jun 2016.

[28] Enej Ilievski, Marko Medenjak, Tomaž Prosen, and Lenart Zadnik. Quasilocal charges in integrable lattice systems. *Journal of Statistical Mechanics: Theory and Experiment*, 2016(6):064008, jun 2016.

[29] E.H. Lieb and D.W. Robinson. The finite group velocity of quantum spin systems. *Commun. Math. Phys.*, 28:251, 1972.

[30] Tomaz Prosen. A new class of completely integrable quantum spin chains. *Journal of Physics A: Mathematical and General*, 31(21):L397–L403, may 1998.

[31] P. Jordan and E. Wigner. Über das Paulische Äquivalenzverbot. *Z. Phys.*, 47:631, 1928.

[32] Marcos Rigol, Vanja Dunjko, Vladimir Yurovsky, and Maxim Olshanii. Relaxation in a completely integrable many-body quantum system: An ab initio study of the dynamics of the highly excited states of 1d lattice hard-core bosons. *Phys. Rev. Lett.*, 98:050405, Feb 2007.

[33] M.L. Mehta. *Random Matrices*. Pure and Applied Mathematics. Elsevier Science, 2004.

[34] Eugene P. Wigner. On a class of analytic functions from the quantum theory of collisions. *Annals of Mathematics*, 53(1):36–67, 1951.

[35] Eugene P. Wigner. On a class of analytic functions from the quantum theory of collisions. *Annals of Mathematics*, 53(1):36–67, 1951.

[36] Eugene P. Wigner. Characteristics vectors of bordered matrices with infinite dimensions ii. *Annals of Mathematics*, 65(2):203–207, 1957.

[37] Eugene P. Wigner. On the distribution of the roots of certain symmetric matrices. *Annals of Mathematics*, 67(2):325–327, 1958.

[38] Freeman J. Dyson and Madan Lal Mehta. Statistical theory of the energy levels of complex systems. iv. *Journal of Mathematical Physics*, 4(5):701–712, 1963.

[39] Tabor M. Berry M. and Ziman J. M. Level clustering in the regular spectrum. *356 Proc. R. Soc. Lond. A*, 1977.

[40] D Poilblanc, T Ziman, J Bellissard, F Mila, and G Montambaux. Poisson vs GOE statistics in integrable and non-integrable quantum hamiltonians. *Europhysics Letters (EPL)*, 22(7):537–542, jun 1993.

[41] Vadim Oganesyan and David A. Huse. Localization of interacting fermions at high temperature. *Phys. Rev. B*, 75:155111, Apr 2007.

[42] Y. Y. Atas, E. Bogomolny, O. Giraud, and G. Roux. Distribution of the ratio of consecutive level spacings in random matrix ensembles. *Phys. Rev. Lett.*, 110:084101, Feb 2013.

[43] Romain Vasseur and Joel E Moore. Nonequilibrium quantum dynamics and transport: from integrability to many-body localization. *Journal of Statistical Mechanics: Theory and Experiment*, 2016(6):064010, jun 2016.

[44] Pasquale Calabrese and John Cardy. Evolution of entanglement entropy in one-dimensional systems. *Journal of Statistical Mechanics: Theory and Experiment*, 2005(04):P04010, apr 2005.

[45] Marko Ljubotina, Marko Znidaric, and Tomaæ Prosen. Spin diffusion from an inhomogeneous quench in an integrable system. *Nature Communications*, 8, 02 2017.

[46] Dmitry A. Abanin, Ehud Altman, Immanuel Bloch, and Maksym Serbyn. Colloquium: Many-body localization, thermalization, and entanglement. *Rev. Mod. Phys.*, 91:021001, May 2019.

[47] P. W. Anderson. Absence of diffusion in certain random lattices. *Phys. Rev.*, 109:1492–1505, Mar 1958.

[48] D.M. Basko, I.L. Aleiner, and B.L. Altshuler. Metal-insulator transition in a weakly interacting many-electron system with localized single-particle states. *Annals of Physics*, 321(5):1126 – 1205, 2006.

[49] Marko Žnidarič, Tomaž Prosen, and Peter Prelovšek. Many-body localization in the heisenberg xxz magnet in a random field. *Phys. Rev. B*, 77:064426, Feb 2008.

[50] Arijeet Pal and David A. Huse. Many-body localization phase transition. *Phys. Rev. B*, 82:174411, Nov 2010.

[51] J. Šuntajs, J. Bonča, T. Prosen, and Vidmar. Quantum chaos challenges many-body localization. *arXiv:1905.06345*, 2019.

[52] Vincenzo Alba and Pasquale Calabrese. Entanglement and thermodynamics after a quantum quench in integrable systems. *Proceedings of the National Academy of Sciences*, 114(30):7947–7951, 2017.

[53] Pasquale Calabrese and John Cardy. *Int.J.Quant.Inf.*, 4:429, 2006.

[54] Jens H. Bardarson, Frank Pollmann, and Joel E. Moore. Unbounded growth of entanglement in models of many-body localization. *Phys. Rev. Lett.*, 109:017202, Jul 2012.

[55] Maksym Serbyn, Z. Papić, and Dmitry A. Abanin. Universal slow growth of entanglement in interacting strongly disordered systems. *Phys. Rev. Lett.*, 110:260601, Jun 2013.

[56] Maksym Serbyn, Z. Papić, and Dmitry A. Abanin. Local conservation laws and the structure of the many-body localized states. *Phys. Rev. Lett.*, 111:127201, Sep 2013.

[57] J. Eisert, M. Cramer, and M. B. Plenio. Colloquium: Area laws for the entanglement entropy. *Rev. Mod. Phys.*, 82:277–306, Feb 2010.

[58] Mark Srednicki. The approach to thermal equilibrium in quantized chaotic systems. *Journal of Physics A: Mathematical and General*, 32(7):1163–1175, jan 1999.

[59] Luca D'Alessio, Yariv Kafri, Anatoli Polkovnikov, and Marcos Rigol. From quantum chaos and eigenstate thermalization to statistical mechanics and thermodynamics. *Advances in Physics*, 65(3):239–362, 2016.

[60] Marcos Rigol, Vanja Dunjko, and Maxim Olshanii. Thermalization and its mechanism for generic isolated quantum systems. *Nature*, 452:854–8, 05 2008.

[61] M. C. Bañuls, J. I. Cirac, and M. B. Hastings. Strong and weak thermalization of infinite nonintegrable quantum systems. *Phys. Rev. Lett.*, 106:050405, Feb 2011.

[62] R. P. Feynman. Simulating Physics with Computers. *Int. J. Theor. Phys.*, 21:467, 1982.

[63] Toshiya Kinoshita, Trevor Wenger, and David S Weiss. A quantum newton's cradle. *Nature*, 440:900–3, 05 2006.

[64] Tim Langen, Sebastian Erne, Remi Geiger, Bernhard Rauer, Thomas Schweigler, Maximilian Kuhnert, Wolfgang Rohringer, Igor Mazets, T Gasenzer, and Jrg Schmiedmayer. "experimental observation of a generalized gibbs ensemble". *Science (New York, N.Y.)*, 348, 11 2014.

[65] Michael Schreiber, Sean S. Hodgman, Pranjal Bordia, Henrik P. Lüschen, Mark H. Fischer, Ronen Vosk, Ehud Altman, Ulrich Schneider, and Immanuel Bloch. "observation of many-body localization of interacting fermions in a quasirandom optical lattice". *Science*, 349(6250):842–845, 2015.

[66] Zi Cai, Congjun Wu, and U. Schollwöck. Confinement: A real-time visualization. *Phys. Rev. B*, 85:075102, Feb 2012.

[67] A. K. Bera, B. Lake, F. H. L. Essler, L. Vanderstraeten, C. Hubig, U. Schollwöck, A. T. M. N. Islam, A. Schneidewind, and D. L. Quintero-Castro. Spinon confinement in a quasi-one-dimensional anisotropic heisenberg magnet. *Phys. Rev. B*, 96:054423, Aug 2017.

[68] Fangli Liu, Rex Lundgren, Paraj Titum, Guido Pagano, Jiehang Zhang, Christopher Monroe, and Alexey V. Gorshkov. Confined quasiparticle dynamics in long-range interacting quantum spin chains. *Phys. Rev. Lett.*, 122:150601, Apr 2019.

[69] Yoshihito Kuno, Shinya Sakane, Kenichi Kasamatsu, Ikuo Ichinose, and Tetsuo Matsui. Quantum simulation of $(1 + 1)$-dimensional u(1) gauge-higgs model on a lattice by cold bose gases. *Phys. Rev. D*, 95:094507, May 2017.

[70] Elliott Lieb, Theodore Schultz, and Daniel Mattis. Two soluble models of an antiferromagnetic chain. *Annals of Physics*, 16(3):407 – 466, 1961.

[71] B. Andersson, G. Gustafson, G. Ingelman, and T. Sjstrand. Parton fragmentation and string dynamics. *Physics Reports*, 97(2):31 – 145, 1983.

[72] Barry M. McCoy and Tai Tsun Wu. Two-dimensional ising field theory in a magnetic field: Breakup of the cut in the two-point function. *Phys. Rev. D*, 18:1259–1267, Aug 1978.

[73] Gesualdo Delfino, Paolo Grinza, and Giuseppe Mussardo. Decay of particles above threshold in the ising field theory with magnetic field. *Nuclear Physics B*, 737(3):291 – 303, 2006.

[74] Pedro Fonseca and Alexander Zamolodchikov. Ising spectroscopy. I. Mesons at T < T(c). *arXiv*, hep-th/0612304, 2006.

[75] Alexander Zamolodchikov. Integrals of motion and $s-$matrix of the (scaled) $t = t_c$ ising model with magnetic field. *International Journal of Modern Physics A*, 04(16):4235–4248, 1989.

[76] S. B. Rutkevich. Energy spectrum of bound-spinons in the quantum ising spin-chain ferromagnet. *Journal of Statistical Physics*, 131(5):917–939, Jun 2008.

[77] Marton Kormos, Mario Collura, Gabor Takács, and Pasquale Calabrese. Real-time confinement following a quantum quench to a non-integrable model. *Nature Physics*, 13:246 EP –, Nov 2016.

[78] G. Vidal. Classical simulation of infinite-size quantum lattice systems in one spatial dimension. *Phys. Rev. Lett.*, 98:070201, Feb 2007.

[79] Paolo Pietro Mazza, Gabriele Perfetto, Alessio Lerose, Mario Collura, and Andrea Gambassi. Suppression of transport in nondisordered quantum spin chains due to confined excitations. *Phys. Rev. B*, 99:180302, May 2019.

[80] S. B. Rutkevich. Decay of the metastable phase in $d = 1$ and $d = 2$ ising models. *Phys. Rev. B*, 60:14525–14528, Dec 1999.

[81] G.H. Wannier. *Elements of solid state theory.* University Press, 1959.

[82] Cheng-Ju Lin and Olexei I Motrunich. Exact strong-eth violating eigenstates in the rydberg-blockaded atom chain. *arXiv preprint arXiv:1810.00888*, 2018.

[83] J. Schwinger. On gauge invariance and vacuum polarization. *Phys. Rev.*, 82:664, 1951.

[84] Julian Schwinger. Gauge Invariance and Mass. II. *Phys. Rev.*, 128:2425, 1962.

[85] C. J. Hamer, J. Kogut, D. P. Crewther, and M. M. Mazzolini. *Nucl. Phys. B*, 208:413, 1982.

[86] T. Pichler, M. Dalmonte, E. Rico, P. Zoller, and S. Montangero. Real-time Dynamics in U(1) Lattice Gauge Theories with Tensor Networks. *Phys. Rev. X*, 6:011023, 2016.

[87] F. Meinert, M. J. Mark, E. Kirilov, K. Lauber, P. Weinmann, A. J. Daley, and H.-C. Nägerl. Quantum quench in an atomic one-dimensional ising chain. *Phys. Rev. Lett.*, 111:053003, Jul 2013.

[88] Hannes Bernien, Sylvain Schwartz, Alexander Keesling, Harry Levine, Ahmed Omran, Hannes Pichler, Soonwon Choi, Alexander S Zibrov, Manuel Endres, Markus Greiner, et al. Probing many-body dynamics on a 51-atom quantum simulator. *Nature*, 551(7682):579, 2017.

[89] C. J. Turner, A. A. Michailidis, D. A. Abanin, M. Serbyn, and Z. Papic. Weak ergodicity breaking from quantum many-body scars. *Nature Physics*, 14(7):745–749, 2018.

[90] Paul Fendley, K. Sengupta, and Subir Sachdev. Competing density-wave orders in a one-dimensional hard-boson model. *Phys. Rev. B*, 69:075106, Feb 2004.

[91] G. Giudici, A. Angelone, G. Magnifico, Z. Zeng, G. Giudice, T. Mendes-Santos, and M. Dalmonte. Diagnosing potts criticality and two-stage melting in one-dimensional hard-core boson models. *Phys. Rev. B*, 99:094434, Mar 2019.

[92] Federica M. Surace, Paolo P. Mazza, Giuliano Giudici, Alessio Lerose, Andrea Gambassi, and Marcello Dalmonte. Lattice gauge theories and string dynamics in Rydberg atom quantum simulators. *arXiv e-prints*, page arXiv:1902.09551, Feb 2019.

[93] C. N. Yang and C. P. Yang. One-dimensional chain of anisotropic spin-spin interactions. i. proof of bethe's hypothesis for ground state in a finite system. *Phys. Rev.*, 150:321–327, Oct 1966.

[94] Sergei B. Rutkevich. Kink confinement in the antiferromagnetic XXZ spin-(1/2) chain in a weak staggered magnetic field. *EPL (Europhysics Letters)*, 121(3):37001, feb 2018.

[95] Alessio Lerose, Federica Surace, Paolo P. Mazza, Gabriele Perfetto, Mario Collura, and Andrea Gambassi. Slow dynamics by quantum confinement of excitations. *In preparation.*

[96] Andrew J. A. James, Robert M. Konik, and Neil J. Robinson. Nonthermal states arising from confinement in one and two dimensions. *Phys. Rev. Lett.*, 122:130603, Apr 2019.

[97] Neil J. Robinson, Andrew J. A. James, and Robert M. Konik. Signatures of rare states and thermalization in a theory with confinement. *Phys. Rev. B*, 99:195108, May 2019.

[98] Dmitry Abanin, Wojciech De Roeck, Wen Wei Ho, and François Huveneers. A rigorous theory of many-body prethermalization for periodically driven and closed quantum systems. *Communications in Mathematical Physics*, 354(3):809–827, Sep 2017.

[99] CJ Turner, AA Michailidis, DA Abanin, M Serbyn, and Z Papić. Weak ergodicity breaking from quantum many-body scars. *Nature Physics*, 14:745, 05 2018.

[100] C. J. Turner, A. A. Michailidis, D. A. Abanin, M. Serbyn, and Z. Papić. Quantum scarred eigenstates in a rydberg atom chain: Entanglement, breakdown of thermalization, and stability to perturbations. *Phys. Rev. B*, 98:155134, Oct 2018.

[101] Soonwon Choi, Christopher J Turner, Hannes Pichler, Wen Wei Ho, Alexios A Michailidis, Zlatko Papić, Maksym Serbyn, Mikhail D Lukin, and Dmitry A Abanin. Emergent su (2) dynamics and perfect quantum many-body scars. *arXiv preprint arXiv:1812.05561*, 2018.

[102] Vedika Khemani, Chris R. Laumann, and Anushya Chandran. Signatures of integrability in the dynamics of rydberg-blockaded chains. *Phys. Rev. B*, 99:161101, Apr 2019.

[103] Eric J. Heller. Bound-state eigenfunctions of classically chaotic hamiltonian systems: Scars of periodic orbits. *Phys. Rev. Lett.*, 53:1515–1518, Oct 1984.

[104] Michael Schecter and Thomas Iadecola. Weak Ergodicity Breaking and Quantum Many-Body Scars in Spin-1 XY Magnets. *arXiv e-prints*, page arXiv:1906.10131, Jun 2019.

[105] Sanjay Moudgalya, Stephan Rachel, B. Andrei Bernevig, and Nicolas Regnault. Exact excited states of nonintegrable models. *Phys. Rev. B*, 98:235155, Dec 2018.

[106] Sanjay Moudgalya, Nicolas Regnault, and B. Andrei Bernevig. Entanglement of exact excited states of affleck-kennedy-lieb-tasaki models: Exact

results, many-body scars, and violation of the strong eigenstate thermalization hypothesis. *Phys. Rev. B*, 98:235156, Dec 2018.

[107] Naoto Shiraishi and Takashi Mori. Systematic construction of counterexamples to the eigenstate thermalization hypothesis. *Phys. Rev. Lett.*, 119:030601, Jul 2017.

[108] F. Hebenstreit, J. Berges, and D. Gelfand. Simulating fermion production in 1+1 dimensional qed. *Phys. Rev. D*, 87:105006, May 2013.

[109] M. Dalmonte and S. Montangero. Lattice gauge theories simulations in the quantum information era. *Contemp. Phys.*, 57:388, 2016.

[110] Erez Zohar and J. Ignacio Cirac. Removing staggered fermionic matter in $u(n)$ and $su(n)$ lattice gauge theories. *Phys. Rev. D*, 99:114511, Jun 2019.

[111] A. Celi, B. Vermersch, O. Viyuela, H. Pichler, M. D. Lukin, and P. Zoller. Emerging 2D Gauge theories in Rydberg configurable arrays. *arXiv e-prints*, page arXiv:1907.03311, Jul 2019.

[112] John Kogut and Leonard Susskind. Hamiltonian formulation of Wilson's lattice gauge theories. *Phys. Rev. D*, 11:395, Jan 1975.

[113] M. Maggiore. *A Modern Introduction to Quantum Field Theory*. EBSCO ebook academic collection. Oxford University Press, 2005.

[114] H.B. Nielsen and M. Ninomiya. Absence of neutrinos on a lattice: (i). proof by homotopy theory. *Nuclear Physics B*, 185(1):20 – 40, 1981.

[115] Kenneth G. Wilson. Confinement of quarks. *Phys. Rev. D*, 10:2445, Oct 1974.

[116] Christine Muschik, Markus Heyl, Esteban Martinez, Thomas Monz, Philipp Schindler, Berit Vogell, Marcello Dalmonte, Philipp Hauke, Rainer Blatt, and Peter Zoller. U(1) wilson lattice gauge theories in digital quantum simulators. *New Journal of Physics*, 19(10):103020, oct 2017.

[117] Sidney Coleman. More about the massive Schwinger model. *Ann. Phys.*, 101(1):239, 1976.

[118] Daniel Barredo, Vincent Lienhard, Sylvain de Léséleuc, Thierry Lahaye, and Antoine Browaeys. Synthetic three-dimensional atomic structures assembled atom by atom. *Nature*, 561:79, 2018.

[119] U J Wiese. Ultracold quantum gases and lattice systems: quantum simulation of lattice gauge theories. *Ann. Phys.*, 525(10-11):777, 2013.

[120] E. A. Calzetta and B. L. Hu. *Nonequilibrium Quantum Field Theory*. Cambridge Univ. Press, Cambridge, 2008.

[121] Gunnar S. Bali, Hartmut Neff, Thomas Düssel, Thomas Lippert, and Klaus Schilling. Observation of string breaking in qcd. *Phys. Rev. D*, 71:114513, Jun 2005.

[122] F. Hebenstreit, J. Berges, and D. Gelfand. Real-Time Dynamics of String Breaking. *Phys. Rev. Lett.*, 111:201601, 2013.

[123] S. Chandrasekharan and U. J. Wiese. Quantum link models : A discrete approach to gauge theories. *Nucl. Phys. B*, 492:455, 1997.

[124] Yoshihito Kuno, Shinya Sakane, Kenichi Kasamatsu, Ikuo Ichinose, and Tetsuo Matsui. Quantum simulation of (1 + 1)-dimensional u(1) gauge-higgs model on a lattice by cold bose gases. *Phys. Rev. D*, 95:094507, May 2017.

[125] Boye Buyens, Jutho Haegeman, Henri Verschelde, Frank Verstraete, and Karel Van Acoleyen. Confinement and string breaking for qed_2 in the hamiltonian picture. *Phys. Rev. X*, 6:041040, 2016.

[126] K. Rajagopal and F. Wilczek. Emergence of coherent long wavelength oscillations after a quench: Application to qcd. *Nucl. Phys. B*, 404(3):577–589, 1993.

[127] Wen Wei Ho, Soonwon Choi, Hannes Pichler, and Mikhail D Lukin. Periodic orbits, entanglement and quantum many-body scars in constrained models: matrix product state approach. *Phys. Rev. Lett.*, 122:040603, 2019.

[128] Immanuel Bloch, Jean Dalibard, and Sylvain Nascimbène. Quantum simulations with ultracold quantum gases. *Nat. Phys.*, 8:267, 2012.

[129] Igor Lesanovsky and Hosho Katsura. Interacting fibonacci anyons in a rydberg gas. *Phys. Rev. A*, 86:041601, Oct 2012.

[130] Johannes Zeiher, Jae yoon Choi, Antonio Rubio-Abadal, Thomas Pohl, Rick van Bijnen, Immanuel Bloch, and Christian Gross. Coherent many-body spin dynamics in a long-range interacting ising chain. *Phys. Rev. X*, 7:041063, 2017.

[131] D. Horn. *Phys. Lett. B*, 100:149, 1981.

[132] D. Banerjee, M. Dalmonte, M. Müller, E. Rico, P. Stebler, U.-J. Wiese, and P. Zoller. Atomic Quantum Simulation of Dynamical Gauge Fields Coupled

to Fermionic Matter: From String Breaking to Evolution after a Quench. *Phys. Rev. Lett.*, 109:1, 2012.

[133] B. M. McCoy and M.-L. Yan. *Nucl. Phys. B*, 215:278, 1983.

[134] Natalia Chepiga and Frédéric Mila. Dmrg investigation of constrained models: from quantum dimer and quantum loop ladders to hard-boson and fibonacci anyon chains. *arXiv preprint arxiv.1809.00746*, 09 2018.

[135] Yi-Ping Huang, Debasish Banerjee, and Markus Heyl. Dynamical quantum phase transitions in $u(1)$ quantum link models. *arXiv preprint arXiv:1808.07874*, 2018.

[136] V. Kasper, F. Hebenstreit, M. Oberthaler, and J. Berges. Schwinger pair production with ultracold atoms. *Phys. Lett. B.*, 760:742, 2016.

[137] E. Rico, T. Pichler, M. Dalmonte, P. Zoller, and S. Montangero. Tensor networks for Lattice Gauge Theories and Atomic Quantum Simulation. *Phys. Rev. Lett.*, 112:201601, 2014.

[138] M.C. Bañuls, K Cichy, I. Cirac, and K Jansen. The mass spectrum of the Schwinger model with matrix product states. *J. High Energy Phys.*, 2013:158, 2013.

[139] F. Fucito, F. Marchesoni, E. Marinari, G. Parisi, L. Peliti, S. Ruffo, and A. Vulpiani. Approach to equilibrium in a chain of nonlinear oscillators. *Journal de Physique*, 43(5):707–713, 1982.

[140] Marlon Brenes, Marcello Dalmonte, Markus Heyl, and Antonello Scardicchio. Many-body localization dynamics from gauge invariance. *Phys. Rev. Lett.*, 120:030601, 2018.

[141] Felix Bloch. Über die quantenmechanik der elektronen in kristallgittern. *Zeitschrift für Physik*, 52(7):555–600, Jul 1929.

[142] C. Zener. A Theory of the Electrical Breakdown of Solid Dielectrics. *Proceedings of the Royal Society of London Series A*, 145:523–529, July 1934.

[143] T Hartmann, F Keck, H J Korsch, and S Mossmann. Dynamics of bloch oscillations. *New Journal of Physics*, 6:2–2, jan 2004.

[144] Sidney Coleman. Quantum sine-gordon equation as the massive thirring model. *Phys. Rev. D*, 11:2088–2097, Apr 1975.